กล้องคอลโปสโคป3มิติราคาถูกแบบพกพาเพื่อการตรวจรอยโรคก่อนมะเร็งด้วยปัญญาประดิษฐ์อัตโนมัติบนโทรศัพท์มือถือ

COMPACT 3D CONTEXT-AWARE DEPTH INPAINTING COLPOSCOPE WITH AUTOMATED ARTIFICIAL INTELLIGENCE FOR CERVICAL PRE-CANCER DIAGNOSIS BASED-ON THE SMART PHONE.

นนทิวัฒน์ อำนวยผล

NONTIWAT AMNUAYPHOL

วิทยานิพนธ์นี้เป็นส่วนหนึ่งของการศึกษาตามหลักสูตรปริญญาวิศวกรรมศาสตรมหาบัณฑิต

สาขาวิชาวิศวกรรมชีวการแพทย์

คณะวิศวกรรมศาสตร์

สถาบันเทคโนโลยีพระจอมเกล้าเจ้าคุณทหารลาดกระบัง

พ.ศ.2567

KMITL-2024-EN-M- 317-241

COMPACT 3D CONTEXT-AWARE DEPTH INPAINTING COLPOSCOPE WITH AUTOMATED ARTIFICIAL INTELLIGENCE FOR CERVICAL PRE-CANCER DIAGNOSIS BASED-ON THE SMART PHONE.

BY

NONTIWAT AMNUAYPHOL

A PROJECT SUBMITTED IN PARTIAL FULFILLMENT OF THE

REQUIREMENTS FOR THE DEGREE OF MASTER OF

ENGINEERING IN BIOMEDICAL ENGINEERING

LADKRABANG

ACADEMIC YEAR 2024

KMITL-2024-EN-M- 317-241

หัวข้อวิทยานิพนธ์ กล้องคอลโปสโคป3มิติราคาถูกแบบพกพาเพื่อการตรวจรอยโรคก่อนมะเร็งด้วยปัญญาประดิษฐ์อัตโนมัติบนโทรศัพท์มือถือ

นักศึกษา นาย นนทิวัฒน์ อำนวยผล

รหัสประจำตัว 66016059

ปริญญา วิศวกรรมศาสตรมหาบัณฑิต

สาขาวิชา วิศวกรรมชีวการแพทย์

พ.ศ. 2567

อาจารย์ที่ปรึกษาวิทยานิพนธ์ รศ.ดร. วิบูลย์ ปิยวัฒนเมธา

บทคัดย่อ

งานวิจัยฉบับนี้พัฒนาขึ้นเพื่อสร้างนวัตกรรมเครื่องมือแพทย์เพื่อเพิ่มความแม่นยำในการวินิจฉัยเทียบกับกระบวนการทำคอลโปสโคปีแบบมาตรฐาน โตยเครื่องมือที่ได้รับการพัฒนามีการปรับใช้เทคโนโลยีใหม่ อันประกอบด้วยการสังเคราะห์ภาพสามมิติผ่านโมเดลการต่อเติมภาพเชิงชั้นโดยอ้างอิงบริบท (CA-LDI) การตรวจจับการประเมินภาพถ่ายสารละลายน้ำเกลือบนภาพปากมดลูกโดยใช้โมเดล efficientnetB0 และ เทคนิคการตรวจจับภาพสารเรืองแสงโดยใช้สารย้อม Fluorescein isothiocyanate (FITC) เป้าประสงค์ของงานวิจัยฉบับนี้คือการตรวจจับภาวะก่อนมะเร็ง โดยใช้การเรียนรู้เชิงลึกของปัญญาประดิษฐ์ผนวกกับการใช้งานภาพถ่ายสารเรืองแสงเพื่อวางโครงสร้างพื้นฐานสำหรับการได้รับผลวินิจฉัยในการเข้าตรวจเพียงครั้งเดียว งานชิ้นนี้ยังได้พัฒนาและย่อขนาดชิ้นงานในรุ่นก่อนหน้าโดยย่อขนาดของระบบได้ถึง 71 เท่า และ ลดต้นทุนต้นแบบได้ถึง 500% โดยได้คงไว้ซึ่งระบบจำเป็นทั้งหมดของระบบดังกล่าว อาธิ การสังเคราะห์ภาพ CA-LDI และการเก็บภาพจากสาร FITC รวมถึงการประมวลภาพแบบการจัดหมวดคู่ภายใต้การแบ่งระยะมะเร็งตามสเกลบีเทสด้า ตัวเครื่องของคอลโปสโคปได้รับการต่อยอดจากดีไซน์ดั้งเดิมอ้างอิงจากมหาวิทยาลัย Duke เป็นดีไซน์ใกล้เคียงระบบย่อส่วนซึ่ง

ได้รับคำแนะนำโดยตรงจากอาจารย์แพทย์อาวุโสของโรงพยาบาลศิริราช ในการวิจัยนี้ กล้องคอลโปสโคปได้ถูกพัฒนาขึ้นทั้งหมดสองรูปแบบ โดยประกอบด้วยแบบสอดใส่ภายใน ซึ่งสามารถใช้งานได้เป็นระยะ 0-6 ซม. สำหรับการตรวจภายนอก และ สามารถสอดใส่ได้ถึง 6 ซม. ไปจนถึงกล้องรูปแบบใช้ตรวจภายนอกโดยเฉพาะซึ่งสามารถใช้งานได้ในระยะ 5-12.5 ซม. โดยคิดเป็นความแตกต่างที่ 208% เมื่อประเมินระยะการใช้งานสูงสุด โดยกล้องคอลโปสโคป MOFiE ดังกล่าวสามารถสังเคราะห์ภาพสามมิติคุณภาพสูงได้ทั้งหมด 4 รูปแบบ ซึ่งได้รับการประเมินผ่านอัลกอริทึ่ม SSIM โดยได้รับคะแนนความคล้ายคลึงที่ 95.4% เมื่อเทียบภาพสังเคราะห์กับเฟรมก่อนหน้า โดยแปรผลได้ว่าภาพดังกล่าวไม่สามารถถูกแยกจากภาพแท้จริงได้ผ่านสายตามนุษย์ นอกจากนี้โมดูลการจัดกลุ่มรอยโรคยังถูกฝึกฝนโดยใช้ภาพคอปโปสโคปีในฐานข้อมูลแบบเปิดของ IARC อันประกอบด้วยภาพถ่ายทางคอลโปสโคปทั้งหมด 201 ภาพ โดยใช้ความแม่นยำทั้งหมด 85.7% ในการคัดกรองกลุ่มความเสี่ยงต่ำ (ภาวะปกติไปจนถึงเนื้องอกระดับต่ำ) และ ความเสี่ยงสูง (เนื้องอกระดับสูงไปจนถึงภาวะมะเร็ง) นอกจากนั้นแล้วอุปกรณ์ที่ได้รับการพัฒนายังสามารถจับสัญญาณจากภาพสารฟลูออเรสเซนต์ได้จนถึงความเข้มข้นสารที่ 0.01 โมลา

Thesis Compact 3D context-aware depth inpainting colposcope with automated artificial intelligence for cervical pre-cancer diagnosis based-on the smart phone.

Student Mr. Nontiwat Amnuayphol

Student ID. 66016059

Degree Master of Engineering

Program Biomedical engineering

Year 2024

Thesis Advisor Associate Professor Wibool Piyawattanametha

ABSTRACT

This research endeavors to develop an innovative medical device aimed at enhancing the diagnostic precision of traditional colposcopy procedures. Our device integrates cutting-edge technologies, including 3D image synthesis with context-aware layer depth inpainting (CA-LDI), object detection utilizing efficientnetB0 on saline imaging, and fluorescent imaging techniques employing Fluorescein isothiocyanate (FITC) dye. The primary objective of this study is to elevate cervical cancer screening by creating a highly accurate system for detecting precancerous conditions, facilitated by deep learning algorithms, alongside leveraging fluorescent imaging for comprehensive validation in a single visit. Our research encompasses the refinement and miniaturization of previous mobile platform iterations, resulting in a remarkable 71-fold reduction in size and approximately

500% decrease in production costs. We have retained essential functionalities such as CA-LDI synthesis and FITC imaging while enhancing the artificial intelligence component to enable precancerous detection through a binary classification model based on the Bethesda reporting system. The colposcope hardware has been upgraded from the Duke University design to a Siriraj-based model, as advised by senior oncologists at Siriraj Hospital. Additionally, two camera versions have been developed, including a minimally invasive model operating within a range of 0-6 cm for non-invasive screening and up to 6 cm for minimally invasive tasks, and a non-invasive version with an operational range of 5-12.5 cm, boasting a 208% greater maximum distance compared to the former. Our MOFiE device offers four camera movement patterns, delivering high-fidelity output in 3D synthesis. Evaluation via SSIM matrix indicates a 95.4% similarity between synthesized and previous frames, effectively rendering them indistinguishable to human perception. The image classification module has been trained on the IARC colposcopy digital atlas and Cervical Cancer Screening dataset, comprising 201 colposcopic images. It achieves an accuracy of 85.7% in distinguishing between low-risk (NILM/LSIL) and high-risk (HSIL/Squamous cell carcinoma) groups. Furthermore, our camera demonstrates exceptional precision in capturing fluorescent images, even at concentrations as low as 0.01 Molar.

ACKNOWLEDGEMENTS

I would like to express my sincere gratitude to all those who have played a crucial role in the successful completion of my project on developing a Fluorescence 3D endoscope for early cervical cancer detection based on Deep Learning Technology. It gives me immense pleasure to acknowledge their contribution and support throughout this endeavor.

First and foremost, I would like to express my heartfelt thanks to my project adviser, Assoc. prof. Wibool Piyawattanametha, for his invaluable guidance and assistance throughout the project. Your support, encouragement, and exceptional recommendations helped me navigate through the intricacies of this challenging project with ease. I am grateful for your meticulous preparation and problem-solving methods that inspired me to pursue excellence and achieve remarkable results. I would also like to extend my sincere appreciation to the members of the biomedical department's staff and the institute itself, for the personnel including my seniors and friends, for their unwavering assistance and encouragement. Your constant support and belief in my abilities have been a source of motivation and inspiration for me throughout the project.

Nontiwat Amnuayphol

TABLE OF CONTENTS

LIST OF FIGURES

LIST OF TABLES

CHAPTER 1

INTRODUCTION

1.1 BACKGROUND AND SIGNIFICANCE OF THE STUDY

According to demographic and health surveys in 2018, there is an estimation that within 2021 cervical cancer will become the 4th most common cancer among women globally. Research mentions that the numbers vary among countries based on multiple factors, for example, the capital income of the nation. This is directly reflected in the fatality rate, which significantly increases in lower-income countries. In low-and-middle-income countries, for example, Thailand, gynecological cancer ranks as the 2nd most common and deadliest cancer in females. This is complemented by the analysis in 2020 by the International Agency for Research on Cancer, United States of America. The estimated number of cancer cases has been published as 19.3 million new cases (18.1 million excluding nonmelanoma skin cancer), with a high possibility of almost 10.0 million cancer deaths (9.9 million excluding nonmelanoma skin cancer) according to the same source. As for specific results in cervical cancer, The Global

Cancer Observatory (GLOBOCAN) 2020 estimates 604,127 cervical cancer cases and the same applies to 341,831 deaths.

To determine the cervical cancer status in patients, Papanicolaou (PAP) smearing, and the Human Papillomavirus (HPV) test are two essential screening procedures. The initial step involves collecting cellular samples from a female subject's cervix using a specialized instrument, placing the sample in a reagent bottle, and analyzing it in the laboratory. This process is akin to the antigen test kit (ATK) position in COVID-19 screening, being cost-effective and not requiring expert input to provide classification results for cervical malignancy. However, the PAP smear exhibits minimal precision compared to other cervical cancer screening methods, with only 47.19% specificity and 64.79% sensitivity. Therefore, colposcopy is necessary as a follow-up instruction after the initial screening to ensure accurate results. Colposcopy is an imaging procedure that examines the cervical epithelium to detect cancerous lesions. However, incorrect administration or application of treatment may compromise the effectiveness of the medical procedure. During colposcopy, a metal speculum is inserted into the vagina, which, if done incorrectly, may cause harm to the patient. Pattern evaluation is used to determine the outcome. Colposcopy relies on the assumptions of doctors based on the cervical pattern detected by the colposcope, leading to divergent conclusions based on individual doctor experience, necessitating

time-consuming training of medical staff with the necessary expertise for effective and accurate diagnosis. Nevertheless, colposcopy exhibits limited precision, varying from oncologist to oncologist. Research in 2020 revealed that colposcopist screening results had only a 65.9% agreement score with biopsy validation, which serves as the gold standard. This underscores the necessity of biopsy techniques to remove tissue for examination in the laboratory to determine the final positive diagnosis in each instance. Although biopsy methods offer near-perfect precision, with 98.8% sensitivity and 89% specificity in classifying squamous cell carcinoma, they come with high operational costs and lengthy processing times, thereby eliminating the possibility of single-visit validation.

This research aims to develop a medical device that, when combined with fluorescent imaging, can enhance the diagnostic accuracy of conventional colposcopy. This device can be utilized in two procedures based on both versions of the handheld colposcope: a minimally-invasive and a non-invasive model. Both models are integrated with instantaneous algorithms designed to convert 2D images into 3D videos, thereby reintroducing missing spatial information back into the handheld colposcope. This feature, although common and deemed necessary in traditional colposcopes, has not been satisfactorily achieved in current handheld models.

Through depth map image construction techniques, it becomes feasible to obtain 3D images with a monocular miniature complementary metal-oxide semiconductor (CMOS) camera, eliminating the need for two endoscopes to collect different angles of view. Instead of displaying overlapping images on a polarization screen and separating them via two polarization filters before reaching the photosensory receptor, this approach simplifies the process. With appropriate algorithmic training approaches, there is a strong feasibility for AI to recognize internal patterns underlying medical images more quickly, accurately, and efficiently, potentially setting a new standard for cervical cancer screening processes in the future. Similarly, the development of a fluorescent imaging module aims to facilitate one-visit screening processes.

1.2 OBJECTIVES

1.1.1 Develop a budget-friendly version of the handheld colposcope, encompassing two variations: minimally invasive and non-invasive AIRC colposcopes.

1.1.2 Develop and validate automatic 3D software for colposcopic images, supporting saline, lugol iodine, and acetic acid imaging.

1.1.3 Develop AI for precancerous screening capable of instant diagnosis to enhance evaluation precision standardization.

1.1.4 Develop fluorescent imaging techniques to facilitate one-visit validation.

1.3 SCOPE OF THE STUDY

The scope of this work is to develop a budget-friendly version of the handheld colposcope, encompassing two variations: minimally invasive and non-invasive AIRC colposcopes. Additionally, develop and validate automatic 3D software for colposcopic images, supporting saline, lugol iodine, and acetic acid imaging. This includes the development of AI for precancerous screening capable of instant diagnosis to enhance evaluation precision standardization. Finally, implement fluorescent imaging techniques to facilitate one-visit validation.

CHAPTER 2

REVIEW OF RELATED LITERATURE

2.1 FEMALE REPRODUCTIVE SYSTEM

At the onset of menopause, the female reproductive system halts the production of crucial female hormones necessary for the reproductive cycle. This transition may manifest in irregular menstrual periods, eventually leading to their cessation [1]. Once a woman has experienced a continuous absence of menstruation for 12 consecutive months, she is classified as menopausal.

2.1.1 FEMALE REPRODUCTIVE ORGAN ANATOMY

Comprising a intricate interconnection of organs and tissues, the female reproductive system delineates into external and internal genitalia. The external genitalia encompasses the labia majora and minora, the vestibule, Bartholin glands, clitoris, and periurethral area, situated external to the true pelvis. While this discussion predominantly focuses on ovaries, it's imperative for medical practitioners, particularly those in obstetrics and gynecology, to comprehend the distinct female anatomy,

which includes the vagina, cervix, uterus, and fallopian tubes, all located within the true pelvis [2].

2.1.1.1 EXTERNAL GENITALIA

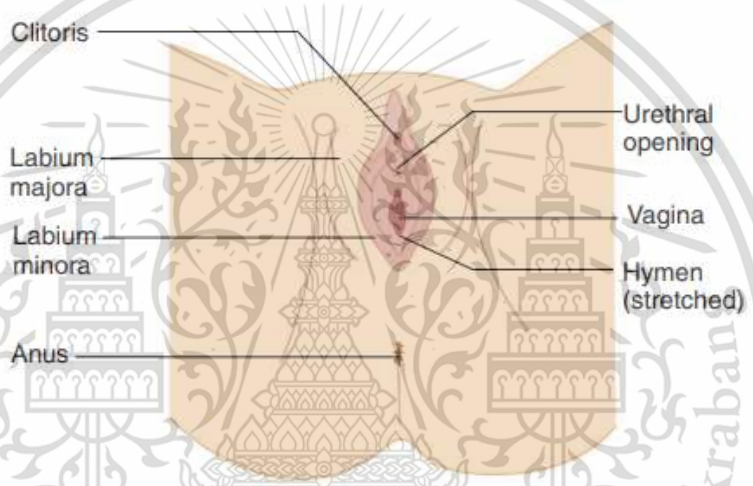

Figure 2.1 female external genitalia [3]

The collective term for the external components of the female reproductive organs includes both the vulva and pudendum. Besides its role as a protective barrier, the vulva contributes to sexual arousal. Components of the vulva encompass the mons pubis, labia majora, labia minora, clitoris, vestibular bulbs, and vestibule [4]. The perineum, located behind the vestibule, completes this anatomical structure.

VULVA

Comprising all anatomical parts of the female external genitalia, the vulva includes the mons pubis, labia majora, labia minora, clitoris, vestibular bulbs, vulva vestibule, Bartholin's glands, and Skene's glands. Additional elements consist of the urethra and vaginal entrance.

MON PUBIS

Situated anterior to the pubic bones, the mons pubis, or pubic fossa, is a mound of fatty tissue more prominent in females, often adorned with pubic hair. It acts as a cushion during sexual activity and hosts sebaceous glands responsible for producing pheromones that stimulate sexual desire.

LABIA MAJORA

Referring to the larger lips, the labia majora are prominent skin folds forming the lateral borders of the vulval clefts. They surround various structures, including the labia minora, clitoris, vulva vestibule, vestibular bulbs, Bartholin's glands, Skene's glands, urethra, and vaginal entrance. During sexual stimulation, they swell with blood, appearing engorged.

LABIA MINORA

The smaller lips, or labia minora, are small cutaneous folds beginning at the clitoris and descending obliquely to form the borders of the vulva vestibule. They encircle

the clitoris, forming its hood and frenulum, and terminate between the labia majora and vulva vestibule. With sexual arousal, they become engorged with blood.

CLITORIS

The clitoris, akin to the male glans penis, is a sensitive organ composed of a glans and body, formed by erectile tissue known as the corpus cavernosum. It is rich in nerves and blood vessels, particularly the glans clitoris, which contains approximately 8,000 nerve endings. During sexual pleasure, it swells with blood.

HYMEN

Primarily composed of elastic and collagenous connective tissue lined with stratified squamous epithelium, the hymen lacks cornification and glandular or muscular components. While ruptured hymens are relatively avascular, significant bleeding upon rupture is unlikely.

2.1.1.2 INTERNAL GENITALIA

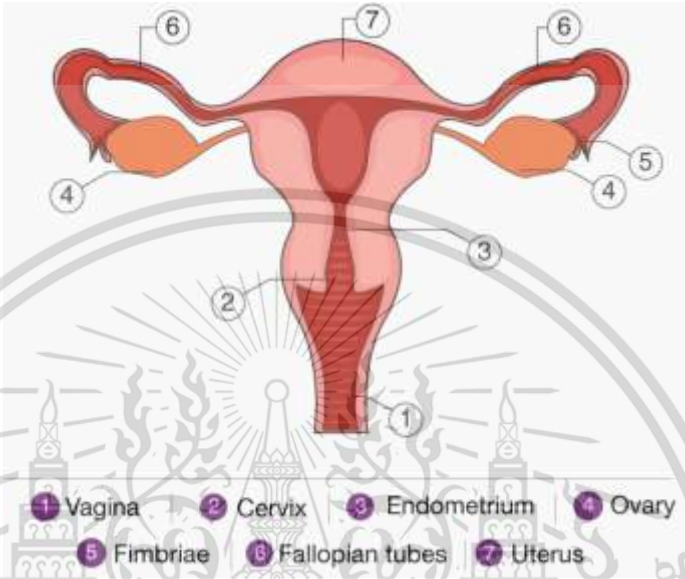

Figure 2.2 representation of internal genitalia [5]

The ovaries, fallopian tubes, uterus, and vagina constitute the internal female genital structures. They facilitate ovum production and release, ovum transportation to potential fertilization sites, sperm access and movement, and provide a conducive environment for fetus implantation, growth, and delivery [4].

VAGINA

Connecting the uterus to the external genitalia, the vaginal canal features inner mucosal folds known as rugae, enhancing flexibility and distensibility. Smooth muscle

forms the superficial layer, contributing to its adaptability. With age, both rugal pattern and flexibility diminish during menopausal and postmenopausal stages.

The vaginal aperture surpasses the urethral opening [6], and arousal induces moisture aiding in penis insertion. During intimacy, vaginal texture generates friction, while lubrication from Bartholin's glands near the vaginal opening and cervix aids in smooth movement. Despite lacking glands, the vaginal wall maintains moisture. Cervical mucus glands secrete various mucus types pre and during ovulation, creating an alkaline environment supportive of sperm survival.

CERVIX

Fig 2.3 inspection of cervix [7]

As a fibromuscular organ, the cervix links the uterine cavity to the vagina, positioned near the uterus's apex. Despite its cylindrical designation, the anterior and posterior walls typically about each other. It spans approximately 3 centimeters in

diameter and 4 centimeters in length. Variations exist based on childbirth history and reproductive age, with postpartum cervixes larger than those of nulliparous women, and those of reproductive age larger than postmenopausal ones. The cervix may be situated internally or externally relative to the uterus. Its lower half, the intravaginal section, extends into the upper vaginal region, while the upper half resides in the pelvic or abdominal cavity above the vagina, with comparable sizes for both halves [8]. Positioned between the bladder anteriorly and the bowel posteriorly, the cervix lies within the birth canal, with the ureters and uterine arteries in close lateral proximity.

URETHRA

The urethra, an extension of the bladder tube, serves as the conduit for urine expulsion from the body. In females, its entrance lies within the vulva vestibule, positioned inferior to the clitoris and superior to the vaginal opening [2].

FALLOPIAN TUBES

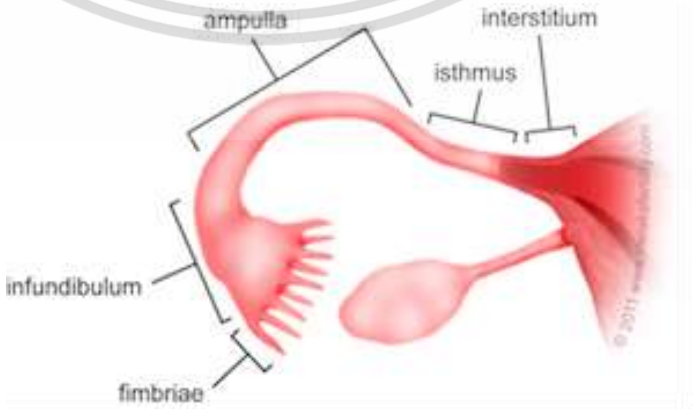

Figure 2.4 anatomy of fallopian tube [9]

Besides its common name, the fallopian tube is also referred to as the oviduct or uterine tube. These muscular tubes, resembling a J-shape, run parallel to the uterus on both sides of the body, extending approximately ten centimeters and protruding into the abdominal cavity. Their primary function involves transporting sperm to the egg within the ovary, facilitating fertilization, and subsequently returning the fertilized egg to the uterus for embryonic development [8]. The fallopian tubes comprise four distinct sections.

2.1.2 FEMALE REPRODUCTIVE ORGAN PHYSIOLOGY

2.1.2.1 MENSTRUAL CYCLE

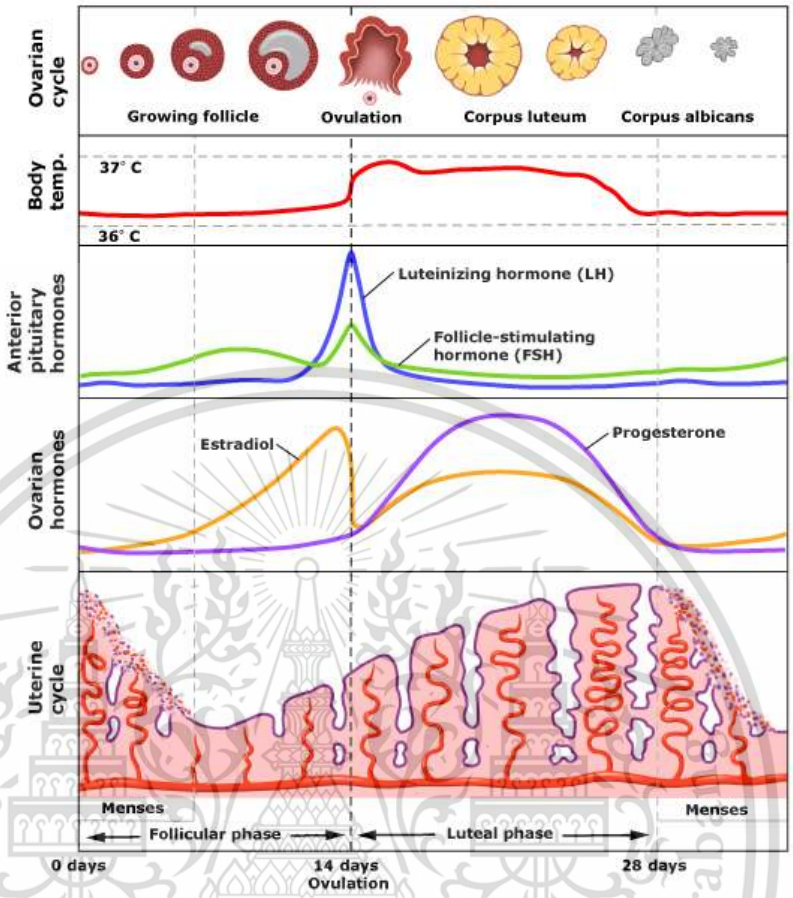

Figure 2.5 table indicating the graph of menstrual cycle [10]

In young girls and women of reproductive age (11 to 16 years old), hormonal cycles occur regularly every month. The term "monthly" stems from the menstrual cycle, where the body readies itself for potential pregnancy each cycle, regardless of the woman's intentions. The shedding of the uterine lining, termed menstruation, marks this monthly event for many women. Typically lasting around 28 days, the menstrual cycle encompasses three phases: the follicular phase (egg development), ovulatory phase (egg release), and luteal phase (hormone levels decrease if implantation does not occur) [13].

2.1.2.2 FOLLICULAR PHASE

The follicular phase, spanning from day 0 (the onset of menstruation) to day 14 (the onset of ovulation), witnesses a decline in estrogen, progesterone, and inhibin A levels post-menstruation as the corpus luteum breaks down. This cascade triggers a positive feedback loop to the hypothalamus and anterior pituitary, prompting the release of GnRH and FSH into the bloodstream. Elevated FSH levels stimulate ovarian granulosa cells, leading to recruitment of multiple follicles from each ovary, with only one Graafian follicle undergoing ovulation per cycle. Consequently, granulosa cells produce more inhibin B due to heightened FSH levels [14]. Inhibin B's impact on FSH production becomes prominent towards the end of the follicular phase, peaking during the LH surge preceding ovulation before swiftly declining.

Transitioning to the mid-follicular phase, rising levels of estradiol and inhibin B from ovarian follicles, spurred by increased FSH, evoke negative feedback, causing FSH levels to decline. At this juncture, the dominant follicle, selected for ovulation, emerges amidst numerous contenders. Theories vary regarding how the dominant follicle is determined. One posits that the follicle with the most FSH receptors prevails, while others are inhibited and undergo atresia. Alternatively, the anti-Mullerian hormone (AMH) may influence dominant follicle selection [15].

As the follicular phase nears its end, estradiol levels surge, flipping the feedback loop from negative to positive, possibly involving kisspeptin neurons [16]. This positive feedback stimulates the hypothalamus and anterior pituitary, triggering increased LH secretion, marking the follicular phase's conclusion and onset of the ovulatory phase.

2.1.2.2 OVULATORY PHASE

Throughout the menstrual cycle, ovulation, the culmination of egg development, is orchestrated by a complex hormonal interplay involving the hypothalamus, hypophysis, and ovary. Debate has long raged over whether ovulation occurs randomly or alternates between ovaries in consecutive cycles. Recent human studies reveal ovulation's randomness, likely influenced by dominant ovary status or follicular phase duration (>14 days), especially pronounced in younger women (<29 years) [17]. Concurrently, endometrial changes prepare for blastocyst implantation in sync with ovulation.

The window for implantation, spanning seven to ten days post-ovulation, sees the uterine walls primed for embryo attachment. Consequently, the blastocyst remains in the fundal intrauterine fluid for three to five days before implantation commences, likely occurring in the fundal region near the isthmus on the ovulated side [18]. Implantation initiates blastocyst penetration into the uterine endometrium, kickstarting placental development.

For fertilization to commence, sperm and egg must traverse from the vaginal fornix and ovary, respectively, to the ampulla region. Subsequently, the zygote, or embryo, journeys from the ovaries through the fallopian tubes to the uterine cavity for implantation, necessitating active transport mechanisms driven by smooth muscles or cilia, responsive to external stimuli [19].

2.1.2.4 LUTEAL PHASE

Throughout the follicular phase of the menstrual cycle, the dominant follicle undergoes maturation. Elevated estradiol levels from granulosa cells within this follicle trigger a surge in pituitary LH. This surge initiates the breakdown of connections between granulosa cells in the cumulus oophorous, leading to the oocyte's entrance into prophase I diplotene and subsequent rupture of the follicle, releasing the egg into the pelvis. Following ovulation, the deflated follicle, devoid of eggs, is disregarded as the oocyte is captured by the fimbria and fertilized in the fallopian tubes. Surviving follicular cells contribute to reproduction and menstrual cycle regulation by generating the corpus luteum [20].

Preceding ovulation, granulosa cells within the dominant follicle commence the transformation process into the corpus luteum. This involves cellular enlargement and increased vacuolation, with lutein pigment uptake imparting the developing corpus luteum's characteristic yellow hue. As granulosa cells become isolated from circulation by

the basal lamina, nutrient and signaling exchange rely on gap junctions. Luteinization entails basal lamina thinning, migration of theca cells into the central layer, and rapid neovascularization primarily controlled by vascular endothelial growth factor and fibroblast growth factor, both elevated in luteinized granulosa cells. Notably, hemorrhagic corpus luteum cases demonstrate significant neovascularization, evident to gynecologists as one of the body's highest blood flows per unit mass [21]. This clinical observation underscores the remarkable neovascularization associated with the corpus luteum.

2.1.2.5 PREGNANCY AND HUMAN DEVELOPMENT

A woman's menstrual cycle typically spans 26 to 35 days, with 28 days considered average. Menstrual bleeding marks the cycle's start, with day 2 often exhibiting peak blood flow. The follicular phase, initiated by pituitary gland FSH release, stimulates primary ovarian follicle formation and estrogen synthesis, promoting uterine lining proliferation. LH surge induced by rising estrogen triggers ovulation and commences the luteal phase. Fertility peaks during the follicular phase, beginning one day pre-ovulation, with the fertile window spanning the five days preceding ovulation and ovulation day itself. Post-ovulation, the corpus luteum produces progesterone, maintaining the endometrial lining for potential fertilization. If fertilization doesn't occur, the corpus luteum degenerates, progesterone levels drop, and menstrual cycle restarts.

Upon normal implantation of a fertilized ovum, trophoblast cells differentiate into syncytiotrophoblasts, secreting hCG, enabling continued progesterone and estrogen release by the corpus luteum, crucial for pregnancy development. Syncytiotrophoblasts collaborate with cytotrophoblasts and extraembryonic mesoderm in placenta formation. The placenta, primarily ensuring pregnancy continuation and fetal needs fulfillment, acts as the fetal respiratory, gastrointestinal, endocrine, renal, hepatic, and immunological systems, facilitating nutrient and gas exchange with the mother's body.

Childbirth concludes the nine-month pregnancy period, with differing views on labor onset. Some research suggests labor initiation results from progesterone decline and uterine wall mechanical stretching, while others propose significant roles for inflammatory mediators like prostaglandins. Subsequently, oxytocin sustains contractions throughout labor and delivery [22].

2.1.3 IN DEPTH OF CERVIX

2.1.3.1 CERVICAL ESSENTIALITY

The cervix's structure is pivotal for maintaining pregnancy by preventing premature embryo expulsion from the uterus and impeding bacteria progression from the vagina. Weak cervix integrity can lead to premature delivery. Despite ongoing research, the underlying cause of this structural deficiency remains elusive. This article delves into cervix

anatomy and function pre- and post-pregnancy, focusing on factors contributing to cervical mechanical breakdown, particularly the internal cervical os. Research methodologies exploring the internal cervical os' role in pregnancy and its significance in preterm birth are examined [24]. Practical application of this knowledge may enable early identification of women who could benefit from interventions to reinforce the internal os, thereby reducing the risk of preterm delivery.

2.1.3.2 CERVICAL COMPONENTS

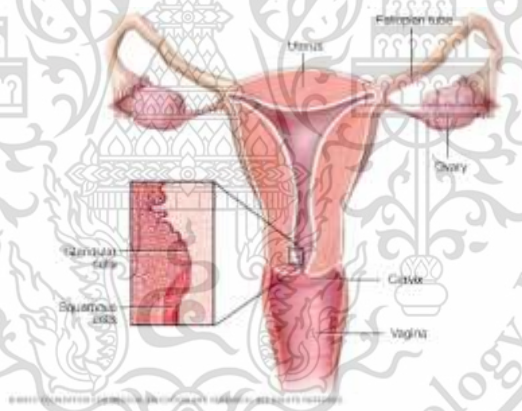

Figure 2.6 Cervical structure [25]

STROMA

The cervix's stroma consists of dense fibromuscular tissue, housing a complex network of blood vessels, lymphatic vessels, and nerves. Blood supply to the cervix originates from the internal iliac arteries, branching into cervical and vaginal branches of

the uterine arteries, ensuring oxygen and nutrient delivery. Cervical branches of the uterine arteries descend into the cervix's lateral aspects at the 3 o'clock and 9 o'clock positions. Nerve supply to the cervix originates from the hypogastric plexus. Unlike the ectocervix, which has fewer sensory nerve endings, the endocervix harbors a significant number of these nerves. The cervix is lined with columnar epithelium and stratified, non-keratinizing squamous epithelium, with the transformation zone being the junction where these two epithelia meet [26].

SQUAMOUS EPITHELIUM

Typically, the ectocervix and the entire length of the vagina are lined with consistent, non-keratinizing stratified squamous epithelium. In non-pregnant women, this epithelium appears smooth and somewhat pink to the naked eye. However, during pregnancy, it becomes more vascular and adopts a blue hue. At the base of the squamous epithelium lies a single layer of spherical basal cells connected to the basement membrane. These cells feature large, darkly stained nuclei and minimal cytoplasm. Acting as a barrier between the epithelium and the underlying stroma, the basement membrane maintains structural integrity. While the epithelial-stromal interface is typically straight, periodic undulations and stromal projections, termed papillae, occur at regular intervals. The regions of epithelium between these papillae are referred to as rete pegs [26].

COLUMNAR EPITHELIUM

The endocervical canal is entirely lined with columnar epithelium, often referred to as glandular epithelium. This structure comprises a single layer of tall cells with darkly stained nuclei located close to the basement membrane. Unlike the cervix's stratified squamous epithelium, which consists of a single layer of cells, the columnar epithelium is much taller. Due to its thin single-cell layer allowing penetration of stromal vascularity, it appears reddish upon visual inspection. In the upper region of the uterine body, it merges with the endometrial epithelium, while at its lower limit, it interfaces with the squamous epithelium at the SCJ. Depending on factors such as age, reproductive status, hormonal condition, and menopausal status, the squamous epithelium may cover varying portions of the ectocervix. During cervical examination, localized overgrowth of the endocervical columnar epithelium may appear as a reddish mass protruding through the external os, indicative of a cervical polyp, potentially a sign of cervical cancer. Typically originating as a localized expansion of a single columnar papilla, a cervical polyp gradually enlarges over time to cover a larger area. It consists of a central region of endocervical stroma surrounded by columnar epithelium with underlying crypts. Multiple polyps originating from the columnar epithelium are also documented [26].

SQUAMOCOLUMNAR JUNCTION

Due to the difference in height between the squamous and columnar epithelium, the squamocolumnar junction may appear as a sharp line with a step under certain circumstances. Throughout a woman's lifetime, the position of the squamocolumnar junction relative to the external os can change. This shift is influenced by various factors, including age, hormonal status, birth trauma, oral contraceptive use, and pregnancy. The original squamocolumnar junction is observable during infancy, perimenarche, puberty, and early reproductive life. Another instance is after puberty when female genital organs continue to develop due to estrogen influence. This growth causes the cervix to enlarge, elongating the endocervical canal and resulting in the emergence of columnar epithelium onto the ectocervix, a condition known as ectropion or ectopy. Visually, this presents as a deeply crimson appearance of the ectocervix, often misconstrued as an erosion or ulcer. Consequently, the squamocolumnar junction is found in a location quite distant from the external os on the ectocervix. During pregnancy, ectropion may arise for the first time or become more pronounced than before [26].

2.1.3.2 CERVICAL CANCER

2.1.3.2.1 OVERVIEW OF CERVICAL CANCER

Figure 2.7 Cervical cancer con cervix [27]

Metaplastic epithelium replaces the columnar lined epithelium of the endocervix during the transformation process, forming the transformation zone, which is a key site of premalignant changes due to chronic HPV infection and the likely origin of cervical cancer. Squamous cell carcinoma (SCC) and adenocarcinoma are the primary histological subtypes observed in cervical cancer. Adenocarcinoma arises from glandular cells producing mucus in the endocervix, while SCC develops from squamous cells in the ectocervix, constituting approximately 75% of cervical carcinoma cases.

In the progression of SCC, cervical squamous cells undergo dysplastic alterations post-HPV infection, forming precursor lesions known as cervical intraepithelial neoplasia (CIN). Most HPV infections resolve within a few years, with only 10–20% leading to cervical cancer. In South Africa, 60 to 80% of women test positive for HPV, with 30.2 cervical cancer cases per 100,000 women detected. The majority of HPV 16- and 18-positive cervical carcinomas exhibit viral integration. A subset of HPV-positive women develops cervical cancer without viral DNA integration, maintaining episomal HPV DNA. Viral E5, E6, and E7

proteins play pivotal roles in inducing and sustaining cervical cancer by exploiting host cell machinery. E5 interacts with host growth factor receptors, inhibits DNA-damaged apoptosis, and evades the immune system. E6 and E7 promote cervical cancer by disrupting cellular checkpoints, degrading tumor suppressors, and mediating malignant transformation. While E5's role diminishes post-HPV DNA integration, E6 and E7 continue to drive the malignant phenotype, as viral DNA integration leads to constitutive production of these proteins [28].

HPV-infected cervical epithelial cells' dysplasia severity is graded, with CIN1 representing mild dysplasia characterized by koilocytes, binucleate cells, and dyskeratotic cells. CIN2 affects two-thirds of the epithelium with various lesions, followed by CIN3, indicating severe dysplasia. Invasive cervical carcinoma has a poor prognosis and metastasizes to the parametrium, vagina, uterus, and surrounding organs. The International Federation of Gynecology and Obstetrics (FIGO) guideline stages invasive cervical cancer as stages I, II, III, and IV. Stage I occurs when cancer extends beyond the cervix's inner lining, while stage II indicates cancer has spread beyond the cervix but not to the pelvic wall and lower part of the vagina. Stage IVA signifies cancer spread to the bladder and rectum, while stage IVB indicates spread to distant sites like the lungs, liver, and skeleton via the bloodstream. The transition from preinvasive CIN to invasive cervical cancer may take 10–30 years [30].

2.1.3.2.2 CERVICAL CANCER SCREENING

The goal of screening for cervical cancer is to detect precancerous changes in cervical cells early, when treatment can prevent the progression to cervical cancer. Sometimes, cervical screening may uncover malignancy. Detecting cervical cancer at an earlier stage makes it easier to cure, as treatment becomes more challenging once symptoms manifest and the cancer has potentially spread.

There are three primary methods for detecting cervical cancer:

PAPANICOLAOU SMEAR (PAP SMEAR)

In most cases, the development of cervical cancer hinges on the presence of a cervical infection caused by a high-risk strain of HPV. However, HPV infection alone does not invariably lead to neoplasia. The majority of high-risk HPV infections are transient and do not progress to cervical intraepithelial neoplasia (CIN), with cervical cancer arising in only a small fraction of infected women. Factors such as smoking, immunosuppression, and HIV infection contribute to the persistence of HPV.

When pap smear results indicate abnormal epithelial cells, further tests like colposcopy and biopsy are recommended. Colposcopy involves visually examining the cervix with a specialized binocular microscope called a colposcope. If abnormalities are detected during colposcopy, a biopsy may be performed for further evaluation. Pap smears can be collected using either the liquid-based or traditional method. During the

procedure, a medical professional inserts a speculum into the vagina to locate the cervix and collects cells from the transformation zone using a brush. In the liquid-based method, the cells are transferred to a vial containing a preservative, while the traditional method involves transferring cells to a slide for preservation. The liquid-based approach allows for additional testing for HPV, gonorrhea, and chlamydia from a single sample, offering potential benefits such as improved interpretation and reduced unsatisfactory findings, although these benefits have not been fully realized in practice.

HUMAN PAPILLOMA VIRUS TEST (HPV TEST)

Persistent genital infection with certain types of HPV is considered a necessary cause of cervical cancer. The association between HPV infection and cervical squamous cell carcinoma is stronger than that between smoking and lung cancer. However, HPV infections are less commonly associated with adenocarcinomas of the cervix, with only about 43% of cases in women aged 60 years or older linked to the infection.

When selecting an HPV test for cervical cancer screening, especially in underserved settings, various factors such as performance accuracy, clinical validation, costs, and logistical requirements need to be considered. It is recommended to supplement or replace population-based cytological screening programs with the direct detection of HPV DNA in cervical or vaginal samples. HPV-based screening tests are more sensitive than

cytology or VIA as a primary screening approach and are particularly useful for triaging minor cytological abnormalities.

HPV tests can be classified into two types:

Hybrid HPV testing which historically, cytologically-based testing such as Pap smears has been the cornerstone of cervical cancer screening efforts worldwide. However, hybrid HPV testing has the potential to significantly enhance these traditional methods. Due to the lower specificity of Pap smears, women with mild cytological abnormalities, such as atypical squamous cells of undetermined significance (ASC-US) and low-grade squamous intraepithelial lesions (LSIL), may undergo triage using more specific molecular-based HPV screening tests in a hybrid approach before being referred for colposcopy if positive for any oncogenic HPV types.

The second type of the test care referred to as primary HPV testing: This approach involves using the HPV test as the primary screening method. HPV tests have much greater sensitivity (96.1%) compared to cytology (53.0%), but their specificity is lower (90.7% vs. 96.3%). While HPV tests are highly sensitive, they cannot differentiate between short-term and long-term infections, making them more suitable as screening tools rather than diagnostic ones. Both the International Agency for Research on Cancer (IARC) and the World Health Organization (WHO) recommend HPV tests as the principal method for detecting precancerous cervical lesions. Consequently, primary HPV screening has

replaced alternative screening methods in most developed countries and many developing ones as well. Despite being more expensive, it is more cost-effective in identifying precancerous cervical lesions when conducted in an organized setting and supported by a robust health infrastructure.

LUGOL'S IODINE

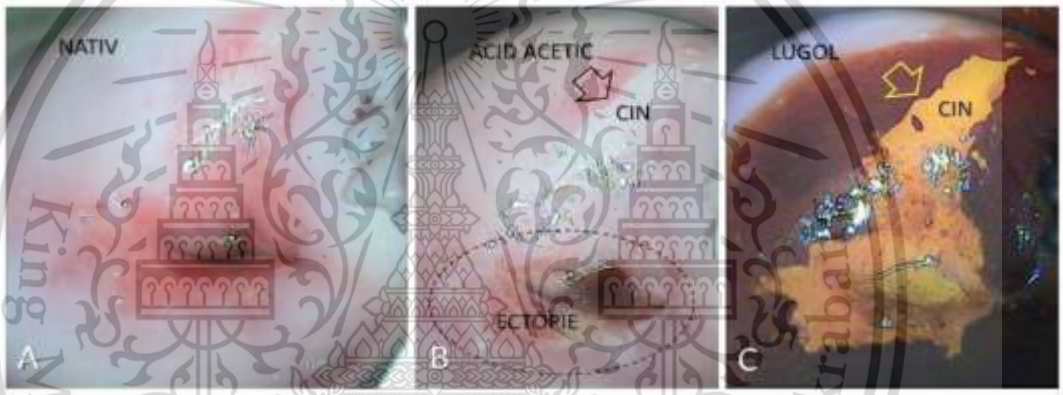

Figure 2.8 Lugol's iodine after applied to precancerous cervix [31]

Cervical cancer screening with Lugol iodine, also known as Schiller's test, is a straightforward and effective method. It involves applying Lugol iodine to the cervix to identify precancerous or cancerous cells.

Each year, over 500,000 women receive a diagnosis of cervical cancer, with most cases being caused by HPV, a sexually transmitted infection.

Early detection of cervical cancer through Lugol iodine testing is crucial for effective treatment. Lugol iodine solution, composed of iodine and potassium iodide, turns the cervix dark brown upon contact with glycogen. Glycogen in cervical tissue reacts with Lugol iodine, resulting in a brownish coloration. Conversely, precancerous or cancerous cells lacking glycogen do not react with Lugol iodine and appear pale or white.

Colposcopy, a procedure utilizing a colposcope to examine the cervix, is typically performed alongside the Lugol iodine test. Lugol iodine is applied to the cervix using a cotton swab or spray bottle during the examination. The colposcope then examines the cervix for any abnormalities. If an abnormal area is detected, a biopsy may be necessary to confirm the diagnosis. A small sample of cervical tissue is taken for microscopic analysis, and the biopsy results guide subsequent treatment, which may include monitoring, surgery, or other interventions.

Lugol iodine-based cervical cancer screening is simple, non-invasive, and requires no special preparation, making it suitable for women of all ages. The examination can be conducted in a doctor's office or clinic within a few minutes.

However, it's important to note that the Lugol iodine test is not infallible. It may overlook certain problematic areas of the cervix and occasionally identify normal ones. Therefore, it's essential to follow up with the screening and tests recommended by the expert as there are multitude of research display the lack of specificity and meaningful sensitivity among lugol iodine colposcopy along. To mitigate this ineffectiveness lugol

iodine is commonly used in conjunction with other straining visualizations for example acetic acid and normal saline. This is also reflected in general guidelines for colposcopic evaluation from World Health Organization in 2011 are in swede score diagnosis matrixes iodine straining is registered as only a part of single component in overall scoring.

The Lugol iodine test for cervical cancer is indeed simple and effective. It involves applying Lugol iodine to the cervix to identify any precancerous or cancerous cells present. If an abnormal area is detected during a colposcopy, a biopsy may be necessary to determine the source and severity of the abnormality. The Lugol iodine test can help detect cervical abnormalities early, allowing for prompt treatment.

In regions where HPV testing or Pap smears are not readily available, the Lugol iodine test can be particularly beneficial. It provides a low-cost and accessible method for detecting cervical abnormalities and reducing the incidence of cervical cancer, especially in resource-limited settings. The Lugol iodine test can complement existing cervical cancer screening programs, filling gaps in areas where more advanced technologies may not be accessible.

COLPOSCOPY

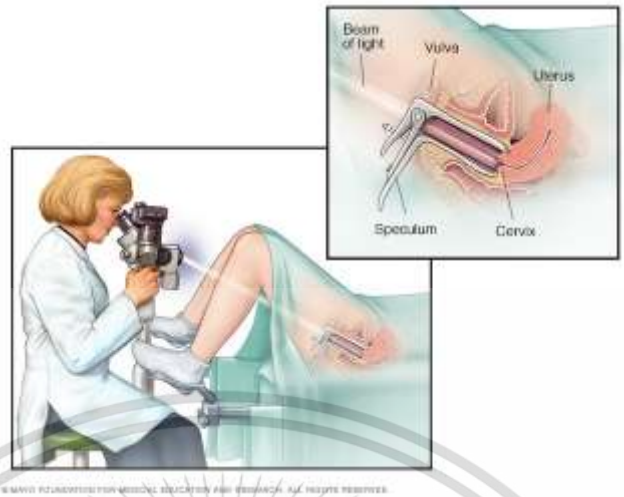

Figure 2.9 Colposcopy process [32]

Colposcopy is indeed a vital diagnostic procedure used to visually examine the cervix, vagina, and vulva, particularly in cases where abnormalities are suspected based on Pap tests, visual inspections with acetic acid (VIA), HPV DNA testing, or suspicious physical appearances. The procedure plays a crucial role in the evaluation of women with abnormal findings and helps guide further management decisions.

Originally introduced as a screening technique for cervical cancer by Hans Hinselmen in 1925, colposcopy has evolved into a fundamental tool in gynecological practice. By providing a magnified view of the tissues, colposcopy allows for the detection of subtle abnormalities that may not be visible to the naked eye, thereby aiding in the diagnosis and treatment of various disorders affecting the cervix and vagina.

The colposcope, equipped with a light source and binocular viewing system, enables healthcare providers to obtain a three-dimensional image of the tissue under

examination. This enhanced visualization facilitates accurate assessment and precise targeting of suspicious areas for further evaluation or treatment. Additionally, the colposcope's maneuverability, often aided by an attached stand or arm, allows for optimal positioning and adjustment during the procedure, ensuring thorough examination and effective diagnosis.

Colposcopy is indeed a crucial diagnostic procedure used to examine the cervix and surrounding tissue for abnormalities, and the colposcope itself plays a central role in this process. Equipped with binocular vision, a dimmable light source, and color and contrast filters, the colposcope enhances visualization and aids in the detection of abnormal cells or growths.

During a colposcopy procedure, the patient typically lies on an exam table with their feet in stirrups, allowing the examiner to access the cervix. A speculum is inserted into the vagina to provide a clear view of the cervix, and the colposcope is positioned near the vaginal entrance to observe the tissue. Acetic acid may be applied to the area to enhance visibility of any abnormalities, and additional solutions like iodine may be used to further aid in detection. If abnormal tissue is identified, a biopsy may be performed for further evaluation.

Colposcopy is not only used for diagnostic purposes but also for monitoring therapy and assessing high-risk patients for future complications. Gynecologists and other

specialists in women's health rely on the colposcope to diagnose and treat a wide range of cervix and vaginal disorders, making it an indispensable tool in their practice.

Performing an adequate colposcopy requires several essential pieces of equipment, including a vaginal speculum, a colposcope, 5% acetic acid, Lugol's solution, biopsy forceps, an endocervical speculum, and a solution or method to stem bleeding. The colposcope, which magnifies the tissue of the cervical, vaginal, and vulvar regions, comes in various models with different features such as lenses, computer-generated graphics, light filters, and cameras capable of capturing images or films.

A proper colposcope should have two magnification settings: one with low power and one with high power, typically ranging between 10x and 18x magnification. It should also include a normal light filter and a green filter to discern vascular patterns that may be challenging to observe with white light.

During the colposcopy procedure, acetic acid (5%) is applied to the cervix using a cotton ball and left to soak for one to two minutes. Dysplastic cells lose their water content and appear as acetowhite lesions after acetic acid application. Some colposcopists may also use Lugol's solution, an iodine-containing solution, to further highlight dysplastic regions through the Schiller's test. Areas that do not retain the iodine stain are considered to have failed the Schiller test.

To perform a comprehensive examination, the cervix and tissue in the upper vaginal region should be thoroughly evaluated. An endocervical speculum may be

required to check the cervical os thoroughly. For cervical biopsy, clinicians may choose from various biopsy forceps, with the Tischler cervical biopsy punch forceps and the Burke biopsy forceps being commonly used options. These instruments are essential for obtaining tissue samples for further evaluation and diagnosis.

After a biopsy, various techniques can be used to stop bleeding, including applying Monsel's solution, using silver nitrate, or performing Bovie cauterization if necessary. Monsel's solution is a hemostatic agent that helps control bleeding by promoting clot formation. Silver nitrate cauterization involves applying silver nitrate directly to the bleeding site to induce coagulation and stop bleeding. Bovie cauterization, or electrosurgery, uses an electrical current to cauterize blood vessels and control bleeding.

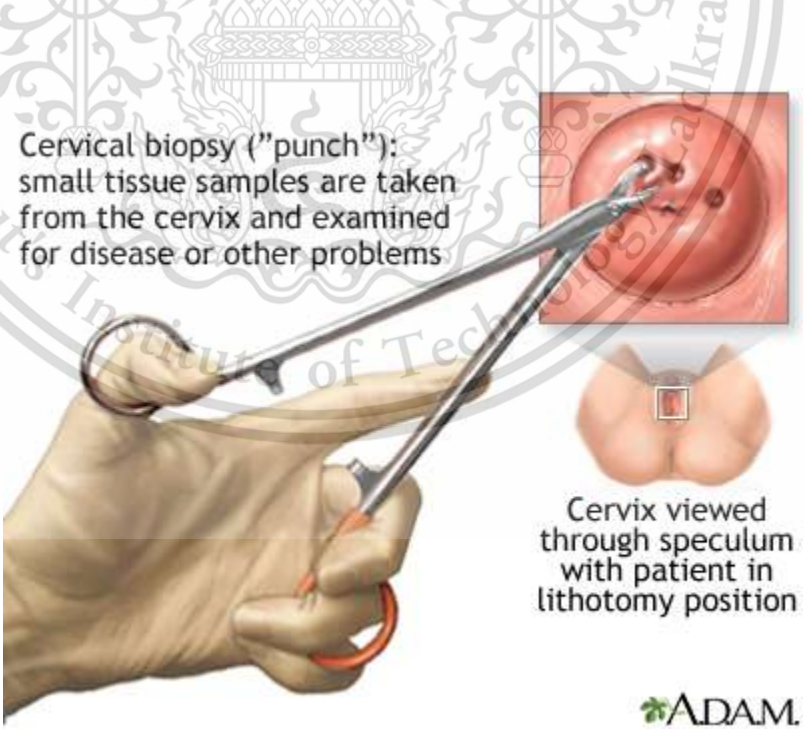

Figure 2.10 Biopsy process reference [33]

A cervical biopsy is a medical procedure where a small piece of tissue from the cervix is removed for microscopic examination. There are various biopsy techniques, each with its own advantages and disadvantages.

Colposcopy-directed biopsy is a common method used in cervical cancer screening. It is typically performed when there is an abnormal Pap test result or when abnormalities are detected during a colposcopy examination. During the procedure, a speculum is inserted into the vagina to visualize the cervix, and a colposcope is used to identify any areas of abnormal tissue. If abnormalities are found, a small tissue sample is taken using biopsy forceps, and it is sent to a laboratory for examination under a microscope.

Cone biopsy is a more invasive procedure often reserved for more advanced cases of cervical cancer or when a colposcopy-directed biopsy does not provide sufficient information. During a cone biopsy, a cone-shaped section of the cervix is removed either by cutting or laser ablation. The removed tissue is then sent to a laboratory for further analysis.

Both colposcopy-directed biopsy and cone biopsy play important roles in the diagnosis and management of cervical abnormalities, allowing healthcare providers to obtain tissue samples for accurate diagnosis and treatment planning. The choice of biopsy technique depends on various factors, including the severity of the condition and the findings from previous screening tests and examinations.

Both colposcopy-directed biopsies and cone biopsies carry minimal risks and potential consequences. While there is a slight risk of bleeding, infection, or damage to the cervix or surrounding tissue, these complications are rare. Patients may experience mild discomfort or cramping during or after the procedure, but this can typically be managed with over-the-counter pain medications.

Following a cervical biopsy, the tissue samples are sent to a laboratory for analysis, which may take several days to a few weeks. Once the results are available, the physician will review them with the patient and provide any necessary follow-up treatment recommendations.

Biopsy plays a crucial role in diagnosing and identifying cervical cancer at an early stage. Colposcopy-directed biopsies and cone biopsies are just two examples of biopsy techniques used in this context. Despite the low risks and consequences associated with these procedures, their findings are essential for early detection and effective treatment of cervical cancer.

Routine cervical cancer screenings, such as Pap tests and HPV testing, are important for women's health. If abnormalities are detected during these screenings, a biopsy may be necessary to further evaluate the source and severity of the abnormality. Before undergoing a biopsy, patients should discuss the potential benefits and risks with their healthcare provider. Early detection and treatment of cervical cancer can significantly

improve outcomes, making screening tests and biopsies critical tools in combating this disease.

POCKET COLPOSCOPE

Figure 2.11 Pocket colposcope from the Duke university [34]

The pocket colposcope accurately visualizes the cervix for the purpose of cervical cancer diagnosis and screening, despite its diminutive size and portability. The device's portability, ease of use, and minimal training prerequisites render it appropriate for implementation by an extensive range of medical personnel. The light and camera of the pocket colposcope are utilized to capture images of the cervix, which are subsequently transmitted to a computer or mobile device for additional analysis.

In an effort to improve the detection and testing of cervical cancer, scientists invented the pocket colposcope in the late 1990s. In settings with limited resources, where

standard screening and diagnostic tools are not easily obtainable, there is an urgent demand for solutions that are easily accessible. A biomedical engineer at Duke University, Dr. John Schmitt, was among the pioneers in the development of a portable colposcope. Early in the twenty-first century, Dr. Schmitt and his colleagues initiated the development of a portable device capable of capturing high-quality images of the cervix for the purpose of cervical cancer screening and diagnosis. To increase enrollment in cervical cancer treatment facilities, the device was designed with portability, affordability, and user-friendliness in mind.

Over the subsequent several years, Dr. Schmitt and his colleagues laboriously refined the pocket colposcope. They conducted clinical trials on numerous prototypes in order to determine which one was the most effective and safest. They exerted effort to improve the device's usability by incorporating wireless networking and touch-screen options.

The first pocket colposcope to be made available for commercial use was introduced to the world by MobileODT in the year 2012. MobileODT was founded by a group of businesspeople and medical professionals who recognized the potential of the portable colposcope to improve treatment for cervical cancer all over the world. The company's headquarters are located in Israel. Since that time, the company has expanded its product line to include digital cervicography as well as other diagnostic instruments that are powered by artificial intelligence.

The pocket colposcope has seen widespread use not only in regions with limited resources but also in regions where access to conventional screening and diagnostic instruments is restricted. There have been thousands of women in countries such as India, Uganda, and Haiti who have been screened for cervical cancer using the device. This has resulted in the collection of significant data regarding the frequency and incidence of the illness in those countries. Additionally to its current application in cervical cancer screening and diagnosis, there is a growing interest in expanding the use of the pocket colposcope to include other applications. In order to investigate the possibility of using the device to take pictures of the skin and the interior of the mouth, for example, researchers are currently conducting research. It has not yet been determined what this means for the early diagnosis of other cancers and disorders, but it is possible that it will have a significant impact.

The portability of the pocket colposcope and the fact that it does not involve any invasive procedures are two of its primary selling points. In contrast to regular colposcopes, which require the use of a speculum in order to take pictures of the cervix, the pocket colposcope does not require the use of a speculum. Through the process of making the screening process more bearable for women, this may help improve the number of women who participate in cervical cancer screening programs. The fact that the pocket colposcope can be used in conjunction with a lubricated condom or sleeve contributes to the fact that it is a minimally invasive method of examination. The creation of a

protective barrier between the device and the cervix comes about as a result of inserting the condom or sleeve into the vagina. In addition to making the operation more bearable for the patient, this has the potential to reduce the likelihood of an infection spreading to other parts of the population.

Within the realm of clinical practice, the portable colposcope has a multitude of applications, including the detection and prevention of cervical cancer. Detecting abnormal cells in the cervix and monitoring the progression of lesions in the cervix are both possible applications of this technique. It is possible to use the device to guide biopsies and other diagnostic procedures, in addition to its application in monitoring the effectiveness of treatment for cervical cancer. Additionally, the portable colposcope has the potential to expand access to cervical cancer screening and diagnosis in regions that have a limited medical infrastructure. It has the potential to reduce inequalities in the incidence and death rates of cervical cancer, and the fact that it is portable and easy to use makes it an extremely useful instrument for medical professionals working in areas that are underserved or located in remote areas.

The utilization of a pocket colposcope comes with a number of advantages, but it also has a few disadvantages. It is possible that the pictures that are taken by the device are not as detailed as those that are obtained by conventional colposcopes. Additionally, it is possible that the technology is not as useful as traditional colposcopes when it comes to identifying minor or subtle problems. In addition, additional research is necessary in

order to accurately evaluate the device's safety and effectiveness, particularly in comparison to traditional colposcopes. In spite of these drawbacks, the portable colposcope holds a great deal of promise for enhancing cervical cancer screening and diagnosis, particularly in regions with limited access to resources. Additional research is necessary in order to properly evaluate the device's efficacy and safety, as well as to devise methods that will allow for the most effective utilization of the device in clinical settings.

2.1.3.2.3 STAGE OF CERVICAL CANCER

Table 4: Comparison of the 2009 and 2018 FIGO Staging Classifications

Stage	2009 FIGO Definition	2018 FIGO Definition
I	Confined to the cervix	Confined to the cervix
IA	≤5 mm depth and ≤7 mm width	≤5 mm depth*
IA1	≤3 mm depth	≤3 mm depth
IA2	>3 mm and not >5 mm depth	>3 mm and ≤5 mm depth
IB	>5 mm depth	>5 mm depth
IB1	≤4 cm maximum diameter	≤2 cm maximum diameter*
IB2	>4 cm maximum diameter	>2 cm and ≤4 cm maximum diameter*
IB3	...	>4 cm maximum diameter*
II	Beyond the uterus but not involving the lower one-third of the vagina or pelvic sidewall	Beyond the uterus but not involving the lower one-third of the vagina or pelvic sidewall
IIA	Upper two-thirds of the vagina	Upper two-thirds of the vagina
IIA1	Upper two-thirds of the vagina and ≤4 cm	Upper two-thirds of the vagina and ≤4 cm
IIA2	Upper two-thirds of the vagina and >4 cm	Upper two-thirds of the vagina and >4 cm
IIB	Parametrial invasion	Parametrial invasion
III	Lower vagina, pelvic sidewall, and ureters	Lower vagina, pelvic sidewall, ureters, and lymph nodes*
IIIA	Lower one-third of the vagina	Lower one-third of the vagina
IIIB	Pelvic sidewall	Pelvic sidewall
IIIC	...	Pelvic and para-aortic lymph node involvement*
IIIC1	...	Pelvic lymph node involvement*
IIIC2	...	Para-aortic lymph node involvement*
IV	Adjacent and distant organs	Adjacent and distant organs
IVA	Rectal or bladder involvement	Rectal or bladder involvement
IVB	Distant organs outside the pelvis	Distant organs outside the pelvis

Source.—Reference 18.
*Changes made in the 2018 FIGO staging classification.

Figure 2.12 FIGO staging in the classification of cervical cancer [35]

Staging methods endorsed by the International Federation of Gynecology and Obstetrics (FIGO) are predominantly employed in cases involving cervical cancer and other tumors affecting the female reproductive organs. The clinical stage is utilized when diagnosing cervical cancer. It is established based on the results of the patient's physical examination conducted by the attending physician, biopsies, imaging tests, and a few additional procedures that may be performed under specific conditions, including proctoscopy and cystoscopy. It is not contingent upon the outcomes of the surgical intervention. The pathologic stage of the cancer can be determined through postoperative assessment; however, this does not have any bearing on the clinical stage. Stage I (1) represents the earliest stage of cervical cancer and progresses to stage IV (4). A smaller score generally signifies that the cancer has not metastasized to an excessive degree. A greater stage designation, such as stage IV, signifies a more pronounced progression of the cancer. Additionally, a subsequent letter within a stage signifies a greater level than an initial letter. Cancers that are in similar stages often exhibit similar prognoses and are frequently managed in a similar fashion [36].

FIGO STAGE I

The malignant cells have already migrated from the outermost layer of the cervix to the deeper tissues of the organ at this juncture. The lymph nodes in the vicinity do not appear to have been affected by the cancer. No indications have emerged of the malignancy metastasizing to an offshore site.

STAGE I - IA

The utilization of a microscope is imperative for the identification of the cancer due to its subtle nature. There have been no documented instances of the disease metastasizing to the lymph nodes within the vicinity. It appears that there has been no dissemination to remote locations.

STAGE I – IA1

The depth of the malignant area is less than 3 millimeters (approximately 1/8 of an inch), rendering it visible solely under a microscope. It has not metastasized to the nearby lymph nodes. Its transmission to other areas has not been substantial.

STAGE I – IA2

Due to its depth of 3 to 5 millimeters (approximately 1/5 of an inch), the malignant lesion necessitates the application of a microscope in order to be observed. No lymph node involvement has been observed in the vicinity. It appears that there has been no dissemination to remote locations.

STAGE I – IB

Cancer has met the criteria for stage I when it has metastasized beyond the cervix by a distance of at least 5 mm (1/5 inch). The disease does not appear to have spread to any of the lymph nodes in the area. As of yet, there has been no discernible dispersion to remote regions.

STAGE I – IB1

When expressed in centimeters, the depth of the cancer is greater than 5 millimeters (approximately 1/5 of an inch) but falls below 2 centimeters (approximately 4/5 of an inch). There have been no documented instances of the disease metastasizing to the lymph nodes within the vicinity. It appears that there has been no dissemination to remote locations.

STAGE I – IB2

When measured at its widest point, the diameter of the carcinoma must be a minimum of 2 centimeters and a maximum of 4 centimeters. There have been no documented instances of the disease metastasizing to the lymph nodes within the vicinity. It appears that there has been no dissemination to remote locations.

STAGE I – IB3

The malignant proliferation is confined to the cervix and has a diameter of no more than four millimeters. There is no evidence that the cancer has metastasized. There have been no documented instances of the disease metastasizing to the lymph nodes within the vicinity. It appears that there has been no dissemination to remote locations.

FIGO STAGE II

Currently, the malignancy has metastasized beyond the uterus and cervix, but it has not yet infiltrated the vaginal or pelvic cavity walls. No instances of the malignancy metastasizing to the lymph nodes within the vicinity have been documented. There have been no reports of the disease expanding to additional regions.

STAGE II – IIA

Despite the fact that the cancer has metastasized beyond the uterus and cervix in this instance, it has not yet infiltrated the parametria, which are the tissues immediately adjacent to these organs. There have been no documented instances of the disease metastasizing to the lymph nodes within the vicinity. It appears that there has been no dissemination to remote locations.

STAGE II – IIA1

The tumor's diameter is significantly less than 4 centimeters (approximately 1 3/5 inches). No lymph node involvement has been observed in the vicinity. It appears that there has been no dissemination to remote locations.

STAGE II – IIA2

Malignancy is frequently identified in tumors measuring four centimeters or larger in diameter. There have been no documented instances of the disease metastasizing to the lymph nodes within the vicinity. It appears that there has been no dissemination to remote locations.

STAGE II – IIB

In addition to extending throughout the cervix and uterus, the malignant tumor has also infiltrated the adjacent tissues (the parametria). There have been no documented instances of the disease metastasizing to the lymph nodes within the vicinity. It appears that there has been no dissemination to remote locations.

FIGO STAGE III

Metastasis of the cancer has occurred in the pelvic floor or lower vagina. A ureteral obstruction may be attributable to the cancer; ureters are the conduits that transport urine from the kidneys to the bladder. Although there is a possibility, there is no evidence

that it has spread to the local lymph nodes. It appears that there has been no dissemination to remote locations.

STAGE III – IIIA

Despite its metastasis to the lower vagina, the cancer remains confined to the pelvic walls, its site of origin. There have been no documented instances of the disease metastasizing to the lymph nodes within the vicinity. It appears that there has been no dissemination to remote locations.

STAGE III – IIIB

The infection of the pelvic walls and clogging of one or both ureters have occurred as a consequence of the malignant progression, leading to renal failure medically referred to as hydronephrosis. There have been no documented instances of the disease metastasizing to the lymph nodes within the vicinity. It appears that there has been no dissemination to remote locations.

STAGE III – IIIC

It is inconsequential to the extent of the tumor. The findings from the imaging and biopsy analyses indicate that the cancer has metastasized to the lymph nodes situated in

the pelvis (stage IIIC1) and in close proximity to the aorta (stage IV) (IIIC2). It appears that there has been no dissemination to remote locations.

FIGO STAGE IV

The cancer has been identified as having metastasized to additional anatomical sites, specifically the lungs and bones.

STAGE IV – IVA

Evidence of cancer has been detected in either the rectum or bladder, in addition to metastasis of cancer from the pelvis.

STAGE IV – IVB

At this time, the lymph nodes, lungs, and bones, which are situated at a considerable distance from the pelvis, have been affected by the cancer.

2.4 Artificial intelligence

AI has progressed since the mid-20th century period. Artificial intelligence has rapidly developed into a potent technology that has the potential to revolutionize society. This article will discuss the history, applications, and drawbacks of artificial intelligence.

the emergence of AI during the 1950s and 1960s. The goal of computer scientists' AI experiments was to develop robots capable of learning and thought similar to humans. The scarcity of computers and data storage impeded expansion.

The Turing Test of 1950 was a significant AI milestone. The test was conceived by Alan Turing to determine whether or not a machine could simulate human intelligence. Text was used to facilitate communication between a human judge, a computer, and another human during the examination. Passage was granted if the judge was unable to distinguish the machine from the individual. Instigating AI research was the Turing test. A decade of programming languages and algorithms that emulated human cognition and reasoning propelled AI forward in the 1960s and 1970s. Simply put, simple algorithms and computing power impeded progress.

AI systems that emulated human judgment in professional settings, known as expert systems, achieved significant progress during the 1980s. A medical expert system, akin to a physician, could evaluate the state of a patient by employing rules and heuristics. The legal, engineering, healthcare, and finance sectors all utilized expert systems. They were incapable of learning and required human input for data and programming. Large datasets, potent computers, and machine learning techniques have all contributed to the development of AI in the twenty-first century. Instructing computers to identify patterns and draw conclusions from data is the goal of machine learning. Intelligent robotics, Siri, Alexa, and driverless cars are all made possible by this technology.

Universities, governments, and businesses have increased funding for AI research. Amazon, Google, and Facebook are all investing significantly in AI research. It has numerous applications in finance, healthcare, and entertainment.

AI is challenging as well. AI bias could be detrimental to certain populations, which is a major concern. The AI is prejudiced if the data is skewed. In order to facilitate human understanding of AI decision-making, researchers are making AI systems more transparent and explicable. A further concern is the impact that AI will have on employment. Some experts believe that AI could disrupt some occupations while creating others. This presents difficulties regarding how society can best prepare for labor changes driven by AI. AI has advanced throughout the current era since its inception. AI is now capable of altering the world. AI has disadvantages, but its benefits are enormous. Society must confront these challenges and ensure that AI benefits all as it develops.

2.2.1 TYPES OF ARTIFICIAL INTELLIGENCE

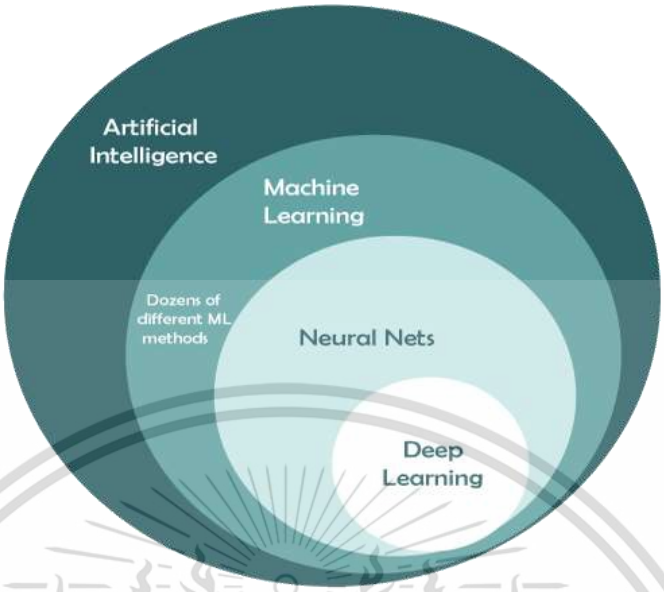

Figure 2.13 A visual chart describe types of general AI [36]

AI research is growing in tandem with the proliferation of AI systems in use. In this section, rule-based systems, machine learning, and deep learning will be contrasted.

Rule-based AI bases its decisions and actions on predefined regulations. The majority of these rules conditionally execute an action using "if-then" statements. "If the patient has a fever and a sore throat, then they have strep throat." When faced with complex decisions, rule-based systems are susceptible to failure.

Machine learning enhances performance through the analysis of data using algorithms. Machine learning systems analyze enormous datasets utilizing statistical methods. Algorithms for machine learning consist of reinforcement, unsupervised, and supervised learning. Supervised learning applies to target-tagged samples to teach the algorithm. Unsupervised learning is the process of teaching algorithms to extract meaning

from unlabeled data. Reinforcement learning trains algorithms through the use of rewards and punishments. NLP, recommendation systems, and image and speech recognition may be aided by machine learning. Complex problems may be resolved by machine learning systems, but they may be difficult to train and require a great deal of data.

Artificial intelligence that employs "deep learning" teaches neural networks to solve complex problems. These networks, like the human brain, utilize numerous interconnected nodes to discover subtle data correlations. Image and audio recognition, natural language processing, and autonomous vehicles all make use of deep learning. Specialized hardware is required for deep learning systems due to the computational complexity they entail.

Variants of AI systems have distinct advantages and disadvantages. Prominent are rule-based systems due to their straightforward development process and provision of clear guidance for decision-making. Although machine learning algorithms discover intricate correlations and patterns in data, they may be challenging to instruct. Despite being excellent at recognizing patterns, deep learning algorithms are resource intensive. In order to develop AI solutions that are both effective and efficient, it is imperative to initially comprehend their advantages and disadvantages.

Swarm intelligence, fuzzy logic, expert systems, and evolutionary algorithms are all components of AI. Expert systems for problem-solving employ human knowledge and guidelines. Fuzzy logic emphasizes decision-making under uncertainty. Evolutionary

algorithms have the potential to enhance search results through the simulation of natural selection and mutation processes. Swarm intelligence solves problems using the strategies of ants and bees. Each strategy has pros and cons.

Expert systems, computer programs that execute human-like tasks, are another key part of AI. Rule-based expert systems make decisions and take action by utilizing knowledge. They are constructed upon the expertise and knowledge of human beings and collect data from domain specialists.

Engineering, medicine, law, and finance are all fields that utilize expert systems. In order to arrive at a diagnosis, an expert system for medical diagnosis might inquire about the patient's medical history and symptoms. On the contrary, investment recommendations provided by a financial planning expert system may be customized to align with the financial goals and risk tolerance of the client.

A mathematical approach to AI decision-making, fuzzy logic accommodates imprecise and ambiguous data. Fuzzy logic assigns variables a specified degree of membership as opposed to true or false. This facilitates more advanced decision-making and the management of incomplete or ambiguous data.

Fuzzy logic is utilized in methods such as automatic control, pattern recognition, and decision support systems. Using temperature sensor data, a fuzzy logic control system may modify the temperature of a room.

To solve complex problems, evolutionary algorithms in artificial intelligence imitate natural selection and mutation. These algorithms construct a population of potential solutions and iteratively improve them through the processes of selection, crossover, and mutation over multiple generations.

Optimization challenges in the fields of machine learning, finance, engineering, and game theory are addressed by evolutionary algorithms. A genetic algorithm may optimize the performance of machine learning models by adjusting their parameters. Another AI technique, swarm intelligence, draws inspiration from ants and bees. Without a leader, a swarm of intelligent agents solves a problem or accomplishes a task.

Problems with work allocation, optimization, and routing are resolved by swarm intelligence. In order to save money and time, swarm intelligence algorithms can optimize the route of delivery trucks.

AI research is progressing and there are a multitude of approaches to developing AI systems. Deep learning, rule-based systems, and machine learning are prominent techniques with advantages and disadvantages. Swarm intelligence, fuzzy logic, expert systems, and evolutionary algorithms each have unique applications and advantages. For numerous domains and applications, it is vital to comprehend AI techniques in order to develop AI solutions that are both effective and efficient.

2.2.2 MACHINE LEARNING IN IMAGE CLASSIFICATION FOR MEDICAL USE

	ANN	CNN	RNN
Basics	One of the simplest types of neural networks.	One of the most popular types of neural networks.	The most advanced and complex neural network.
Structural Layout	Its simplicity comes from its feed forward nature – information flows in one direction only.	Its structure is based on multiple layers of nodes including one or more convolutional layers.	Information flows in different directions, which gives it its memory and self-learning features.
Data Type	Fed on tabular and text data.	Relies on image data.	Trained with sequence data.
Complexity	Simple in contrast with the other two models.	Considered more powerful than the other two.	Fewer features than CNN but powerful due to its self-learning & memory potential.
Commendable Feature	Ability to work with incomplete knowledge and high fault tolerance.	Accuracy in recognizing images.	Memory and self-learning.
Feature type: spatial recognition	No	Yes	No
Feature type: Recurrent connections	No	No	Yes
Main Drawback	Hardware dependence.	Large training data required.	Slow and complex training and gradient concerns.
Uses	Complex problem solving such as predictive analysis.	Computer vision including image recognition.	Natural language processing including sentiment analysis and speech recognition.

Figure 2.14 Comparison of ANN, CNN, and RNN [37]

An area that was previously stagnant, object categorization has been completely upended by artificial intelligence's capability to enable robots to recognize and categorize objects automatically. The field has witnessed a significant surge in interest surrounding neural network designs due to the advancements made in deep learning methodologies. In this section, we will examine numerous practical examples of neural network architectures in use for real-world object categorization tasks, including an explanation of their operation and a few medical applications.

Regarding the classification of objects, Convolutional Neural Networks (CNNs) are among the most frequently implemented neural network architectures. Convolutional

layers are employed to detect and extract spatial characteristics from photographs in an automated manner. A CNN consists of convolutional layers initially, followed by a pooling layer, and finally an activation layer. A fully connected layer renders the ultimate classification determination subsequent to receiving the flattened output from the final convolutional layer. Face recognition, traffic sign recognition, and medical image analysis are a few examples of tasks requiring object categorization in which CNNs have demonstrated efficacy.

For object categorization, Recurrent Neural Networks (RNNs) are an additional type of neural network architecture. RNNs perform exceptionally well with sequential data, including time series and text. In object classification, RNNs are utilized to classify items based on their temporal relationships. By categorizing activities in videos based on the sequence in which they transpire in the footage, an RNN can be implemented. Natural Language Processing (NLP) and voice recognition and language modeling are a few of the many applications of RNNs.

For object classification, Fully Convolutional Networks (FCNs) represent the third type of neural network architecture. Extended CNNs, also known as FCNs, are capable of pixel-level image segmentation. They convert an input image into a corresponding output image, with each pixel representing a class label. FCNs have been identified in the medical imaging industry for a variety of purposes, including segmentation of blood vessels, organs, and tumors.

The importance of applying artificial intelligence to the task of object categorization has increased within the medical field. The classification and identification of anatomical characteristics is an essential component of medical image analysis; however, when performed manually, it can be a laborious and susceptible to error procedure. This can be facilitated by AI's dependable and automated object categorization. For instance, AI may be utilized in mammography to analyze images for indications of breast cancer.

Medical object categorization includes the identification of lung cancer nodules in CT images as one application of artificial intelligence. Researchers have developed various neural network architectures for the purpose of identifying and classifying lung nodules. One study employed a convolutional neural network (CNN) to accurately detect lung nodules in CT images with an accuracy of 89 percent. The mean dice similarity coefficient utilized in the segmentation of lung nodules from CT data utilizing an FCN was 0.81.

The utilization of artificial intelligence in medical object categorization is not limited to the detection of diabetic retinopathy. In the United States, untreated diabetic retinopathy is the leading cause of blindness. Analyzing retinal images, artificial intelligence may aid in the diagnosis and severity assessment of diabetic retinopathy. In one experiment, a CNN was instructed to classify instances of diabetic retinopathy with an accuracy of 90%.

In conclusion, artificial intelligence has enabled robots to recognize and sort objects into predefined categories. CNNs, RNNs, and FCNs are among the neural network architectures that have demonstrated efficacy in the domain of object categorization. The utilization of artificial intelligence in the medical field has been increasingly expanding to encompass anatomy detection and categorization. Positive results have been observed with the application of AI to the classification of medical objects, indicating that this method could assist physicians in providing patients with more accurate and timely diagnoses.

2.2.3 CREATING PROFESSIONAL AI TAILORED TO THE USE CASE

Constraintless development and implementation of a series of procedures are required to establish an AI from the ground up. The primary goal of business is to determine which artificial intelligence system is most aptly equipped to confront the given challenge. Upon the resolution of this matter, one can commence the process of organizing information and formulating plans. Prior to divided into training and testing sets, the data necessitates feature selection, cleaning, and organization. Selecting an appropriate machine learning approach to train the AI model is the subsequent step. Models should be tested to ensure they generate accurate predictions following training. Once the AI model has been adequately tested, it is permissible to implement it in

production. Over time, the efficacy and productivity of the AI model must be routinely assessed and modified.

Detailed procedures for each process consist of:

STEP 1: SELECT A NETWORK.

Determining the appropriate network architecture is the primary step in the training procedure of an artificial intelligence system to classify objects. In addition to the complexity and size of the provided data, the nature of the categorized subject must be taken into account throughout the process. Convolutional Neural Networks (CNNs), Residual Neural Networks (ResNets), and DenseNets are illustrative instances of networks that are widely employed in the domain of research.

STEP 2: PREPARATION OF DATA

Once a network has been selected, the data must be collected and organized in preparation for analysis. In the training process, the quality and size of the dataset utilized have a substantial impact on the dependability of the model. It is imperative to assign category labels to the photographs at this juncture. It is advisable to partition the data into distinct sets, namely the test set, validation set, and training set.

Image preprocessing techniques, such as resizing, normalizing, and augmenting, can be implemented to improve the diversity and quality of the dataset. In order to achieve uniform dimensions, images can be resized, and normalization can aid in maintaining consistent pixel values everywhere. A number of techniques, including rotation, mirroring, and cropping, can be employed as augmentation methods to introduce diversity into the dataset.

STEP 3: TRAINING AND VALIDATION

Following data preparation and cleansing, the subsequent step is to train the model using the dataset. During the training phase, the model gains knowledge of the attributes and patterns that are associated with the classes of objects. The loss function serves as a quantitative measure to assess the extent to which the actual values differ from the anticipated ones.

It is critical to fine-tune the model's hyperparameters, including learning rate, batch size, and optimizer, to maximize the training process. Due to the destructive potential of overfitting and underfitting, it is critical to validate the model frequently with the validation dataset. One can monitor the development of the model during training by examining the validation accuracy.

STEP 4: MODEL EVALUATION

After the model has undergone training, its performance is assessed using a test dataset. Standard evaluation criteria encompass accuracy, precision, recall, and F1-score; nevertheless, the exact metrics utilized depend on the nature of the problem at hand. The confusion matrix provides an indication of the model's performance with respect to true positives, true negatives, false positives, and false negatives.

STEP 5: ADJUST AND FINE-TUNE IN

Fine-tuning can be employed to enhance the precision of the model in the event that its performance fails to meet anticipated levels. Elements are modified to the network's architecture or hyperparameters throughout the process of fine-tuning. The model can be implemented in real-world scenarios once its performance has been optimized to its intended level.

Object classification AI has numerous potential applications in the medical field, including the identification of abnormal cells in microscope images, the diagnosis of diseases from medical imaging, and the detection of tumors using MRI scans. The trained models have the potential to assist physicians in making accurate diagnoses promptly, thereby resulting in improved health outcomes.

There are numerous moving parts involved in the development of an effective artificial intelligence for object categorization. The aforementioned procedures comprise network selection, data preprocessing, training, validation, and testing. Upon completion of the procedures, the researcher will possess a functional model suitable for practical implementation, be it within the medical field or another domain.

2.2.3 PRACTICAL NEURAL NETWORKS ARCHITECTURES FOR MEDICAL OBJECT CLASSIFICATION

Neural networks are a fundamental component of artificial intelligence, and the term "neural network architecture" pertains to the configuration and structure of these networks. The network's efficacy and precision in producing outcomes are contingent upon its architecture as well as the methods employed for data processing and analysis. Neural networks possess a discernible architecture consisting of layers of neurons that are interconnected. An assortment of "layers" within the model are tasked with performing analysis-related functions, including feature recognition and classification. Depending on the difficulty of the task at hand and the quantity and nature of data that will be processed by the network, the overall architecture may differ.

The efficacy and precision of a neural network's output are substantially influenced by its architecture. A well-designed network architecture will enable accurate evaluation

and interpretation of the data, leading to outcomes that are more dependable. Conversely, an architecture that is inadequately designed may yield unreliable outcomes due to analysis that is either inaccurate or insufficient.Additionally, the network's effectiveness may be influenced by its architecture. A more complex architecture comprising multiple layers would necessitate additional processing power and time, while a simpler architecture might yield quicker outcomes but at the expense of precision.

Precision, efficacy, and overall utility of artificial intelligence may be substantially influenced by the architecture of the neural network. Architecture that is designed and implemented with the utmost precision will produce the highest quality outcomes.

Common neural network architectures include the following:

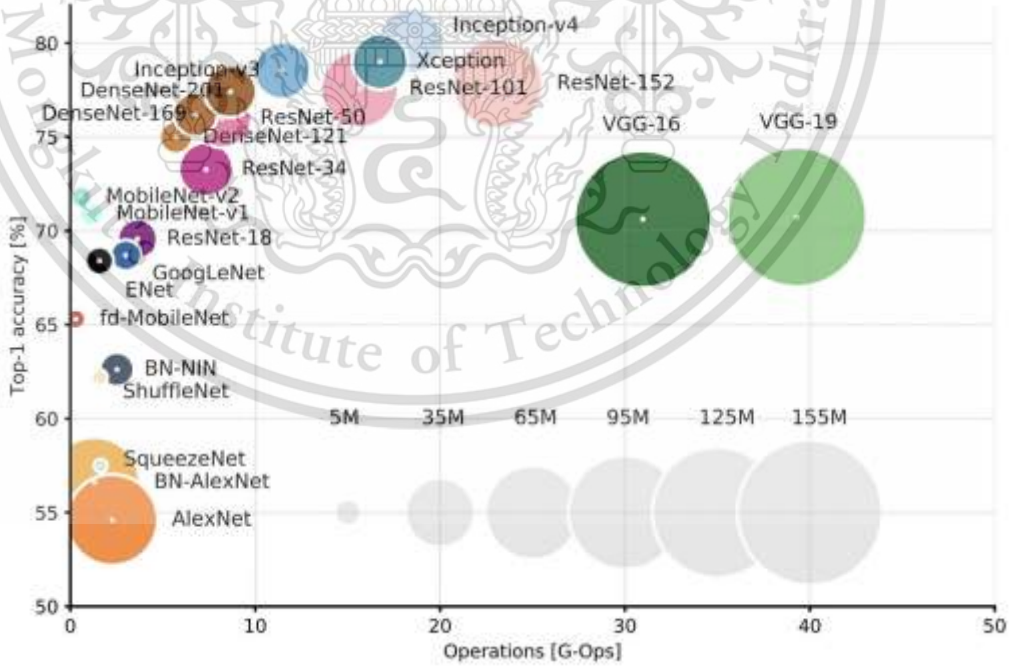

Figure 2.15 Comparison of neural network size to accuracy [38]

YOLOv5, an approach that utilizes a solitary neural network, is designed to detect and classify objects in real-time. Due to its rapidity and precision, it has become a favorite in computer vision applications. Each cell of the input image is utilized by YOLOv5 to estimate bounding boxes and class probabilities. Following this, the system eliminates duplicate detections by utilizing non-maximum suppression before generating its predictions.

To classify images, ResNet (Residual Network), a well-known deep neural network architecture, is utilized. It is widely recognized for its ability to streamline the training process of extremely deep neural networks and has demonstrated exceptional performance on several benchmark datasets. The primary innovation of ResNet is the implementation of residual connections, which circumvents the vanishing gradient problem when training extremely deep neural networks. The gradient can traverse directly from the output of one layer to the input of a layer several levels below it in a network with residual connections.

VGG16 (Visual Geometry Group), a convolutional neural network architecture developed by Oxford University's Visual Geometry Group It is frequently employed for image classification and consists of sixteen layers. The usability of VGG16 is widely recognized and it has demonstrated exceptional performance across numerous benchmark datasets. Convolutional layers, max pooling layers, and finally completely

linked layers comprise the architecture. The convolutional layers make use of diminutive 3x3 filters that possess a pixel stride.

Convolutional neural networks comprise Inception-v3, the third iteration of Google's Inception neural network architecture. It has established an exceptional standing in terms of both speed and accuracy, surpassing all alternative methods across a multitude of test datasets. The architectural design incorporates the Inception module, which comprises an assortment of convolutional layers featuring filters of varying sizes. As a result of this capability, the network can acquire data at an extensive range of scales and resolutions. Additional techniques that improve performance, including factorized convolutions and batch normalization, have been incorporated into Inception-v3.

A common application of the convolutional neural network architecture U-Net is image segmentation. Although its initial purpose was to segment biomedical images, it has subsequently been implemented in various other domains. The final segmentation mask is generated when the encoder network downsamples the input image and the decoder network upsamples the encoder's output. U-Net is distinguished by the fact that it employs skip connections, which link nodes of the encoder and decoder networks that are identical. By retaining the spatial characteristics of the input image, the network is capable of producing segmentation masks that are more precise.

MobileNet is a lightweight and efficient convolutional neural network architecture. It is frequently employed in embedded systems for the identification and classification of

objects. In order to optimize performance, MobileNet combines depthwise and pointwise convolutions to generate depthwise separable convolutions. Pointwise convolutions combine the results of multiple depthwise convolutions using a 1x1 filter, whereas depthwise convolutions independently apply a filter to each input channel. As a result, both the computational complexity and parameter count of the network are diminished.

In pursuit of object recognition and segmentation, a considerable number of scholars have implemented the widely recognized Mask R-CNN neural network framework. Furthermore, it produces object bounding boxes and pixel-level segmentation masks, constituting an improvement over the Faster R-CNN method. To accomplish its goal, Mask R-CNN initially employs a Region Proposal Network (RPN) to generate object proposals. After these assessments, a variety of techniques are employed to enhance the recommendations.

2.2.5 PREPROCESSING TECHNIQUES AND ITS IMPACT ON ARTIFICIAL INTELLIGENCE PRODUCTS

Figure 2.16 Examples between non-preprocessing and pre-processed images [39]

In terms of enhancing the accuracy and precision of artificial intelligence models, preprocessing techniques are indispensable. These techniques aim to improve the quality of unprocessed data through the extraction of valuable attributes and the reduction of noise. In the domain of image processing, preprocessing techniques are frequently utilized to prepare images for neural network analysis. This article will examine several widely used preprocessing methods and their respective applications.

The process of adjusting the proportions of an image without modifying the image itself is known as image resizing. Utilizing this approach will ensure that every photograph in the dataset has an identical size. Resizing is essential when working with neural networks that demand a particular input size. Either downsampling or upsampling is performed on

the image in order to accommodate the specified input size. There are numerous resizing techniques in existence, such as nearest neighbor, bilinear, bicubic, and Lanczos.

Image processing modifies luminance to ensure uniform illumination. "Normalization" modifies the contrast, brightness, and ambient light. Intensity values can be normalized by rescaling them to a range of 0–1 or -1–1, or by establishing the mean as zero and the standard deviation as one. By utilizing rotations, translations, inverts, and cropping, image augmentation generates new images from existing ones. Augmenting images increases the size and diversity of a dataset while decreasing overfitting. Examples include Keras, TensorFlow, and PyTorch.

Filtering improves the quality of an image by eliminating extraneous elements. This necessitates numerous photo adjustments. The application of a filter reduces noise, blur, and clarity. Filtering includes structures such as the Gaussian, Median, Sobel, and Laplacian.

Image segmentation is the process of dividing an image into regions that share aesthetic, textural, or geometric attributes. The aforementioned technique is commonly utilized in the domains of image classification, boundary extraction, and object detection. Watershed, thresholding, and clustering are a few of the techniques that can be employed for segmentation.

To prevent the favoritism of one class over another, the distribution of classes in a dataset can be altered via data balancing. In order to ensure that the model is trained with a representative sample size for each class, this technique is frequently implemented. Mixed-method balancing, oversampling, and undersampling are all viable alternatives.

The "image registration" process is utilized to construct a composite image from multiple photographs of the same scene. By applying this technique to a series of low-resolution photographs, it is possible to generate a high-resolution image. Additionally, it is commonly used to compensate for camera shake. There are various approaches available to address the registration task, such as affine, elastic, and non-rigid registration.

Preprocessing techniques are essential for improving the precision and accuracy of AI models. These techniques aim to improve the quality of unprocessed data through the extraction of valuable attributes and the reduction of noise. Scaling, normalizing, augmenting, filtering, segmenting, balancing, and registering images are typical operations. Each method has advantages and disadvantages; therefore, selecting one necessitates consideration of the available data and the task at hand.

2.2.6 METHOD OF QUALITATIVE REPRESENTATION FOR AI RESULTS

		Predicted	
		Negative **(N)** -	Positive **(P)** +
Actual	Negative -	True Negative **(TN)**	**False Positive (FP) Type I Error**
	Positive +	**False Negative (FN) Type II Error**	True Positive **(TP)**

Figure 2.17 Confusion metric [40]

As the application of AI systems expands into numerous industries, there must be a standardized method for assessing their accuracy and value. In order to ensure that an AI system meets the required standards and can be relied upon to produce accurate judgments, it is vital to assess the system's quality. This dissertation will examine a number of the most widely used methods for assessing the quality of an artificial intelligence system.

F1 RESULTS

The F1 score is a widely used metric in classification tasks to assess the predictive ability of a model. It serves as a statistical indicator of the ideal equilibrium between precision and long-term memory retention. Recall is equal to the same fraction divided

by the number of accurate diagnoses, whereas recall is the proportion of accurate diagnoses relative to all positive outcomes. The F1 score is calculated by averaging the accuracy and recall metrics. It serves as an indicator of both. The F1 score ranges from 0 to 1, where a value of 1 signifies optimal recall and accuracy.

ACCURACY ASSESSMENT

An additional widely used metric for assessing the performance of AI systems is the accuracy score. It represents the system's proficiency in generating predictions. In binary classification, the accuracy score is calculated as the proportion of accurate predictions to the total number of guesses. In multi-class classification, the accuracy score is calculated by dividing the quantity of correct predictions by the overall number of guesses. The accuracy score may range from 0 to 1, where 1 denotes the highest level of precision.

RECEIVER OPERATING CHARACTERISTICS, OR ROC CURVE

A graphical representation of the sensitivity and specificity of a classification model can be found in the Receiver Operating Characteristics (ROC) curve. Sensitivity refers to the ability of a test to identify true positive results, while specificity denotes the frequency of false negative outcomes. Comparing the proportion of accurate diagnoses (1 minus

specificity) to the proportion of incorrect positives (sensitivity) yields the ROC curve. The area under the receiver operating characteristic curve (AUC) is utilized to assess the performance of a classifier. AUC is measured on a continuous scale from 0 to 1, with 1 indicating optimal sensitivity and specificity.

MEAN ABSOLUTE ERROR (MAE)

The mean absolute error (MAE) measures the average deviation of the predictions from the true value. It is commonly utilized within the framework of regression concerns. In order to calculate the mean absolute error (MAE), the sum of every discrepancy between the predicted and actual values is utilized. MAE, or maximum allowable error, is equal to zero; therefore, perfect precision is opposed to an infinite MAE.

SD (STANDARD DEVIATION)

The MSE is another well-known tool for determining the accuracy of a regression model. A useful metric is the average squared deviation between predicted and observed values. The mean squared error (MSE) quantifies the deviation of one's predictions from the actual value. The MSE maximum that is permissible is infinity, while an MSE value of zero signifies absolute precision.

THE CURVE OF RECALL-ACCURACY

An additional metric for assessing the accuracy of a classifier is the precision-recall curve. A graph of accuracy versus recall is presented, encompassing a range of cutoff values. Recall quantifies the proportion of accurate predictions relative to the total number of positives, while precision quantifies the proportion of correct positives that occurred. To evaluate the quality of a classification model, one computes the area under the precision-recall curve (AUPRC).

2.2.7 FINE TUNING FOR BETTER ACCURACY

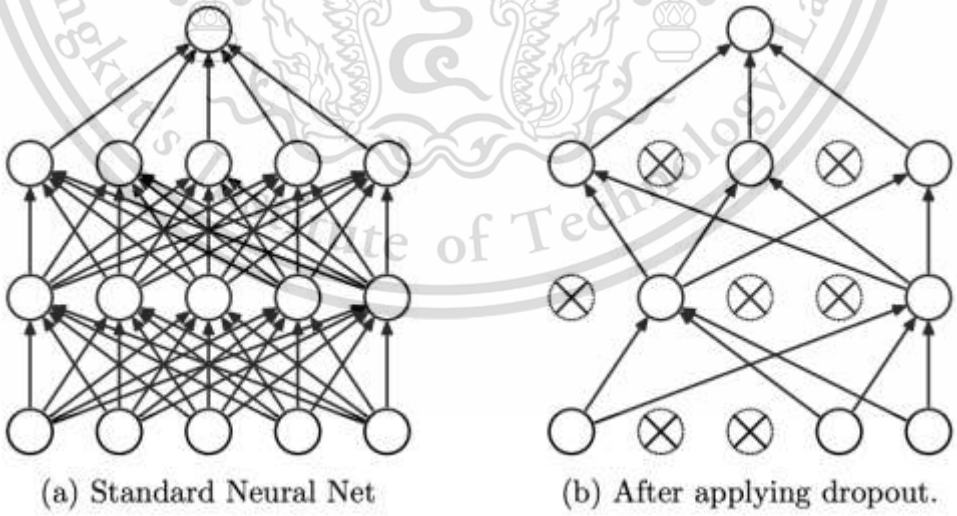

Figure 2.18 Droup out algorithm [41]

The development of an AI model that can execute its intended function with optimal effectiveness and efficiency requires meticulous fine-tuning. The procedure of fine-tuning entails making adjustments to the parameters of a pre-trained model in order to optimize its performance on an alternative assignment or dataset. This stage is critical in enhancing the model's performance and generating precise predictions. Frequent adjustment techniques encompass the subsequent:

Transfer learning is a fine-tuning technique wherein the input for a separate task is provided by a model that has already been trained. By utilizing data from a model that has been previously trained, the performance of the model is enhanced for the present task. Transfer learning has gained significant traction as an approach to enhancing AI models due to its ability to optimize computational resources and time, while also establishing a robust framework for the development of new models.

The learning rate is a critical hyperparameter of AI models that necessitates strategic planning. The sizing of the optimization stages throughout model training is under its control. The learning rate can be gradually slowed down throughout the training process by employing a method called "learning rate scheduling." By employing this approach, the model's capacity to adjust to novel data is enhanced as it is prevented from becoming entangled in local minima.As AI models are susceptible to overfitting, regularization is a useful fine-tuning technique. When a model performs exceptionally well on training data but poorly on testing data, this is known as overfitting. Overfitting is

mitigated through the application of regularization techniques L1 and L2, which penalize the model's excessive weights.

The dropout method is a fine-tuning technique utilized to decrease the probability of overfitting in deep learning models. In this approach, certain network nodes are omitted from the training procedure by arbitrary setting to zero. By employing this approach, the network is compelled to acquire more resilient features that exhibit enhanced generalizability to novel data.

A technique utilized during training to prevent gradients from expanding is known as "clipping gradients." Extremely large gradients result in an eruption of model parameters. This could potentially lead to the model experiencing unpredictability and failing to converge. By implementing a maximum gradient value, which is alternatively referred to as "clipping," the gradient is limited to a predetermined threshold.

2.3 FLUORESCENT IMAGING

2.3.1 HISTORY OF FLUORESCENT IMAGING

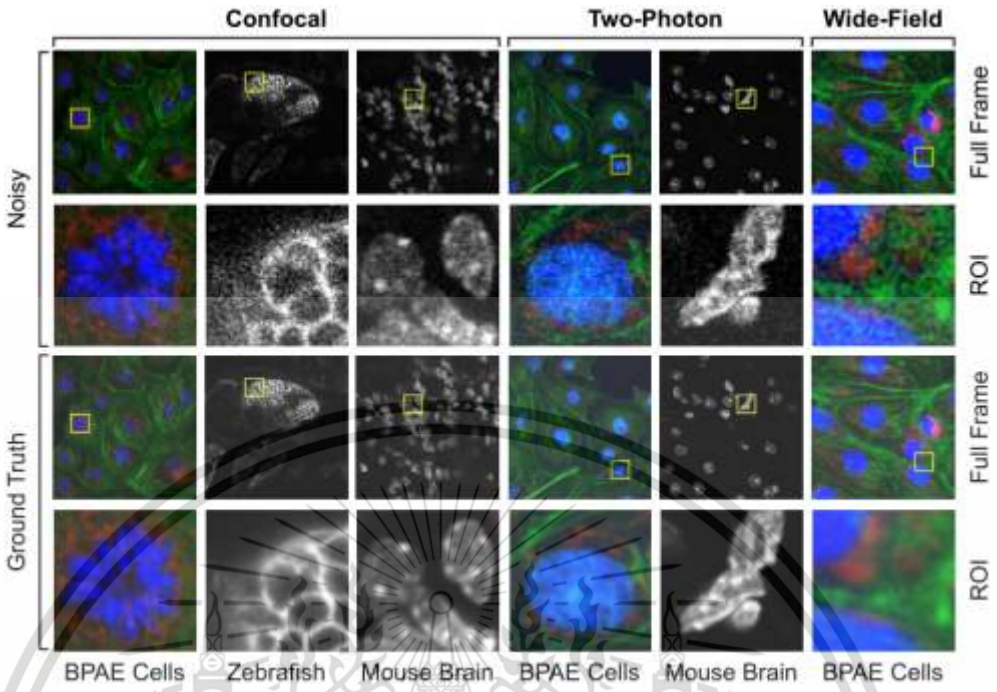

Figure 2.19 Examples of fluorescent imaging [42]

In the fields of materials research, biology, chemistry, and physics, fluorescent imaging is indispensable. It revolutionized molecular and cellular research. The history, evolution, and applications of fluorescence imaging will be covered in this article. Early in the 20th century, researchers investigating light developed fluorescence imaging. A 1912 discovery by William Lawrence Bragg that crystals scatter X-rays was the impetus for X-ray crystallography. Molecular structure research was profoundly transformed by this method, which was awarded numerous Nobel Prizes in chemistry and medicine.

When George Placzek discovered in 1928 that ultraviolet radiation caused certain substances to emit light, he had discovered fluorescence. The advent of fluorescence microscopy in the 1940s enabled researchers to observe living cells in action. Initially, fluorescence imaging employed naturally occurring fluorescent substances, such as

chlorophyll, that emit light upon activation at a specific wavelength. The effectiveness of these techniques was limited by the concentrations of fluorescent molecules and the wavelength range.

In the 1960s, synthetic fluorescent dyes significantly advanced fluorescence imaging. Cellular DNA was stained using acridine orange, one of the earliest synthetic dyes. In 1971, fluorescein isothiocyanate (FITC) established fluorescence imaging as the norm. Proteins can be conjugated with FITC, the first synthetic dye to exhibit intense green fluorescence, in order to label specific cell structures. Influenced by confocal microscopy, fluorescence imaging was transformed in the 1980s. A sample plane that was illuminated with a laser was capable of producing images of greater resolution and three-dimensional reconstructions. Organelles and the cytoskeleton must be examined with confocal microscopy.

In the 1990s, GFP in jellyfish once more revolutionized fluorescence imaging. GFP can be introduced genetically into cells in order to label proteins and monitor their activity. Studies of signaling pathways and protein interactions were facilitated by FRET. For biomedical research, fluorescence imaging continues to be highly effective. The expansion of fluorescence probes made possible by synthetic dyes and genetic engineering has enabled more precise labeling of cellular processes and structures. Super-resolution microscopy has expanded the boundaries of resolution by enabling the investigation of nanoscale structures. Fluorescent imaging is utilized in both clinical and

fundamental research. In cell biology, fluorescent imaging is employed to examine the dynamics of the cytoskeleton and organelles. In neuroscience, it investigates neural signaling and synaptic plasticity. With fluorescent imaging, cancer progression and metastasis are investigated. Fluorescence imaging in clinical settings detects and monitors disease.

In the development of biosensors, fluorescent imaging is intriguing. Fluorescent probes are utilized by biosensors to identify hormones or glucose in blood or urine. These technologies have the potential to revolutionize healthcare through more frequent and precise monitoring of diabetes and cancer. Similar to any technological advancement, fluorescent imaging also possesses limitations. Photobleaching is a significant concern as it involves the gradual loss of fluorescence from fluorescent molecules. GFP was produced by Aequorea victoria jellyfish in the mid-1990s. The protein emits a green glow when exposed to ultraviolet light. The protein could potentially be synthesized in living cells to enable real-time observation.

GFP pioneered novel imaging techniques. Protein fluorescence constituted molecular tags. By labeling them, this method enabled scientists to monitor the mobility and interactions of cell proteins. In consequence, FRET, a method for quantifying molecular interactions within living cells, was created. Confocal microscopy completely transformed fluorescence imaging in the 1980s. Thick specimens are sectioned optically in this manner,

which permits three-dimensional cell imaging. The utilization of confocal microscopy has propelled the fields of cell biology and disease research forward.

Imaging with fluorescence transformed biomedical research. Studies of cells and organisms in real time aid scientists in understanding biological processes and the etiology of diseases. As a consequence, novel diagnostics and treatments have emerged. Fluorescent imaging facilitates cancer research. By enabling the tracking of cancer cell migration, fluorescent imaging improves treatment. Additionally, fluorescent imaging has assisted scientists in understanding neurological diseases such as Alzheimer's and Parkinson's.

Advancements in fluorescent imaging have been testing the boundaries. An increase in the variety of hues and properties of fluorescent proteins permits more precise cell labeling and imaging. Using super-resolution microscopy, minuscule cellular processes and structures can be observed. The history of fluorescent imaging is fascinating. Biomedical research has been profoundly altered by fluorescent imaging ever since its inception in the 19th century. As fluorescent imaging advances, comprehension of disease mechanisms and biological processes is further expanded.

2.3.2 TYPES OF FLUORESCENT DYES

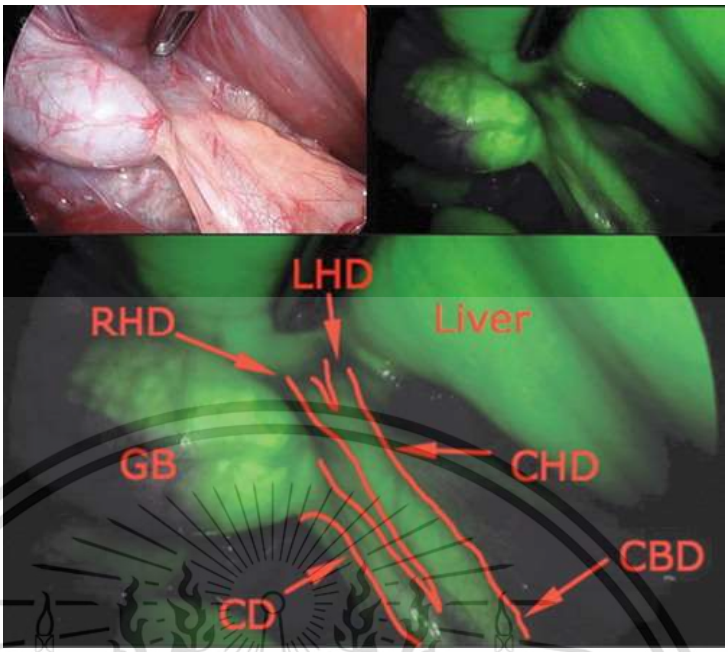

Figure 2.20 Examples of ICG imaging [43]

Utilized in biomedical research for a variety of purposes, fluorescent dyes have been implemented to image cellular and subcellular structures, detect molecules and interactions, and monitor biological processes. The luminous signal generated by fluorescent dyes is due to their characteristic of absorbing light at a specific wavelength and subsequently emitting light at a longer wavelength.

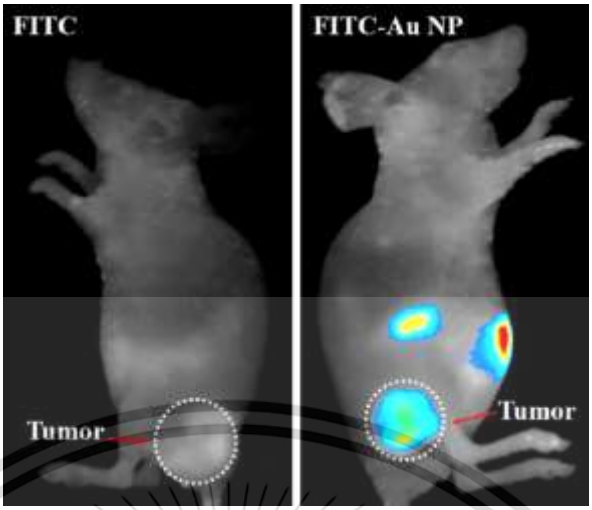

Figure 2.21 Examples of FITC imaging [44]

Flow cytometry, immunofluorescence, and protein labeling frequently employ fluorescein isothiocyanate (FITC), a fluorescent dye distinguished by its high quantum yield and excitation wavelength of 488 nanometers. FITC demonstrates a green fluorescence at 525 nm upon light activation and is easily conjugable to antibodies, proteins, and peptides.

Indocyanine green (ICG), owing to its fluorescence and near-infrared absorption characteristics, is an additional fluorescent dye that finds extensive application in medical imaging and diagnostics. ICG, which exhibits its maximum absorption at 780 nm and fluorescence at 820 nm, enables the visualization of deeper tissue layers while concurrently mitigating the impact of ambient noise. ICG has been utilized in numerous diagnostic procedures, including angiography, liver function testing, and lymphatic imaging.

Cy3, which, similar to numerous other fluorescent dyes, undergoes red fluorescence at 570 nm after activation at 550 nm. To achieve multicolor labeling and imaging, it is frequently utilized in combination with additional fluorescent dyes such as Cy5 or FITC. Cy3 is also utilized extensively in fluorescent in situ hybridization (FISH), a technique that can identify specific DNA sequences in cells and tissues.

A type of fluorescing dye, Cellbrite fixed 488 is a patented fluorescent dye that identifies the cell membrane and fluoresces orange at 488 nm when stimulated at that wavelength. Since changes in the concurrent motion and interaction of the cell can be observed in real time, this dye is utilized in the tracking and imaging of cells

Additionally, there are numerous fluorescent dyes available for general applications, each with its own set of distinguishing characteristics, for instance. One example of such a protein is green fluorescent protein (GFP), which generates a fluorescent signal internally rather than requiring the introduction of extraneous colors. GFP has established extensive applications in live-cell imaging and tracking owing to its capacity to be genetically encoded and targeted to specific cellular components.

In a similar fashion, when stimulated at 345 nm, the DNA-binding fluorescent dye DAPI (4',6-diamidino-2-phenylindole) emits a blue fluorescence at 358 nm. Due to its ability to offer clear visualization of DNA structure and distribution within cells and tissues, DAPI is frequently utilized in the fields of nuclear labeling and imaging.

A diverse array of functional groups and molecules can be conjugated with fluorescent dyes to enable the targeting and visualization of specific biological processes. By putting calcium ions, mitochondria, or lysosomes to use It is feasible to generate distinct fluorescent probes that correspond to particular modifications of molecules. Researchers employ these exceptional advancements to observe and track dynamic biological processes, such as autophagy, signal transduction in cells, and apoptosis.

However, the implementation of fluorescent dyes is not devoid of challenges. Photobleaching is a significant concern due to the gradual reduction in fluorescence intensity caused by the irreversible destruction of the dye molecule by light. This may reduce the duration and quality of imaging investigations and requires the modification of imaging techniques and settings.

An additional concern arises when multiple fluorescent dyes with identical excitation and emission spectra are utilized, as this may result in spectral overlap and cross-talk. In order to avoid producing false-positive or false-negative signals, this requires the meticulous choice and refinement of fluorophores and targets.

2.3.3 FLUORESCENT FILTER SELECTION AND USAGE

Figure 2.22 Examples of Semrock's filter [45]

It is a robust method to image biological specimens using fluorescence microscopy. This property enables fluorescent dyes and other compounds to generate a fluorescent signal by absorbing light at one wavelength and subsequently emitting light at a longer wavelength. To detect this signal using fluorescence microscopy, specialized filters are utilized to selectively transmit or obstruct different wavelengths of light. This paper will examine and describe the operation of the semrock bandpass filter as well as other types of fluorescent filters.

The principal fluorescent filters utilized in fluorescence microscopy are the excitation filter, the dichroic mirror, and the emission filter. Dichroic mirrors are employed to reflecate excitation light while permitting emission light to pass through. Conversely, excitation filters are utilized to select the optimal light wavelength for stimulating the fluorescent molecule. In order to isolate the fluorescent signal and

remove any residual excitation light, researchers employ emission filters. Then, a filter cube containing these filters is inserted into the light path of the microscope.

In order to selectively permit the transmission of light wavelengths that align with the excitation spectrum of the fluorescent molecule, narrowband filters known as "excitation filters" are constructed. Placing themselves in the intermediate region between the light source and the sample, their purpose is to obstruct all wavelengths of excitation except for the ones specified. Excitation filters are frequently constructed from glass or quartz, and their bandwidths can vary between 10 and 100 nanometers.

Beamsplitters, which are thin layers of metal or dielectric material, are employed to selectively block the transmission of specific wavelengths of light while permitting the transmission of others. The emission light is directed to the detector due to the 45-degree angle at which the excitation light is reflected back toward the sample. Dichroic mirrors are designed with the dual purpose of optimizing the transmission efficiency of the emission wavelength and enhancing the reflection efficiency of the excitation wavelength.

In order to isolate the fluorescent signal, residual excitation light is eliminated using narrowband filters known as emission filters. They are positioned between the sample and the detector in order to restrict the wavelengths of light that reach the detector to those that were actually emitted. Commercially available emission filters often consist of glass or quartz and span a wavelength range of 10 to 100 nanometers.

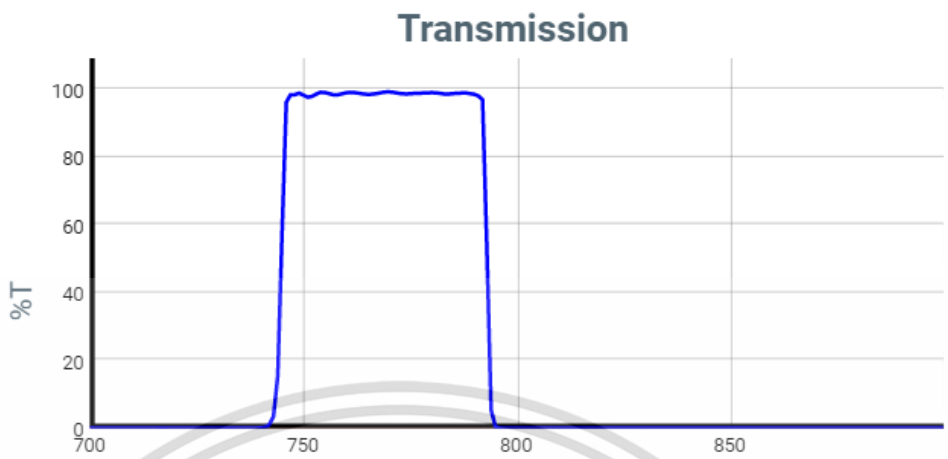

Figure 2.23 Operation range for semrock's ICG filter [46]

An instance of a fluorescent filter, the Semrock Bandpass Filter is a narrowband emission filter that possesses a high transmission efficiency at a specific wavelength. This is produced by applying a thin film of dielectric material to a glass or quartz substrate. The bandpass filter of the Semrock is distinctive due to the abrupt transition from the passband to the stopband.

The Semrock bandpass filter functions by utilizing interference. When light traverses a thin layer, certain wavelengths experience reinforcement, whereas others are nullified, as a result of constructive and destructive interference. By manipulating the refractive index and thickness of the thin film, the bandpass filter of the semrock can be modified to confine transmission to a specific range of wavelengths.

In conclusion, fluorescent filters are utilized by fluorescence microscopy to detect fluorescent signals selectively. To ensure that transmission and detection are limited to the specified wavelengths, an apparatus consisting of emission filters, dichroic mirrors, and

excitation filters is employed. The Semrock bandpass filter is an instance of an interference-based narrowband emission filter designed to optimize transmission at a specific wavelength. In order to develop and optimize fluorescence microscopy investigations, knowing the concepts underlying these filters is essential.

2.3.4 FIBER BUNDLE AND LIGHT SOURCES

Fluorescent dyes are stimulated by light sources that possess appropriate wave lengths. Fluorescence imaging employs a variety of light sources, each of which has advantages and disadvantages.

Mercury lamps are attractive because they convert ultraviolet to visible light. Mercury lamps are utilized in fluorescence microscopy owing to their low cost and widespread availability. They are delicate and require ongoing upkeep. Likewise, Xenon lamps stimulate fluorescence. Xenon lamps emit a comparable spectrum of light to mercury lamps, but they are more durable and require little maintenance. When imaging tasks require a high signal-to-noise ratio, brighter light may be utilized.

Lasers are frequently utilized as sources of excitation due to their capability of being tuned to specific wavelengths. Laser emission of a collimated and monochromatic light beam is ideal for excitation of fluorescent dyes with a narrow tuning. By delivering

stimulation in a more targeted manner, lasers have the potential to improve signal-to-noise ratios and spatial resolution. Lasers are more durable and require less upkeep than traditional lighting.

Figure 2.24 Laser fiber light source example [47]

Frequently, lasers with wavelengths of 488 nm and 789 nm are employed to stimulate fluorescence. A common application of the 488 nm laser in the life sciences is to stimulate dyes such as green fluorescent protein (GFP) and fluorescein isothiocyanate (FITC). The 789 nm laser is frequently utilized in medical imaging to stimulate dyes such as indocyanine green (ICG).

In fluorescence imaging, light delivery from the source to the sample is another prominent application of fiber bundles. Fiber bundles are formed by combining flexible optical fibers; these bundles can subsequently be arranged in an extensive variety of

patterns. Imaging applications that require accurate illumination can benefit from their functionality, which enables them to concentrate light exclusively on particular regions of the material.

Two of the most significant benefits of laser light sources over more conventional light sources are their high intensity and narrow bandwidth. The consistent wavelength of light emitted by a laser source renders it highly suitable for the excitation of fluorescent dyes. The capability for enhanced spatial resolution and rapid frame rates in imaging is attributed to the substantial intensity exhibited by laser light sources.

Additionally, laser light sources are more durable and require less maintenance than conventional alternatives. Mercury lamps and other traditional lighting methods necessitate routine replacement and maintenance. Conversely, laser light sources are more durable and require less maintenance, potentially resulting in long-term cost savings.

Furthermore, due to their compact dimensions and adaptable nature, laser light sources can be effortlessly integrated into established imaging configurations. In order to achieve the intended excitation wavelength using conventional light sources such as mercury lamps, supplementary elements including shutters and filters are frequently required. On the contrary, laser light sources can be easily integrated into novel configurations and are controlled through user-friendly interfaces.

In general, the optimal light source for fluorescence excitation will be determined by the requirements of the imaging application. Mercury lamps and xenon lamps, which are two instances of conventional light sources, are frequently employed due to their widespread availability and affordability. On the contrary, laser light sources are frequently chosen for applications that require increased signal-to-noise ratios or more precise excitation. The utilization of fiber bundles can potentially yield advantages for numerous fluorescence imaging applications by augmenting the precision and adaptability of illumination.

2.3.5 CMOS AND FLUORESCENT IMAGING

Figure 2.25 Zoom-in picture of CMOS sensor [48]

CMOS chips are utilized in medical imaging devices, cellphones, and digital cameras. CMOS sensors convert light into an electrical signal in low light conditions in order to capture both static and moving images. This article will describe the fluorescence image capture process of the CMOS sensor. CMOS sensors consist of columns and rows of pixels. Each pixel contains photodiodes that convert light to electricity. The pixel charge is luminosic. ADCs convert the electrical charges of pixels into digital signals. The image is generated by a DSP using digital signals.

The CMOS sensor's image capture is powered by the photoelectric effect identified by Albert Einstein in 1905. Electrons are struck by photons, which induces the photoelectric effect. Electrons may be expelled from substances by photons, generating electrical charges. Semiconductor photodiodes are utilized by CMOS sensors to convert light into electrical charge.

CMOS sensors exhibit superior speed and efficiency in comparison to traditional imaging technologies. Rapid reading speeds enable CMOS sensors to capture images and videos at high speeds. Due to their low power consumption, CMOS sensors are ideal for battery-operated devices such as smartphones and portable medical imaging equipment. CMOS sensors are utilized to detect fluorophores in fluorescent imaging. Fluorophores emit light after absorbing it. To visualize a molecule of DNA or protein, a fluorophore is introduced. Fluorophores become excited upon absorbing excitation wavelength light. Light with longer wavelengths is detected by the CMOS sensor via excited fluorophores.

Excitation light is required for CMOS sensors to detect the fluorescence of fluorophores. Fluorescence microscopy concentrates and intensifies light at a specific wavelength using laser light sources. This improves the signal-to-noise ratio of the fluorescence image and controls the excitation light. By directing laser excitation light to samples via fiber bundles is a common practice. Light can be transmitted without loss over vast distances using multi-fiber bundles. From fiber bundles, excitation light is focused by means of a lens device. The objective of the microscope gathers and guides the fluorescence of the sample towards the CMOS sensor.

Light sources that utilize lasers are superior for fluorescent excitation. They emit narrow-bandwidth, high-intensity excitation light in order to excite fluorophores selectively and without producing background noise. Imaging with fluorescence improves both sensitivity and specificity. Laser light sources require no calibration or maintenance due to their durability and constancy.

Contemporary imaging is dependent on CMOS sensors. It is possible to explain how electrons respond to photons of light via the photoelectric effect. CMOS sensors are utilized to detect fluorophores in fluorescent imaging. Due to the fact that laser light sources concentrate light, fluorescent microscopy employs them.

CHAPTER 3

METHODOLOGY

This chapter focuses on the review of the newest setup for the construction of the updated model of the **M**inimally-Invasive **O**bject Detection **F**luorescent **I**maging **3**D **Colposcope** (**MOFiE-Colposcope**). This thesis section includes an in-depth method of development on colposcope hardware (minimally-invasive and non-invasive), desktop application programming, mobile deep learning platform, automated 3D software, precancerous detection artificial intelligence, fluorescent computer vision, and support modules (for example, foot switch, shelf, mechanical arm, etc.) respectively.

In this project, we have integrated two commercial endoscopes with customized 3D casings to develop a cost-effective colposcope. Enhancements include three advanced features: 3D modeling facilitated by context-aware layer depth inpainting using open-source software, an AI-based precancerous image classification system trained on the WHO atlas of colposcopy dataset, and fluorescent imaging that combines FITC techniques with a 488 nm excitation laser via a fiber bundle. To validate these innovations, we conducted a series of experiment: hardware distance assessments, a triple evaluation matrix (SSIM,

PSNR, and LPIPS) for the 3D modeling, a confusion matrix for the AI classification model (EfficientNetB0), and visibility experiments using a bandpass filter for the FITC imaging.

For overview summarization of each subsection, the information can be concluded as followed:

COLPOSCOPE HARDWARE: Minimally-invasive and non-invasive models have been developed, both of which developed under monocular design, covered major physical configuration of both equipment.

DESKTOP APPLICATION PROGRAMMING: The core capabilities of the Windows platform, including the connectivity network between each of its sub-components, are explored in detail. This includes an in-depth explanation of the development of internal features, as well as the GUI arrangement and the thought process behind the layout.

DEEP LEARNING ARTIFICIAL INTELLIGENCE (DL/AI): in detailed review of deep learning architecture, the inclusion of dataset analysis is emphasized. This covers the representation of the coding process for training, validating, and testing the model, along with the utilization of preprocessing techniques during machine learning development.

FLUORESCENT COMPUTER VISION: Providing information on the fluorescent imaging module, which offers the capability of fluorescein isothiocyanate emissive detection with 488nm laser excitation.

SUPPORT MODULES: The supplementary components encompass mechanical units, each serving specific functions, electrical devices interfacing with the system through USB ports, and structural components establishing the system's foundational support.

3.1 HARDWARE

3.1.1 MINI-INVASIVE DESIGN

Figure 3.1 comparison between MOFiE-BiM222 design and MOFiE-MoP0135 design

On the first iteration of the MOFiE-Colposcope design, the model was developed with reference to the functionality of the Duke University prototype in 2018. However, following a visit to Siriraj Hospital with senior oncologists, several points of failure were identified due to an engineer-centric design rather than practical medical usability. For instance, the diameter of the original binocular model (BiM130 and BiM222) was calculated based on the maximum elasticity of vaginal expansion, leading to cases where the previous scope model could not physically fit into the canal structure, even with the largest size of speculum. Additionally, there were concerns regarding the Duke-based camera's bulky tube obstructing the oncologists' view, limiting observation to digital images rather than providing organic visibility of the scene and increasing the risk of collision accidents, despite being made of medical-grade stainless steel. To address these issues highlighted by the experts, two versions of the camera were developed, including a minimally invasive and a non-invasive colposcope, both supporting connections to computers and Android devices, while another variant only supports computer display.

Typically, commercial colposcopes are stationary inspection machines designed to visualize cervical structures using visible light from a fixed distance. However, this setup can result in minor missing information during the inspection process, as the view of the images is predetermined in a fixed position without the ability to freely readjust. By reengineering the traditional colposcope into a handheld device with the option for temporary attachment to a movable mechanical arm, more spatial information can be

captured from different angles and distances compared to the conventional approach. Or in alternative, the newly budget model can operate outside mechanical support from the imaging cart and be apply as a standalone device with mobile display.

3.1.2 MINI-INVASIVE COLPOSCOPE MODELS

In the current stage of development, three camera models have been constructed for individual medical carts, each tailored to specific needs. These include a 30-mm diameter binocular colposcope (circular shaft), a 20-mm diameter binocular colposcope (ovary shaft), and a 13.5-mm monocular colposcope (circular shaft), all utilizing advanced 3D image generation techniques. Each model comprises three main parts: a plastic handle, an endoscope case, and a tip cover. The 30-mm model is the largest, featuring components larger than those of the other models, while the 20-mm and 13.5-mm colposcopes share the same handle design with variations in casing diameters, lengths, and tip designs. In terms of material, biocompatibility is a key consideration. The 20-mm and 30-mm models feature a medical-grade ABS plastic handle approved by the FDA, with shafts made from stainless steel 316LVM (low-carbon vacuum melted), ensuring non-toxicity to human biology. For the 13.5-mm colposcopes, still in the prototyping phase, 3D printing has replaced local metal fabrication due to its speed, cost-effectiveness, and flexibility. Currently, the 13.5-mm monocular colposcope utilizes white PLA+ filament from the eSUN manufacturer. As detailed information on the 20-mm and 30-mm

colposcope designs has been documented in previous senior student theses, this thesis paper focuses primarily on the detailed analysis of the 13.5-mm monocular model.

3.1.3 NON-INVASIVE COLPOSCOPE MODELS

While minimally invasive model has image resolution of 1920×1080 pixels non-invasive camera utilizing a web camera CMOS censor with the resolution of 4,096 x 2,160 pixels, twice the active pixel of previous model. As per diameter, the noninvasive model has cross sectional diameter equal to 40 mm with built in LED light source. To increase the usability of the device, ergonomic handle has been designed and print under eSUN PLA+ filament so support the foldability of the machine, hence provided organic adjustment of observing angles.

3.1.4 CAMERA SELECTION

The primary aim of this project is to develop the smallest possible colposcope while retaining all necessary functions without causing compatibility issues with the software. To achieve this objective, a pair of endoscopes was initially purchased from Alibaba to build two prototypes for the system, each with diameters of 20 mm and 30 mm, respectively, designed for commercial use in invasive medical inspections. The selected type of endoscope core is the complementary metal oxide semiconductor

(CMOS) due to its excellent noise immunity, low operating temperature, minimal power consumption, and impressive image resolution. Although various sizes and brands of endoscopes are available, the chosen model for the system is a cost-effective 8-mm diameter version, noted for its disposability, ease of replacement, and suitability for prototyping purposes.

However, as the project evolved to incorporate new fluorescent imaging tasks, it became evident that the previous endoscope model had limitations, particularly in its auto adaptations to optical exposure. Therefore, a new endoscope with modifiable software had to be selected for the 13.5-mm 3D colposcope to ensure the validity of the data obtained for scientific analysis. In the latest iteration, the monocular colposcope (minimally invasive model) is equipped with a 1080p endoscope as the primary CMOS sensor. Meanwhile, for the noninvasive monocular device, a webcam camera has been sourced from the same supplier, featuring an upgraded CMOS sensor with a larger overall design and casing.

3.1.5 3D MODELING

For both of the monocular model of the scope (13.5 mm and 40 mm), all designs were created using Autodesk Inventor software, which allows for simultaneous visualization of the design on-screen and is fully compatible with Ultimaker Cura 5. Once

the design is completed, it can be saved as a Standard Triangle Language (.stl) file in Inventor, which can then be directly sliced into G-code for 3D printing using Ultimaker Cura 5. The production time for each component ranged from 3 to 8 hours.

3.1.6 Hardware design and manufacture

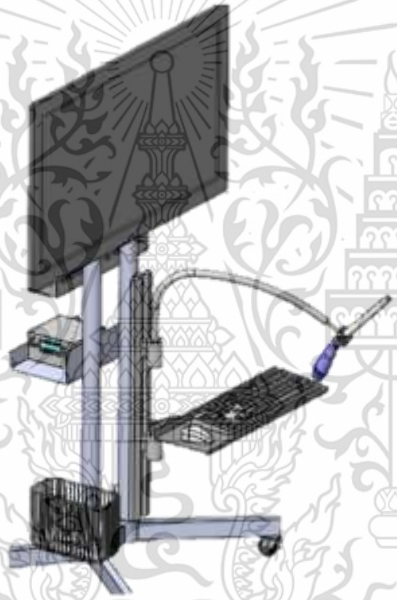

Figure 3.2 3D design for standard MOFiE cart and data acquisition system (DAQ)

The device was crafted in alignment with the anatomical structure of the female vaginal canal, adhering precisely to its characteristics. The vaginal canal is a straight, cylindrical passage terminating in a circular structure known as the cervix, with a depth of 10-15 cm from the vulva. Reflecting these physiological attributes, the instrument has

been designed as a long, perfectly straight tube, equipped with a handle that can be easily grasped with one hand for user convenience.

The casing of the 1.35 cm 3D colposcope consists of three components; two of these pieces serve as the support handle for gripping, while the remaining segment contributes to the structural support of the CMOS camera. With the tubing tip bent at an angle of 20 degrees, the two main elements of the handle can be securely fastened together to ensure a firm grip on the device. In the prototype stage, the section forming the camera barrel is designed as an 18-centimeter-long circular tube with a diameter of 1.35 centimeters. However, the ultimate objective, once the automatic 3D software has completed its task and the equipment has produced the desired results, is to reduce the barrel diameter to one centimeter in the final product.

Regarding the noninvasive devices, the original foldable design of the webcam has been retained, with the addition of a custom tube-shaped handle resembling a flashlight, providing support for a 180-degree operating angle similar to that of the original device. Both the CMOS camera and the PLA handle are secured together using an M10 screw.

3.2 DESKTOP APPLICATION PROGRAMMING

3.2.1 3D COLPOSCOPE WITH DL/AI AND FLUORESCENT IMAGING SOFTWARE

In the previous iteration of the application, two functional user interfaces were incorporated: one for inputting patient information and another for selecting modes. Initially, data was logged by consolidating all input characteristics into a folder name and then depositing all recorded files into a specified directory. However, with the development of the monocular colposcope hardware, a new Python-based desktop application has been developed. The goals of this redesign are to introduce a more efficient data storage approach utilizing SQL programming queries, enhance the graphical user interface (GUI) for a modern look, improve information accessibility through a patient search page, and implement a dashboard for displaying statistically relevant data. The upcoming sections will delve into each software function in greater detail to provide insight into the current state and revisions of the modules.

3.2.2 GRAPHICAL USER INTERFACE (GUI)

The GUI for version 2 of the modulation software was constructed by utilizing the Tkinter library within the main Python code base. The application was developed through a hardcoding approach, resulting in a functional design with a somewhat dated visual presentation. In pursuit of goals centered around introducing new informative windows and enhancing the user experience, new tools have been integrated into the development process. Version 3 of the modulation software has been created using Tkinter Designer

software, which is openly available on GitHub. Tkinter Designer represents a modern approach to Tkinter development, allowing developers to finalize page designs interactively on third-party web applications like Figma and then seamlessly import the finished product directly into Python source code.

3.2.2.1 TKINTER

Python's Tkinter stands as the standard library for crafting graphical user interfaces (GUIs). Leveraging Python alongside the Tkinter toolkit simplifies the creation of GUIs, as Tkinter serves as an object-oriented wrapper for the Tk graphical user interface toolkit, amplifying its capabilities [1].

Tkinter boasts a diverse array of advantageous features. Its cross-platform nature ensures that the same code can seamlessly execute on Windows, macOS, or Linux systems. By harnessing native components of the operating system to generate visual elements, Tkinter-based applications exude a sense of native integration with the platform on which they operate. Despite Tkinter's status as the default Python GUI framework, one common critique revolves around the perceived antiquated appearance of GUIs developed with Tkinter.

Nevertheless, Tkinter remains an appealing choice for GUI development due to its lightweight nature and relative ease of use. Additionally, it boasts a smaller footprint

compared to competing frameworks, making it an attractive option for swiftly constructing functional, cross-platform GUI applications, especially in scenarios where immediate functionality and cross-platform compatibility take precedence over modern aesthetics [2].

3.2.2.2 TKINTER DESIGNER

Tkinter Designer was conceived to streamline the process of developing Python GUIs by leveraging the renowned design tool Figma. This innovative approach simplifies the creation of visually appealing Tkinter GUIs. Tkinter Designer harnesses the Figma Application Programming Interface (API) to analyze design files and automatically generate the requisite code and files needed for the GUI. Notably, even Tkinter Designer's own GUI is designed using Tkinter Designer.

The benefits of utilizing Tkinter Designer are manifold. Its drag-and-drop interface simplifies design tasks, resulting in a faster development cycle compared to traditional methods. Moreover, the end products are more aesthetically pleasing. Tkinter Designer has been released globally as open source under the BSD 3-Clause "New" or "Revised" License and was developed by Parth Jadhav, an Indian developer. The project has garnered significant attention, boasting over 4,800 stars and 452 forks on Jadhav's Github repository page [3].

The execution process of generating Python code with Figma design involves three stages, with varying degrees of user involvement. While some interactions require user input, others are automated. To initiate the process, the user must provide a URL of the completed Figma design as an API token in Tkinter Designer. Subsequently, the application executes a script, generating a Python file and multiple Portable Network Graphic (PNG) files based on the initial design. Throughout this process, Tkinter Designer accesses the Figma database via the provided API to retrieve file data, which is then utilized to generate picture files and Python source code.

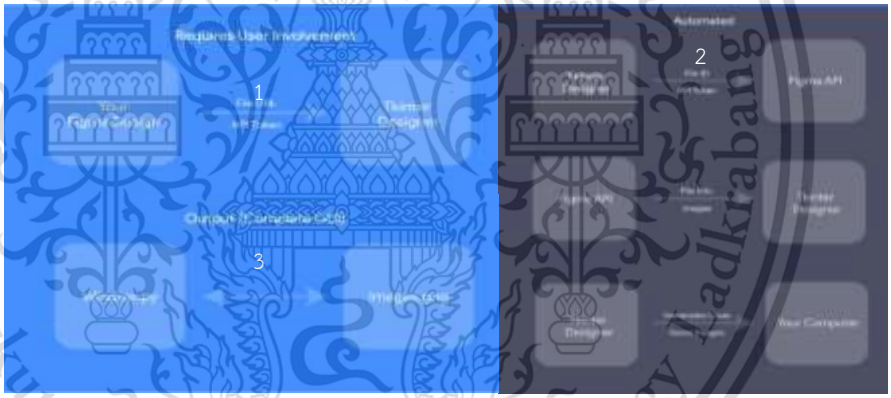

Figure 3.3 Workflow behind the tkinter system [49]

3.2.2.3 FIGMA

Figma is a specialized web application designed for the purpose of generating user interfaces (UI). In 2015, a small group of Google developers established the initiative. The principal objective was to provide developers involved in user interface (UI) projects with

a more adaptable solution, given that team members were dissatisfied with established tools such as Photoshop and Sketch, perceiving them as insufficient for contemporary design endeavors. Figma, an innovative web application, empowers users to accomplish more within a reduced timeframe. Decades of thousands of illustrious designers utilize it, which has been downloaded millions of times. The unparalleled number of features that Figma possesses has contributed to its meteoric rise in popularity. Its forte is the development of wireframes, mockups, and prototypes for digital products and websites [50]. Figma offers numerous advantages, such as its cloud-based infrastructure, availability of a free plan, and easy access to plugins. It also provides real-time collaboration, seamless file sharing, and serves as an all-in-one tool for design, prototyping, and handoffs to software developers. Additionally, Figma offers plugin accessibility [51]. On September 15, 2022, both the Figma and Adobe blogs announced that Adobe will soon acquire Figma [6].

3.3 CONTENTS OF THE SOFTWARE INTERFACES

The previous iteration of the software integrated three distinct operational pages and two interactive windows into a unified interface. The initial window consisted of a data input page where the user was prompted to enter the patient's name and identification number. The subsequent window served as a selection page, directing the

user to the appropriate function based on their choice. After making changes to the design, the third version of the software now includes three interactive pages. The pages consist of a log-in page, a dashboard, a camera selection page, and separate operating pages for each camera function.

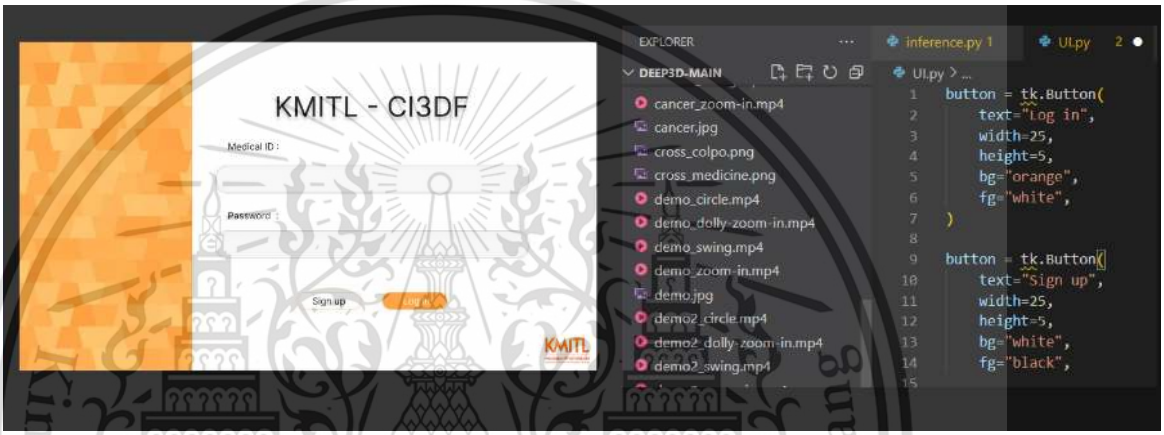

Figure 3.4 design and coding behind new software interfaces

3.3.1 LOG-IN PAGE

The login page adheres to the KMITL color code guidelines, prominently featuring the colors orange and white. At the top of the page, the camera's product name is displayed in text. Below this, users encounter two input fields—one for entering their medical identification and the other for their password. Positioned at the bottom of the page are two buttons. One button leads users to the signup page for the service, while

the other button navigates registered users to the dashboard, serving as the system's central hub.

3.3.2 SIGN-UP PAGE

Upon clicking the sign-up button, users without registered accounts will be redirected to the sign-up page, where they must provide essential personal details for medical staff. These include the user's name, gender, medical ID, medical position, age, and a chosen password. Once these details are successfully inserted into the SQL database, users will gain authorization to commence diagnosis procedures.

3.3.3 DASHBOARD

The program's control panel features five graphs, each presenting different percentages of negatives observed throughout the day, month, and year. Additionally, there are two sections on the window displaying photographs of the first and last instances diagnosed on that day. At the bottom of the window, a bar includes two string displays and four icons enabling users to navigate to the previous page, access information, use the in-application search engine, and exit the program instantly.

3.3.4 SELECTION PANEL

The colposcope serves three primary functions: fluorescent computer imaging, artificial intelligence with deep learning, and three-dimensional video synthesis. Each function is accessible through a single interactive page represented by its corresponding icon. Users can simply click on the symbol to access the desired function.

3.3.5 3D SYNTHESIS DIAGNOSIS

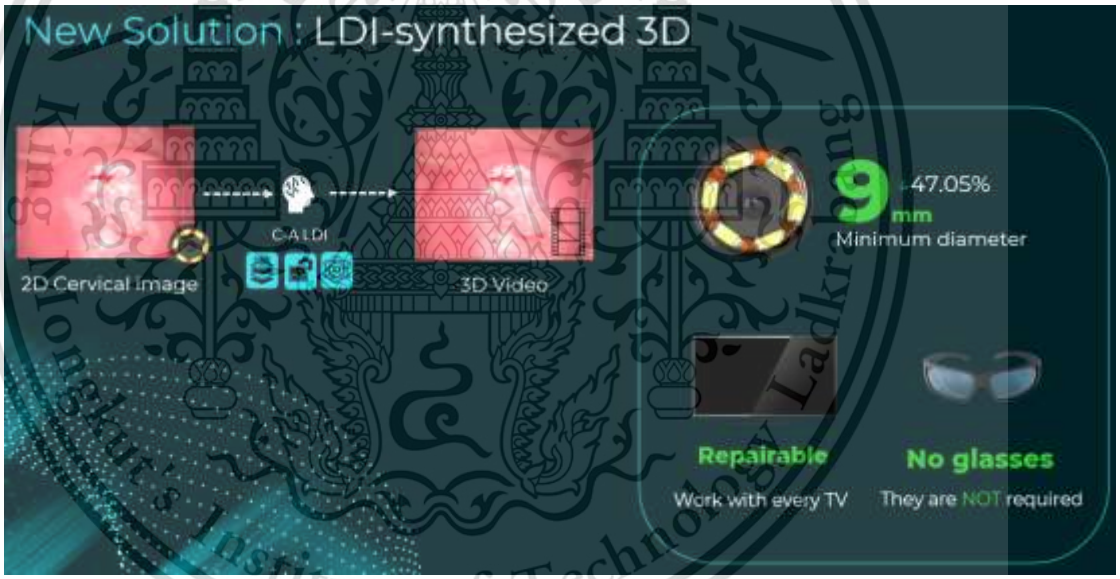

Figure 3.5 Overview for C-A LDI and its advantages

In this section of the display, the screen will be divided into two symmetric rectangular areas: the left area will show a synthesized mp4 video, while the right area will display a real-time image from the connected camera. The video is generated by an automated script that utilizes all four models of artificial intelligence. The original source

code was downloaded from the Github repository of the original developer on Google Colab and then modified. This modification involved removing example inputs that were left in the production folder, addressing a few errors in the deployed code to accommodate updates in the VisPy module, and implementing Linux protocols to clean unused folders and connect the virtual machine to an external virtual database (Google Drive). This allows the synthesized video to be permanently saved and accessed via external operations, as the necessary libraries for the conversion process are limited to the Linux platform rather than Windows, which is the main system deployed.

3.3.6 DEEP LEARNING ARTIFICIAL INTELLIGENCE

To execute this function, the program will employ a real-time version of an OpenCV script equipped with a pre-trained AI model capable of performing instantaneous classification on the cervix. A bounding box will be generated around the exposed region with a label indicating whether it is normal or abnormal. These labels represent the diagnosed class and will always be displayed along with the numerical confidence values generated by the model.

3.3.7 FLUORESCENT COMPUTER IMAGING

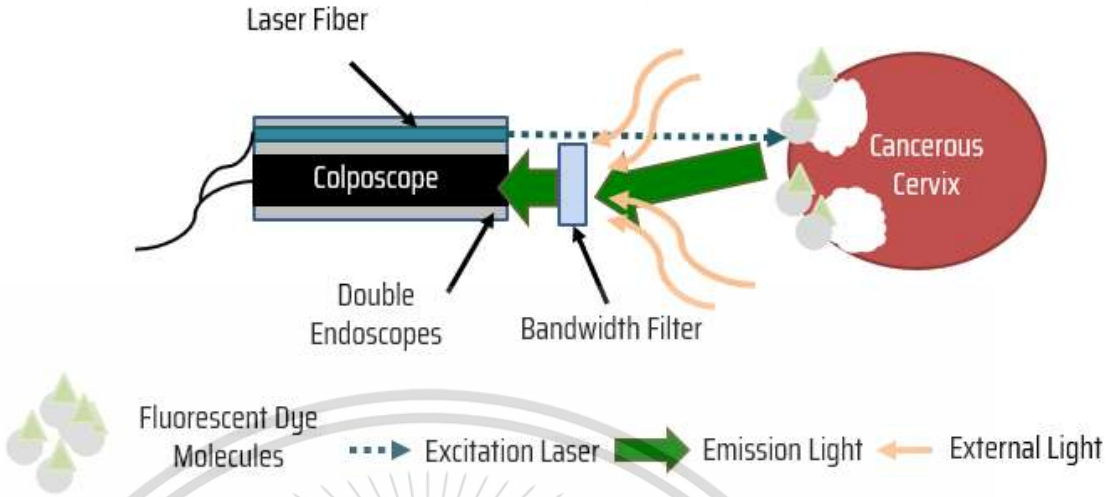

Figure 3.6 diagram behind the fluorescent system

For fluorescence imaging, the program solely presents real-time spatial information captured by the connected camera. This technique relies on exciting a specific frequency within the optical spectrum, resulting in emitted light that can be filtered through an exclusive bandpass filter designed to eliminate unwanted frequencies. This camera mode aims to capture referenced biochemical phenomena and showcase the results on the screen, requiring no additional software for the task.

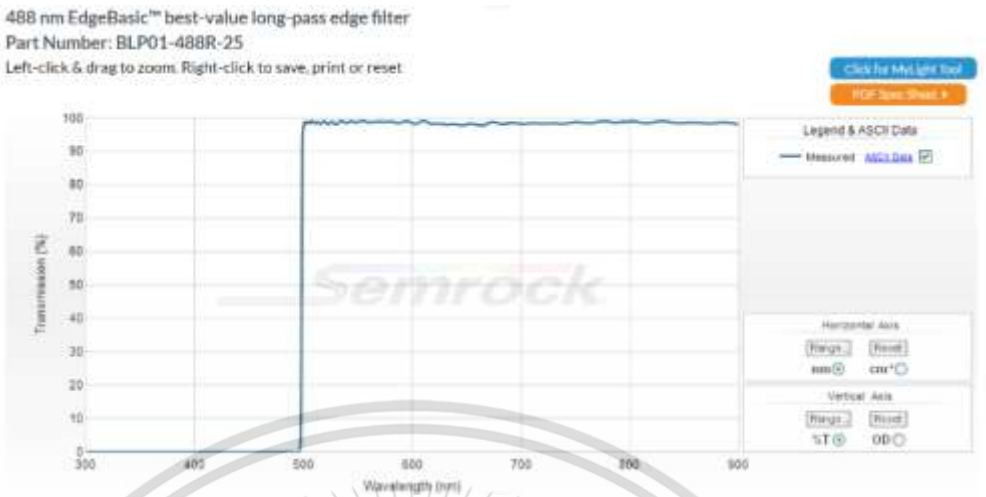

Figure 3.7 The attribute of semrock's filter in the experimentation [52]

3.4 DATABASE

FIGURE 3.8 THE DATA BASE DESIGN FOR SQL DATABASE

The database was built using structured query language (SQL), which stores data in .csv files using table storage structures. In database architecture, both SQL and NoSQL techniques are suitable for data processing, but there are significant operational differences between the two. SQL is the predominant method of data storage due to its

longevity and industry-wide familiarity. However, SQL's fixed row-based table-centric approach may not offer the flexibility users need, making NoSQL techniques more innovative in this regard.

While SQL structures are designed for vertical scalability, requiring additional funding for hardware upgrades and installations as data stores grow, this may not be ideal for larger enterprises. In contrast, NoSQL structures tend to be more efficient in such scenarios. Since the data sizes in the third modulation software's database are relatively modest, the structured approach of SQL architecture would be advantageous due to its speed, compactness, and robust support.

3.5 DEEP LEARNING ARTIFICIAL INTELLIGENCE

In the previous version of the colposcope, specifically the binocular model, the fifth version of the You Only Look Once (YOLO) architecture was employed. YOLO is an object detection algorithm designed for real-time processing of single input images. YOLOv5, developed for regression problems, provides class probabilities of detected objects using convolutional neural networks (CNNs) to recognize objects in real-time. As the name suggests, YOLO requires only a single forward propagation through a neural network to detect objects while simultaneously generating their bounding boxes.

The AI development process for real-time cervical cancer diagnosis can be broadly categorized into stages such as data preparation, model training, model testing, and

integration of the model into the system. However, during evaluation by senior medical personnel at the NRIIS board meeting, it was found that the YOLOv5 model could only distinguish between carcinoma in situ and normal types, which may be obvious to an untrained eye and therefore limited in its real-world impact.

To address this limitation, the focus of deep learning development shifted towards the development of AI with precancerous detection capabilities. In pursuit of this goal, YOLOv5 was replaced by EfficientNetB0, an image classification network capable of tackling more complex problems. While YOLOv5 excels in quick real-time evaluation, the medical evaluation process can afford a few additional processing seconds if higher accuracy can be achieved.

3.5.1 DATA PREPARATION

For the original model of the MOFiE-colposcope, which can distinguish between normal and cancerous classes, this model offers the capability of constructing a bounding box on the cervical image. Two sources of datasets were used for training the model: the colposcopy digital atlas from the World Health Organization (WHO) website and a cervical cancer screening Kaggle competition. The dataset from the WHO website has been categorized into many classes of diagnostic results, ranging from normal to cancerous, and other substantial cervical inflammations, while the Kaggle dataset primarily comprises normal photos. Since YOLOv5 is intended for classification based on the given item, the

region of interest must be labeled prior to input into the network; hence, LabelImg was used to bind the cervical position of the patient to each relevant picture.

As for the second model, only the World Health Organization image has been preprocessed, as the source provides complementary features including patient age, HPV result, and biopsy status, with finer separation of classes including 8 major categories: normal, low grade, high grade, early and advanced cancer, inflammation and cervicitis, squamous metaplasia and ectropion, miscellaneous, and post-treatment. This dataset also contains 25 subtypes with overall 200 cases and 913 images, including normal, atrophy, pregnancy, squamous cell cancer, adenocarcinoma, candidiasis, trichomonas vaginalis, inflammation, ectropion, metaplasia, inflammation and cervicitis, cervical polyp, condyloma, congenital transformation zone, leukoplakia, stenosis of the cervix, post-LLETZ, post-cryotherapy, and post-radiation changes. However, only limited cases were relevant, as there are overall 4 major categories and 5 subtypes that contribute to the task (normal, low grade, high grade, and cancer). Each cases has multiple images stored in non-structural storage which ranges from saline image to lugol iodine and acetic acid.

3.5.2 PREPROCESSING

Among the four preprocessing techniques that have been applied to the dataset, data cleaning and image processing are particularly noteworthy. The Isolation Forest

algorithm is designed to identify anomalies by utilizing binary trees. It is used for data cleaning algorithms. A linear time complexity and a low memory requirement are characteristics of the algorithm, which allows it to function effectively with large amounts of data. K-nearest neighbors is an algorithm that detects anomalies by utilizing binary trees. The algorithm only requires a small amount of memory and has a linear time complexity, making it suitable for processing large amounts of data successfully. as well as principal component analysis, which is a method for reducing the linear dimension of data and has applications in exploratory data analysis, visualization, and data preprocessing. The data is transformed linearly onto a new coordinate system in such a way that the directions (principal components) that capture the most significant variation in the data can be easily identified. This transformation has been applied. Furthermore, in order to carry out additional testing, an algorithm for color conversion is established on the dataset.

3.5.3 MODEL TRAINING

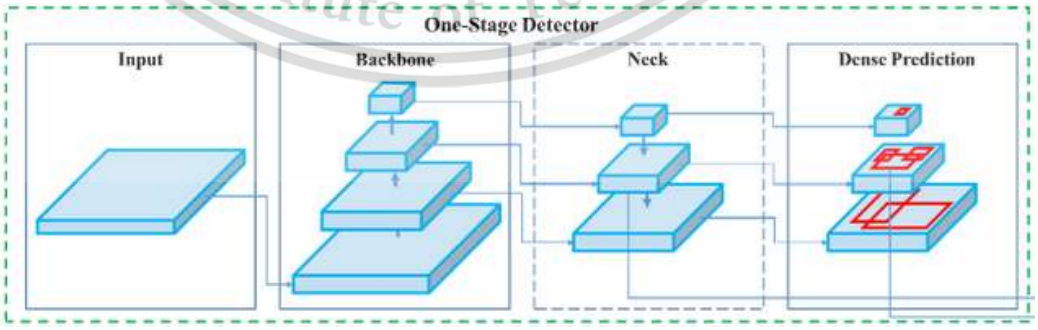

Figure 3.9 Attributes behind the Yolov5 [53]

The labeled dataset has been divided into several smaller training sets, each of which contains unique images for the purposes of training, validation, and testing. Following the completion of the process of organizing the photographs into their respective directories, a Python script that made use of the pre-built Yolov5 package was developed in order to initiate the training procedure. The utilization of confusion matrices in each iteration of the artificial intelligence system was done in order to evaluate the optimal performance of the trained real-time object detection model. This was done to guarantee that the most superior remodeling product was achieved through numerical validation.

In the process of identifying precancerous lesions, a total of 27 models were incorporated into the dataset through a series of iterations. Pretrained models such as EfficientNetB0 to EfficientNetB7, ResNet50, ResNet152, MobileNet, Xception, VGG16, and Inception-resnet-v2 were among those that were included in this category. In addition, a number of bespoke models were developed and tested under conditions that were comparable to those utilized. An example of this would be the investigation of a triple-input model that included three EfficientNetB0 models as feature extractors, in addition to Bi-Gradient Rate Units (Bi-GRU) and a bespoke perceptual network.

3.5.4 Model testing

To evaluate the performance of an artificial intelligence, it is necessary to test its ability to detect patterns in a recently introduced data set. In this specific case, the dataset had already been divided into a subsection prior to the setup process. After selecting several models with high accuracy from the training batches, these models were evaluated using the testing dataset. The output of this particular method is a confusion matrix that provides values for sensitivity, specificity, accuracy, and precision.

3.6 Fluorescent imaging

Four illumination dyes, namely indocyanine green (ICG), fluorescein isothiocyanate (FITC), Sulfo-Cyanine3 (Cy3), and commercial cellbrite-fixed 488, have been prepared to enable access to the fluorescent image using a CMOS camera. All substances, including ICG and FITC, were individually tested in separate experiments. ICG and FITC were tested using a pure solution in the AIRC laboratory at KMITL. Cy3 and cellbrite488 were tested at the Institute for Quantitative Health Sciences and Engineering, Michigan State University. Both substances were applied in vivo on rat colon tissues. Once the dyes were applied, all of the samples were stimulated using the corresponding laser fiber within the appropriate spectrum to activate the emission characteristics of the dye. The CMOS sensor was equipped with two integrated filters: a band pass filter with an average wavelength of 813 nm for near-infrared (NIR) imaging in the ICG experiment, and a band pass filter with

an average open frequency of 516 nm for a group of 488 nm dyes. Both of these products have been manufactured by the Semrock company.

CHAPTER 4

RESULTS

4.1 OVERVIEWS

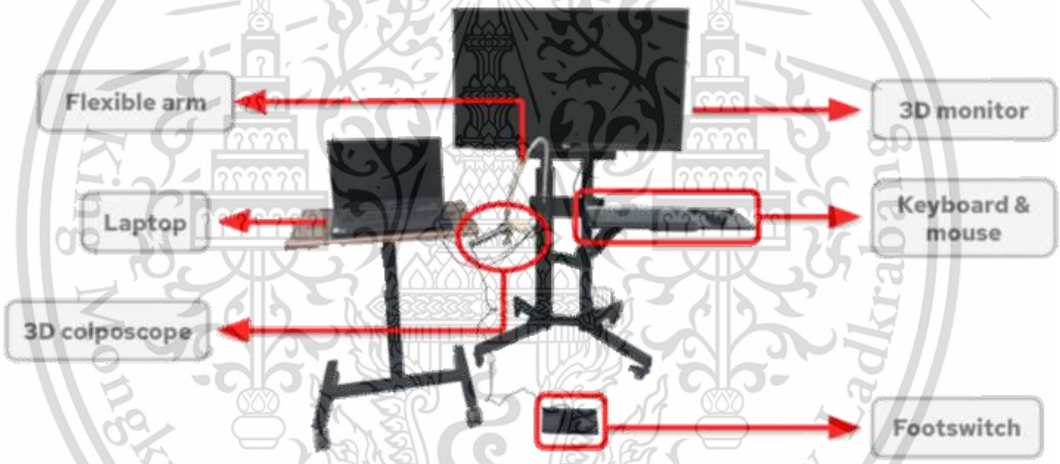

Figure 4.1 Picture of the MOFiE system

In recent years, the field of colposcopy has experienced notable progress due to the emergence of novel technologies and techniques for imaging and diagnosis. One such advancement is the pocket colposcope, a minimally invasive and cost-effective device developed by Duke University. This project draws inspiration from the original concept of the pocket colposcope. In 2018, the pocket colposcope was introduced as a compact

handheld device that offers diagnostic accuracy comparable to traditional colposcopes, but with lower production costs. The objective of this project is to enhance Duke University's pocket colposcope by incorporating revolutionary features such as 3D imaging, instant AI diagnosis, and fluorescent imaging. The results of our research focus on two distinct models of colposcopes: MOFiE-BiM222, which was developed by the 7th batch of KMITL students, and MOFiE-MoP0135, the latest innovation in this group.

MOFiE-BiM222 was developed between 2021 and the first quarter of 2022. It includes older technologies like stereographic polarization 3D imaging and ICG imaging. Integrating two endoscopes with following specification into its system: Specifications:

- Sensor size: 1/9 inch
- Frame rate: 30fps
- View angle: 67 degrees
- Light sensitivity: Automatic
- Focus range: 5 cm - infinity
- Power supply: 5V DC via USB
- Waterproof level: IP68
- Operating temperature: 0 to 70 C
- Resolution: 1920×1080 p

- Lens diameter: 8 mm
- Video format: AVI
- Total length: 1M
- Adjustable LED lighting: 6 light sources

However, MOFiE-MoP0135 incorporates advanced technologies like context awareness layer depth inpainting and FITC imaging. It was developed between mid-2022 and April 2023.The new creation of MOFiE-MoP0135 features updates in four sections, namely hardware, 3D, fluorescent upgrade, and an unchanged AI system from the previous model. The information regarding each system will be provided in the following paragraphs for a concise update.

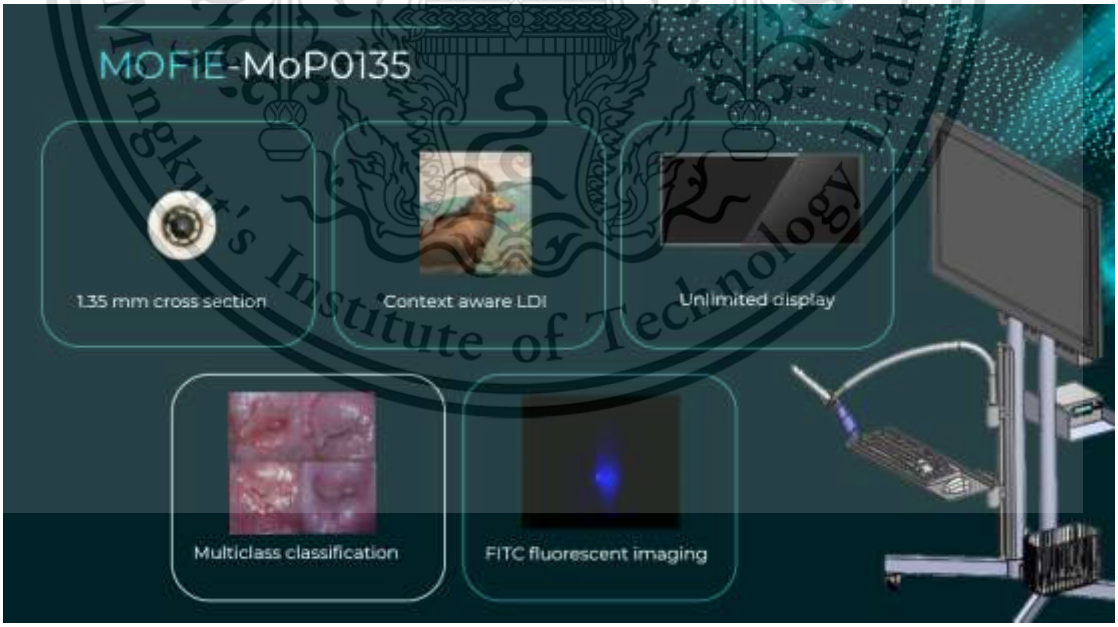

Figure 4.2 brief functionality in MOFiE-MoP0135

4.1.1 HARDWARE UPDATES

The MOFiE-BiM222 is a binocular colposcope that utilizes stereographic polarization 3D imaging to offer a three-dimensional perspective of the cervix. The utilization of polarization imaging glass in the CMOS two-barrel endoscope facilitates the acquisition of distinct images of the cervical tissue, thereby enhancing the precision of diagnostic evaluations. Contrarily, the MOFiE-MoP0135 is a monocular colposcope with a smaller and more manageable design. This innovative design enhances maneuverability during procedures, making it an optimal selection for minimally invasive surgeries. For the non-invasive model, a camera has been developed with a CMOS sensor originated in commercial webcam. This version of colposcope has further focus length hence more suitable for distance imaging.

4.1.2 3D SOFTWARE UPDATES

An important development in colposcopy is the implementation of context awareness layer depth inpainting in MOFiE-MoP0135. This technology utilizes a deep learning algorithm to generate a 3D representation of the cervical tissue by compensating for the absence of depth information. Consequently, this leads to the production of more precise and comprehensive images, thereby enabling enhanced diagnosis and treatment.

On the other hand, MOFiE-BiM222 utilizes stereographic polarization techniques for the purpose of delivering three-dimensional imaging. Although this method is efficient, it necessitates the utilization of specialized glasses (polarization imaging glasses that rapidly switch between horizontal and vertical filters) to perceive the images in a 3D layout. Consequently, this approach becomes less feasible for extended sessions and can cause optical fatigue with prolonged use. In order to assess the quality of 3D images using numerical matrices, three distinct methods have been employed on the device. These methods include the structural similarity index measure (SSIM), peak signal-to-noise ratio (PSNR), and the learned Perceptual Image Patch Similarity (LPIPS).

4.1.3 AI OBJECT CLASSIFICATION UPDATES

Artificial intelligence (AI) is now being utilized in colposcopy to classify and diagnose objects, which is a noteworthy advancement. Utilizing the YOLOv5 algorithm, we have created an artificial intelligence model capable of accurately identifying cervical cancer. Through the analysis of images obtained from both MOFiE-BiM222 and MOFiE-MoP0135, the AI model can swiftly offer a real-time diagnosis, facilitating immediate medical intervention. A total of 27 models were modified and tested for the updated precancerous detection model. These modifications included changes to input types, the

cleaning process, data preprocessing, classes arrangement, architectural customization, and integration of pretrained models.

4.1.4 FLUORESCENT IMAGING UPDATES

Fluorescent imaging is a significant component of colposcopy, and we have assessed the effectiveness of both MOFiE-BiM222 and MOFiE-MoP0135 in this area. MOFiE-BiM222 employs ICG imaging, which is highly proficient in discerning tumor boundaries owing to its exceptional depth of penetration. Nevertheless, MOFiE-MoP0135 utilizes FITC imaging, which offers superior resolution and delivers more distinct images of the cervical tissue. This facilitates more precise diagnosis and formulation of treatment plans.

The research conducted on MOFiE-BiM222 and MOFiE-MoP0135 has shown significant progress in the field of minimally invasive colposcopy technology. Despite utilizing outdated technology, MOFiE-BiM222 still offers substantial capabilities for imaging and diagnosis. However, MOFiE-MoP0135 stands out due to its advanced technology and design, which enables it to provide highly precise and detailed imaging. As a result, it is a more practical option for conducting minimally invasive diagnoses. Furthermore, the combination of fluorescence imaging and object categorization using artificial intelligence enhances the accuracy of diagnosing and treating cervical cancer. The technological

advancements in colposcopy are expected to lead to enhanced patient outcomes and more streamlined therapies. Samples of indocyanine green (ICG) and fluorescein isothiocyanate (FITC) solutions were prepared to assess their visibility when combined with a sample of Sulfo-cyanine3 and CellbriteFix488, which were used to stain freshly prepared rat colon tissue in vivo.

4.2 IN DEPTH RESULTS

4.2.1 3D PROGRESSION FROM MOFIE-BIM222 TO MOFIE-MOP0135

Figure 4.3 the algorithm and the result from C-A LDI synthesis

MOFiE-BiM222, the binocular minimally invasive colposcope, was an innovative invention developed by the seventh cohort of biomedical engineering students at KMITL in the field of gynecological imaging. By employing polarization imaging and glasses, it implemented the principles of stereoscopic 3D imaging. Colposcope images were captured by two endoscopes placed side-by-side and superimposed on a 3D television to represent two distinct perspectives. Following this, the polarization glasses were utilized to perceive the images in three dimensions.

Figure 4.4 Comparison of C-A LDI to other method in 3D synthesis history

Stereoscopic three-dimensional imaging is based on the combination of binocular vision functions, which empowers humans to perceive depth. Two cameras are positioned within the metal casing of MOFiE-BiM222 to replicate the movement of the eyes. By superimposing the images captured by these cameras, the illusion of depth is produced. This methodology may be referred to by various names, such as Multi-View Stereo (MVS)

or Multi-Perspective Imaging (MPI), but both are synonymous with the underlying principle utilized in contemporary iPhone cameras—which empower high-end mobile phones of the most recent generation to capture depth images.

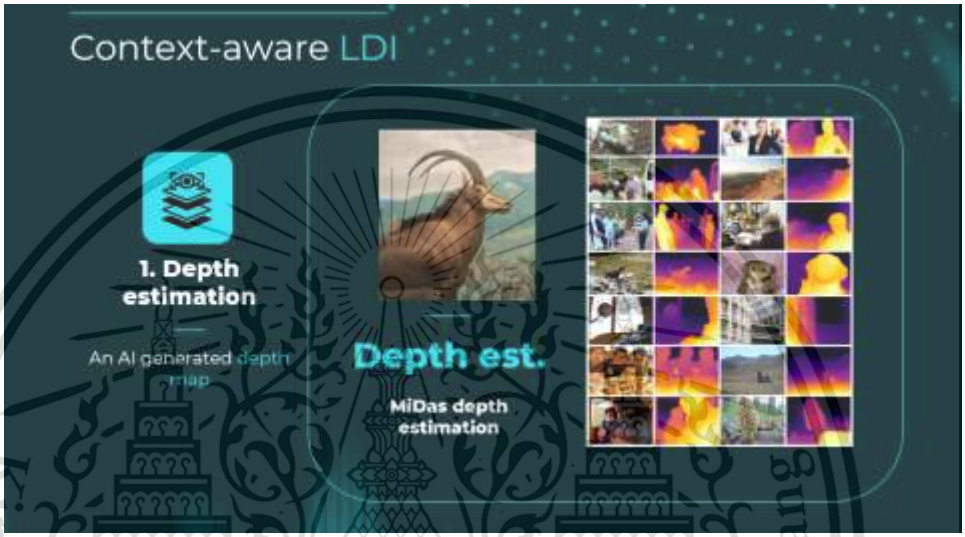

Figure 4.5 Overview of depth estimation process in C-A LDI

Polarization imaging was employed in MOFiE-BiM222 to partition the images acquired by individual endoscopes. By positioning the polarization filters in front of the endoscopes, the light was divided into two distinct polarizations. Following the superimposition of the two polarized images with polarization glasses, the observer was able to discern the three-dimensional image.

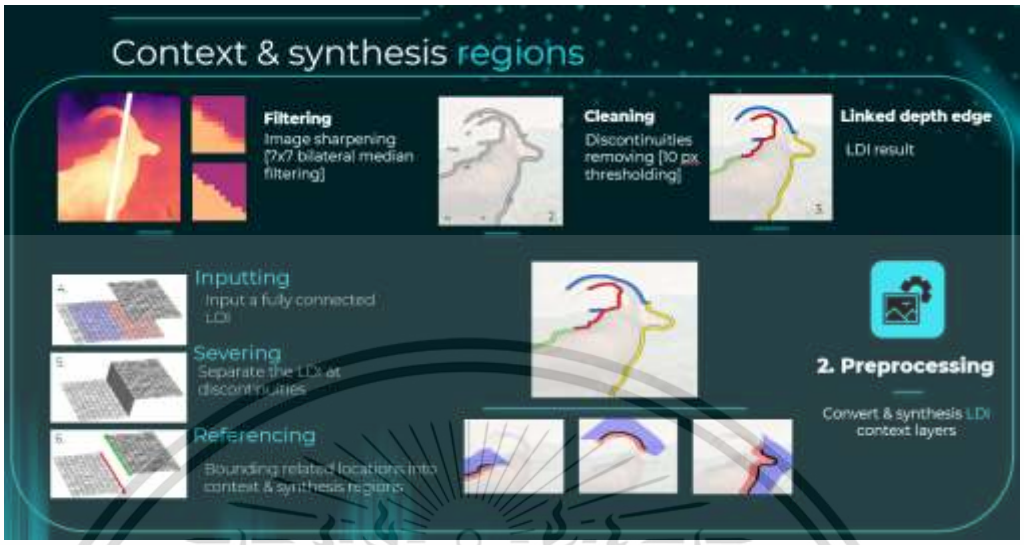

Figure 4.6 Overview of image pre-process in C-A LDI

Although groundbreaking, the MOFiE-BiM222 had a number of limitations. Certain users experienced vertigo due to the application of polarization glasses, while the hardware utilized in the system had been discontinued, thereby complicating its repair. Additionally, the operational necessity of physical glasses rendered the system impractical for extensive implementation. In order to surmount these constraints, the MOFiE-MoP0135 was devised. It is a monocular colposcope that employs Context-Aware Layered Depth Inpainting, a novel technology. The research paper "3D Photography Using Context-Aware Layered Depth Inpainting" by Meng-Li Shih et al. serves as the foundation for this technology.

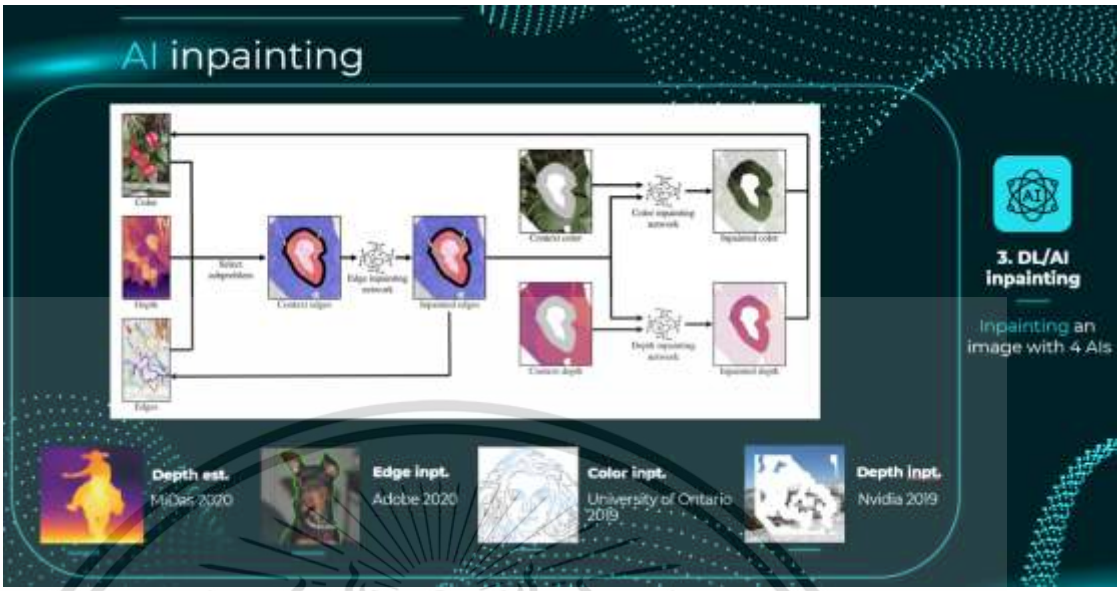

Figure 4.7 Overview of inpainting process in C-A LDI

A computer vision technique, Context-Aware Layered Depth Inpainting, produces a three-dimensional image through the deduction of depth information from a solitary two-dimensional image. The algorithm accurately infers depth information by considering contextual information present in the image. The technology eliminates the requirement for two cameras, polarization filters, or glasses in order to generate a three-dimensional image. As an improvement from MOFiE-BiM222, MOFiE-MoP0135 does not necessitate the use of physical glasses; furthermore, its hardware is easily accessible for large-scale fabrication. However, unlike the previous model, the technology is not yet capable of operating in real time; this represents a limitation.

In contrast, MOFiE-BiM222 and MOFiE-MoP0135 are both groundbreaking innovations that seek to transform gynecological imaging through the integration of essential technologies, including gate-way biopsy and colposcopy, onto a single device.

MOFiE-BiM222 implemented stereoscopic 3D imaging principles by employing polarization filters and glasses. In contrast, MOFiE-MoP0135 generates 3D images from a single 2D image through the utilization of Context-Aware Layered Depth Inpainting. As a result, repairs became feasible and production became scalable, eliminating physical constraints such as dizziness and optical fatigue that hindered the user's ability to use continuously. Therefore, it can be substantiated that MOFiE-MoP0135 exhibits considerable benefits in comparison to MOFiE-BiM222 and MOFiE-BiM130, the primary and secondary models, respectively. Nevertheless, a notable drawback of this model is its lack of real-time functionality, which requires attention. (While both preceding versions operate in real time, MOFiE-MoP0135 requires three to five minutes to load and produce 3D images.)

The testing outcome, which comprised three algorithmic evaluations (SSIM, PSNR, and LPIPS) with respective ranges of 0.9577, 39.7563, and 0.0084, further validates the enhanced quality. Each of these images exceeds the average human perception threshold by >90, >30db, and <0.1, respectively, and can be perceived indistinguishably from non-synthesis images in natural environments.

TABLE 4.1: EVALUATION RESULT OF CA-LDI IN MOFIE-MOP0135

Method	*Minimum*	*Maximum*	*IDTH* threshold*	*Average results*
SSIM	-1	1	>0.9	0.9577
PSNR	<10db	-	>30db	39.7563
LPIPS	1	0	<0.1	0.0084

**Indistinguishable to human eyes*

4.2.2 HARDWARE PROGRESSION

MOFiE-BiM222 and MOFiE-MoP0135 are two distinct colposcopy models that share similar hardware characteristics but are otherwise quite dissimilar in appearance, construction, and operational attributes. MOFiE-BiM222 is a binocular model featuring a metal casing and a medical-grade plastic handle with oval-shaped cross-sections measuring 22 mm. In contrast, MOFiE-MoP0135 is a minimally invasive colposcope constructed entirely of medical-grade plastic with a circular cross-section measuring 13.5 mm.

Figure 4.8 Comparison of each MOFiE colposcope model

The incorporation of metal into the design of MOFiE-BiM222 provides it with strength and longevity; however, it is over twice as heavy as MOFiE-MoP0135, which is composed entirely of medical-grade plastic. The disparity in mass between the two iterations may have a significant bearing on the physician's proficiency when operating the apparatus. As a result of MOFiE-MoP0135's significantly reduced weight in comparison to two preceding models, the inspector who is expected to use the device for the duration of workdays experiences fewer muscular strains. In contrast, the MoFiE-BiM222 has the same weight as smaller dumbbells, which may present difficulties for use cases lasting between 4 and 8 hours. Additionally, the previous design failed to account for ergonomics, which resulted in increased pressure on the user from the elbows to the shoulder, which could potentially lead to long-term injury. Incorporating this updated feature would constitute a significant improvement over the previous design.

The patient is safer as an additional benefit of the MOFiE-MoP0135's design incorporating medical-grade plastic. A long metal pipe that penetrates the vaginal structure during an accident could cause significant tearing and injury, which could result in infection and subsequent surgical intervention. As an alternative, impact with a plastic barrel could, at most, result in minor injuries. Therefore, plastic is a safer material to incorporate into the MOFiE-MoP0135, particularly in light of the device's primary function.

In addition to shifting the center of gravity towards the user to alleviate previous weight distribution issues in the design, MOFiE-MoP0135 reduces the excessive pressure that strikes the user. The ergonomic design of this device has the potential to mitigate discomfort and pain, thereby potentially enhancing the physician's operational efficiency and precision. Additionally, the incorporation of plastic into the design of MOFiE-MoP0135 results in reduced manufacturing costs, which enhances its compatibility with the device's scalability.

In contrast, the colposcope design conventionally consists of a stationary inspection apparatus that can, from a specific distance, discern cervical structures through the utilization of a beam of visible light. In contrast, the mini-invasive design of MOFiE-MoP0135 permits the acquisition of a greater quantity of spatial information from various distances and angles in comparison to the conventional method. The MOFiE-MoP0135 colposcope is one of three camera models that are specifically designed for each medical cart. The remaining two models consist of a binocular colposcope with a 30-mm diameter

and ovary shaft (MOFiE-BiM130 and MOFiE-BiM222, respectively). The 30-mm model is the most sizable among the group due to the fact that every component is larger than that of the other models. In contrast, the 20-mm and 13.5-mm colposcopes have similar handles but feature distinct casing diameters, lengths, and tip designs.

Figure 4.9 Image from the MOFiE-MoP0135 compared to iphone camera

The sole drawback observed in the current prototypes of the MOFiE-MoP0135 is its comparatively shorter barrel length in relation to other models. Measuring 15 meters in length, this device has a shorter barrel than the 20 meters of the other minimally invasive colposcopy instrument. This is because the prototyping of the device's casing is beyond the capabilities of the 3D printer utilized by the device. Due to the lower printing resolution of the cheaper model, it is more difficult to print 20 cm long tubes with uniform interior holes than 15 cm tubes with the same characteristic (it does require multiple

attempts for the machine to function properly). Additionally, the smallest theoretical version achievable with the current endoscope is 9 mm wide (8 mm colposcope with 1 mm thin casing tube). However, due to the printing resolution, it is not feasible to fabricate such a specialized device using the equipment in our laboratory without causing damage or outsourcing.

By capitalizing on advancements in 3D printing technology, it is presently feasible to fabricate an additional MOFiE-MoPx09 model.

In regards to the image quality of the minimally invasive model (MoP0135), a test was performed on an imaging rail using a replica to assess the practical operating range of the device. During non-invasive testing, the most effective distances ranged from 0 to 6 cm from the vaginal entrance. Under this setup, the image quality is considered average, as the cervix is visible to the camera. However, the observed patterns are not as good as those obtained with the exclusive non-invasive camera that was tested (MoN0). At a distance of 6 cm, the MoP0135 is able to capture cervical imaging, although the quality is reduced because the sensor is designed for a focus distance of 4 cm. This pattern consistently occurred within the range of 6 – 8 cm, with the cervix becoming predominantly dark at 9 cm, showing no coherence in the micro-epithelial pattern.

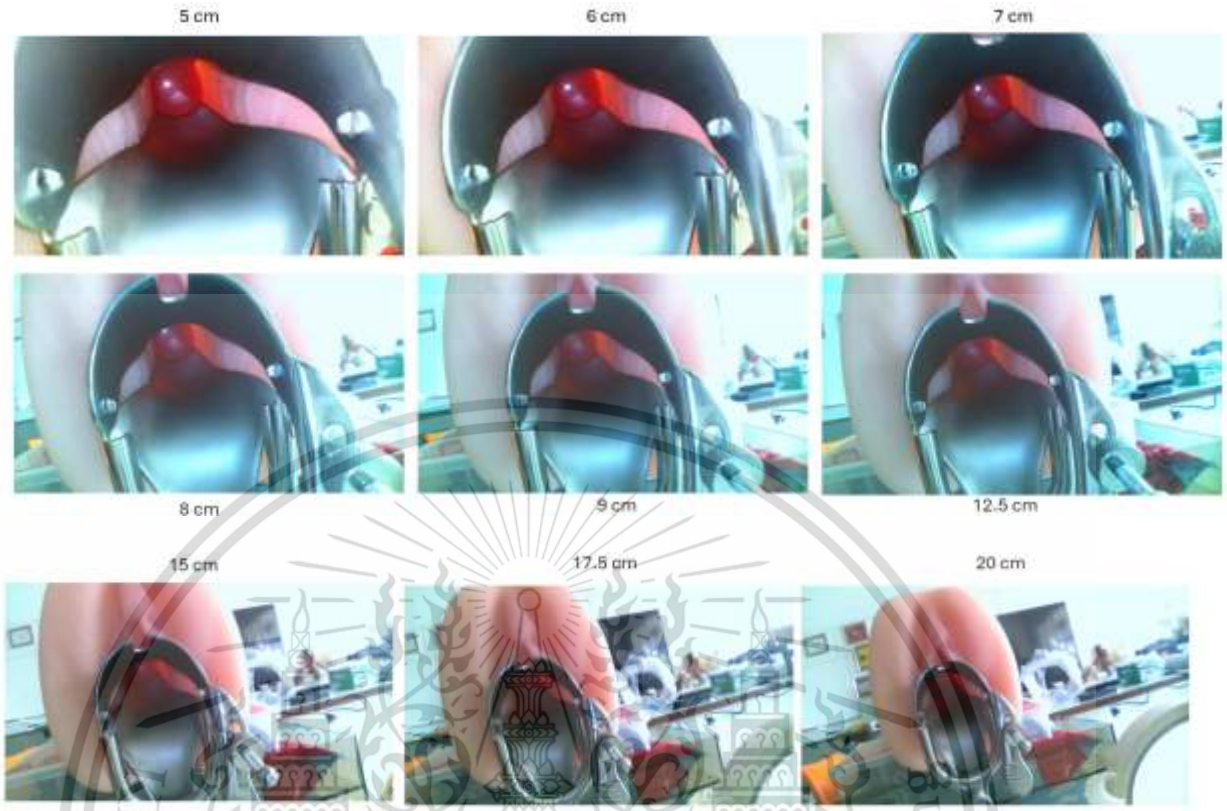

Figure 4.10 Imaging result of MoP0135

The non-invasive model (MoN0) was used in the same experiment, using the same setup and arrangement. The MoN0 device has the capability to capture the visible epithelial pattern on the cervix from a distance of 5 – 9 cm, which exceeds the 8 cm limitation of the MoP0135 model. Additionally, it is capable of observing cervical images at a distance of 9 – 12.5 cm with moderate quality. Therefore, the device outperforms its

alternative in terms of image quality, pixel resolution, and operational distance, exhibiting a significant improvement of 208% in comparison.

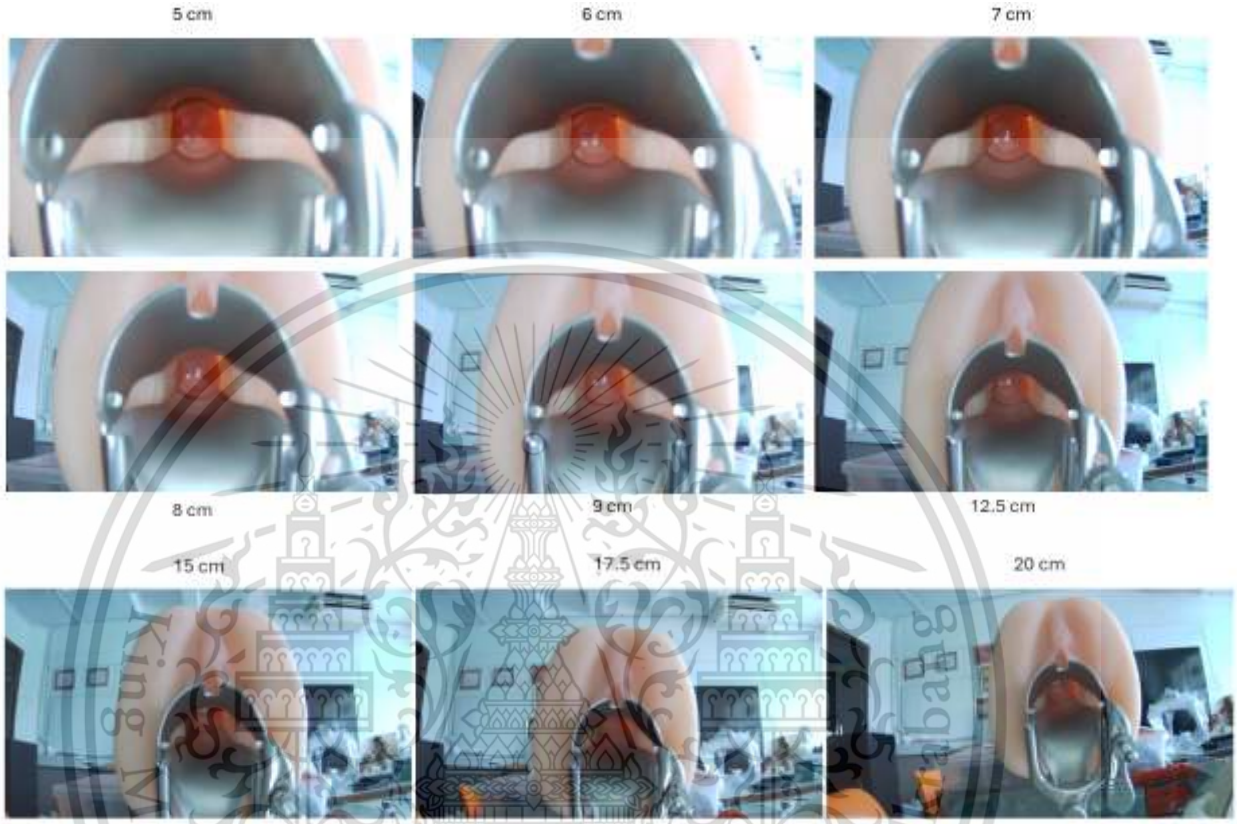

Figure 4.11 Imaging result of MoN0

When directly comparing both models, at a distance of 5 cm which is the closest distance MoP0 can perform, MoP0135 has extremely clear edges on the nearest vaginal surface instead of the target region. This results in a red blob with little epithelial pattern, leading to the conclusion that the quality is of medium resolution due to the fixed focus. When compared to MoN0 at the same distance, the CMOS originated from a webcam has a longer focus length. As a result, the device captures more detailed images of the cervix compared to the vaginal pattern. When the MoP0135 image reaches a length of 12.5 cm,

it becomes predominantly dark and the visibility of the cervical area is almost nonexistent. On the other hand, the MoN0 image is still capable of capturing some of the imaging data, although the quality is lower.

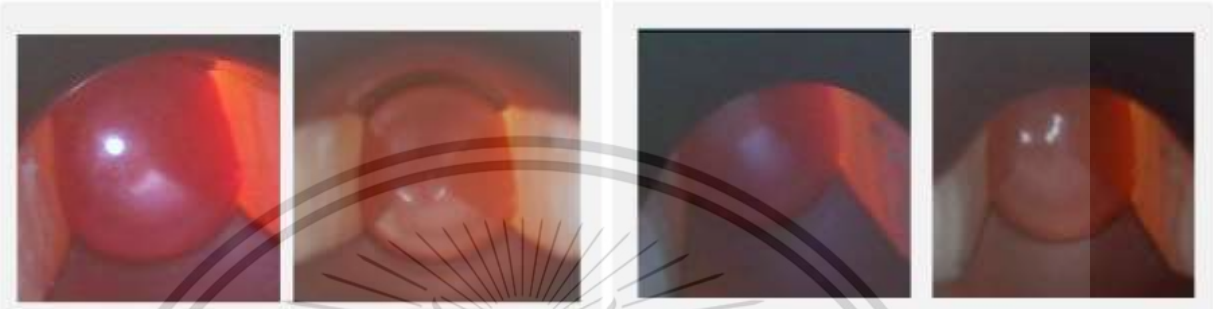

Figure 4.12 Comparison of MoP0135 and MoN0 at 5 cm (left) and 12.5 cm (right)

An experiment was conducted on MoP0135 to obtain internal images using invasive sampling. The images were captured at two different distances: 3 cm and 6.5 cm. Both arrangements produce high-quality images, but the image quality of MoP0135 with a 3 cm insertion cervical detail is slightly better than M0N0 due to improved LED scattering. However, the overall image quality is limited by the near focus length. Therefore, when the CMOS sensor is positioned at a distance of 6.5 cm from the cervix, it becomes closer and achieves optimal focus. As a result, the image quality improves significantly, allowing it to capture the scratch pattern on the cervix, a capability that previous models lacked.

Figure 4.13 Internal image of MoP0135 at -3 cm (left) and -6.5 cm (right)

4.2.3 AI STATUS

Model	Confusion Matrix				Calculation				
	TP	FP	TN	FN	Sensitivity	Specificity	Accuracy	Negative Predict Value	Precision
1	46	4	11	31	0.920	0.260	0.620	0.733	0.597
2	41	9	26	16	0.820	0.620	0.728	0.743	0.719
3	37	13	32	10	0.740	0.760	0.750	0.711	0.787
4	32	18	37	7	0.640	0.840	0.734	0.673	0.823
5	29	21	36	8	0.580	0.820	0.691	0.632	0.784
6	22	28	34	8	0.440	0.810	0.609	0.548	0.733
7	43	7	22	20	0.860	0.520	0.707	0.759	0.683
8	35	15	17	27	0.700	0.390	0.553	0.537	0.565
9	26	24	34	8	0.520	0.810	0.652	0.586	0.765
10	35	15	27	15	0.700	0.640	0.674	0.643	0.700

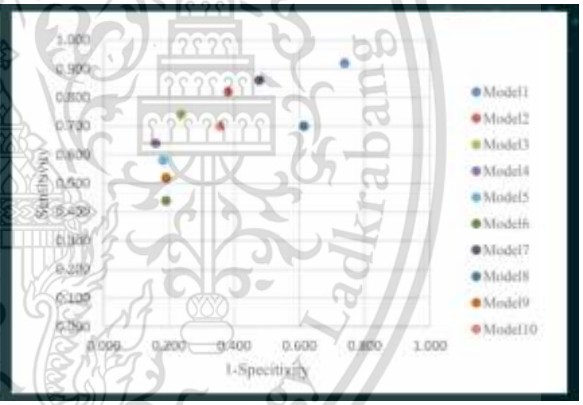

Figure 4.14 Result for AI process for object classification

The results of the study indicated that the application of YOLOv5 AI to the detection of cervical cancer using the two datasets was only marginally successful; further training is necessary before it can be utilized in practice. For the preliminary AI training, the 'Intel & MobileODT Cervical Cancer Screening' Kaggle competition dataset was utilized; it comprised 8,734 cervical images, all of which were of the normal type. A range of

abnormal cervical images, totaling more than 250, were extracted from the WHO dataset in order to supply the study with such images. However, only 25–50 images were devoted to cervical cancer in the WHO dataset; the remainder depicted intraepithelial lesions of varying grades. In order to address the issue of the unbalanced dataset, two methodologies were implemented: batch selection and oversampling through data augmentation.

A sequence of training exercises commenced subsequent to the generation of a fresh set of 914 samples, which comprised 492 normal images and 423 abnormal images supplemented from the initial 50 inputs. Within this results section, ten of the highest quality batches were chosen as the analytical boundary target. The confusion matrix indicated that the final prediction was influenced by a number of random factors. With respect to this subject, the model with the highest sensitivity (0.62) exhibited below-average specificities (0.26), whereas the model with the lowest specificities (0.84) demonstrated superior performance. Consequently, the obtained values are inadequate for pragmatic implementation, and further training is necessary to enhance the model for prospective utilization in the MOFiE-colposcope.

In general, the outcomes indicated that YOLOv5 AI exhibits promise in the detection of cervical cancer utilizing the two datasets; however, further development is required to enhance the model's precision and specificity. In order to ensure accurate and

dependable results, the study also emphasizes the significance of training AI models in medical image analysis with balanced datasets.

For precancerous lesion detection, six categories of adjustments have been applied to the dataset via 27 variations of the models, inputs, and groups, including input types, the cleaning process, data preprocessing, class arrangement, architectural customization, and integration of pretrained models. The initial evaluation was conducted to validate the performance of three feature extractors with Bi-Gradient Rate Units (Bi-GRU) and a custom perceptual network, which represented the state-of-the-art architecture in 2023. This custom model required three-phase inputs of Lugol iodine (Li), acetic acid (A), and normal saline (S) to classify four classes of lesion stages: Negative for Intraepithelial Lesion (NILM), Low-Grade Squamous Intraepithelial Lesion (LSIL), High-Grade Squamous Intraepithelial Lesion (HSIL), and Squamous Cell Carcinoma. In this experimental stage, the state-of-the-art model was tested, followed by the installation of a few pretrained models to evaluate Li images with four classes separation, including ResNet50 and a single EfficientNetB0, all of which returned insufficient testing accuracies of 40%, 24.45%, and 42.85%, respectively.

TABLE 4.2: PRECANCEROUS DETECTION RESULTS WITH MULTIPLE FEATURE EXTRACTORS

Input	Model	Train(%)	Val(%)	Test(%)	Classes	Arrangement
Li,A,S	3EfB0 + GRU + CustomNet	79.59	60	**40**	4	N,L,H,C
Lugol	Resnet50	99.18	44.44	**24.45**	4	N,L,H,C
Lugol	EfficientNetB0	96.23	85.71	**42.85**	4	N,L,H,C

Note: N = Negative for intraepithelial lesion (NILM), L = Low-Grade Squamous Intraepithelial Lesion (LSIL), H = High-Grade Squamous Intraepithelial Lesion (HSIL), C = Squamous cell carcinoma | Li = Lugol's iodine, A = Acetic acid, S = Normal Saline

The dataset was preprocessed by applying a set of cleaning algorithms, including k-nearest neighbor (KNN), isolation forest (IF), and principal component analysis (PCA), before feeding the image into the efficientnetb0 network. This preprocessing step was performed after comparing the performance of multiple feature extractors with a single model architecture using a limited input (Lugol's Iodine). In this experiment, the IF algorithm did not detect any anomalies in the image. However, both the KNN and PCA algorithms identified 4 different anomalies each, resulting in a total of 8 anomalies. Despite excluding these outliers, there was no significant improvement in the final accuracy. In fact, the PCA cleaning process decreased the accuracy by 14.28%, which corresponds to a 33.33% reduction in performance.

TABLE 4.3: PRECANCEROUS DETECTION RESULTS WITH CLEANING ALGORITHM

Model	Cleaning algorithm	Anomaly	Train(%)	Val(%)	Test(%)	Classes	Arrange-ment
EfficientNet B0	KNN	4	97.96	42.86	**42.85**	4	N,L,H,C
EfficientNet B0	IF	0	-	-	-	-	-
EfficientNet B0	PCA	4	96.23	71.43	28.57	4	N,L,H,C

Note: N = Negative for intraepithelial lesion (NILM), L = Low-Grade Squamous Intraepithelial Lesion (LSIL), H = High-Grade Squamous Intraepithelial Lesion (HSIL), C = Squamous cell carcinoma | KNN = K-Nearest Neighbor, IF = Isolation Forest, PCA = Principal Component Analysis

In order to enhance the precision even more, one of the strategies that has been tested is the reorganization of the class. In this phase, instead of dividing the cases into four separate classes, the class has been categorized into low risk and high risk groups. This experiment tested four different arrangements. The first arrangement classified NILM and LSIL as low risk, while HSIL/Cancer were classified as high risk. In the second batch, NILM has been categorized as low risk, while LSIL, HSIL, and cancer have been grouped together as high risk. The final categorization groups NILM and LSIL together in the low-risk category, while HSIL and Cancer are placed in separate categories. Due to the superior

performance of the N/L + H/C arrangement, the same approach has been implemented for saline input, resulting in the highest testing accuracy of 85.71% among all adjustments.

TABLE 4.4: PRECANCEROUS DETECTION RESULTS WITH ARRANGEMENTS

Input	Model	Train(%)	Val(%)	Test(%)	Classes	Arrangement
Lugol	EfficientNetB0	98.11	85.71	71.42	2	N/L + H/C
Lugol	EfficientNetB0	98.11	42.86	57.14	2	N + L/H/C
Lugol	EfficientNetB0	16.98	14.29	14.28	3	N/L + H + C
Saline	EfficientNetB0	90.57	71.43	85.71	2	N/L + H/C

Note: N = Negative for intraepithelial lesion (NILM), L = Low-Grade Squamous Intraepithelial Lesion (LSIL), H = High-Grade Squamous Intraepithelial Lesion (HSIL), C = Squamous cell carcinoma

After identifying the optimal arrangement and input, 13 architectural models were tested on the same setup to determine the most optimal model. The neural networks that have been chosen are ResNet50, MobileNet, VGG16, Xception, EfficientNetB1 – B7, inception-resnet-v2, and ResNet152. Although some models may have comparable performance, none of them surpass the accuracy of EfficientNetB0. While there are models with the same accuracy, they require more computational power, such as EfficientNetB4-B7, which does not meet the selection criteria.

TABLE 4.5: PRECANCEROUS DETECTION RESULTS WITH VARIOUS ARCHITECTURE

Input	Model	Train(%)	Val(%)	Test(%)	Classes	Arrangement
Saline	ResNet50	75.75	71.43	-	2	N/L + H/C
Saline	MobileNet	69.81	85.71	71.42	2	N/L + H/C
Saline	VGG16	75.47	85.71	-	2	N/L + H/C
Saline	Xception	58.49	85.71	-	2	N/L + H/C
Saline	EfficientNetB1	81.13	57.14	-	2	N/L + H/C
Saline	EfficientNetB2	86.79	57.14	-	2	N/L + H/C
Saline	EfficientNetB3	75.47	57.14	-	2	N/L + H/C
Saline	EfficientNetB4	81.13	71.43	-	2	N/L + H/C
Saline	EfficientNetB5	66.04	71.43	-	2	N/L + H/C
Saline	EfficientNetB6	77.36	71.43	-	2	N/L + H/C
Saline	EfficientNetB7	67.92	71.43	-	2	N/L + H/C
Saline	inception-resnet-v2	58.49	57.14	-	2	N/L + H/C
Saline	ResNet152	62.26	71.14	-	2	N/L + H/C

Note: N = Negative for intraepithelial lesion (NILM), L = Low-Grade Squamous Intraepithelial Lesion (LSIL), H = High-Grade Squamous Intraepithelial Lesion (HSIL), C = Squamous cell carcinoma

During the final testing phase, the input image is transformed into grayscale prior to advancing in the training process. The accuracy of the saline image has decreased compared to the previous iteration, while the grayscale acetic image has maintained the same accuracy as the saline image, with no adjustment, at 85.71%.

TABLE 4.6: PRECANCEROUS DETECTION RESULTS WITH IMAGE PROCESSING

Input	Model	Cleaning method	Train	Val	Test	Classes	Arrangement
Saline	EfficientNetB0	Greyscale	86.79	71.43	57.14	2	N/L + H/C
Acetic	EfficientNetB0	Greyscale	84.43	71.43	85.71	2	N + L/H/C

Note: N = Negative for intraepithelial lesion (NILM), L = Low-Grade Squamous Intraepithelial Lesion (LSIL), H = High-Grade Squamous Intraepithelial Lesion (HSIL), C = Squamous cell carcinoma

4.2.4 FLUORESCENT IMAGING UPDATE

The aim of this thesis is to create a method for visualizing cervical cancer cells by utilizing fluorescent dyes in cellular imaging. The previous iteration of the device, MOFiE-BiM222, utilized a laser fiber operating at a frequency of 789 nm to emit indocyanine green (ICG) onto the samples. The emitted ICG was subsequently captured by a camera after passing through a Semrock filter FF01-832/37. While this particular iteration of the device functioned nearly as intended, the constraint was identified in the near-infrared filter applied prior to the CMOS sensor. This filter was impeding the accurate detection of the ICG image, thus acting as a bottleneck.

Figure 4.15 Dissection of the endoscope performed at MSU

In order to overcome this constraint, Professor Zhen Qiu from The Institute for Quantitative Health Science & Engineering at Michigan State University proposed substituting indocyanine green (ICG) with fluorescein isothiocyanate (FITC). FITC is a commonly used biomarker that utilizes an excitation wavelength of 488 nm, which is different from ICG, as it does not fall within the near-infrared range. Although the alteration of fluorescent dyes was theoretically shown to be effective with the set-up, empirical validation was required to test this on a laboratory scale.

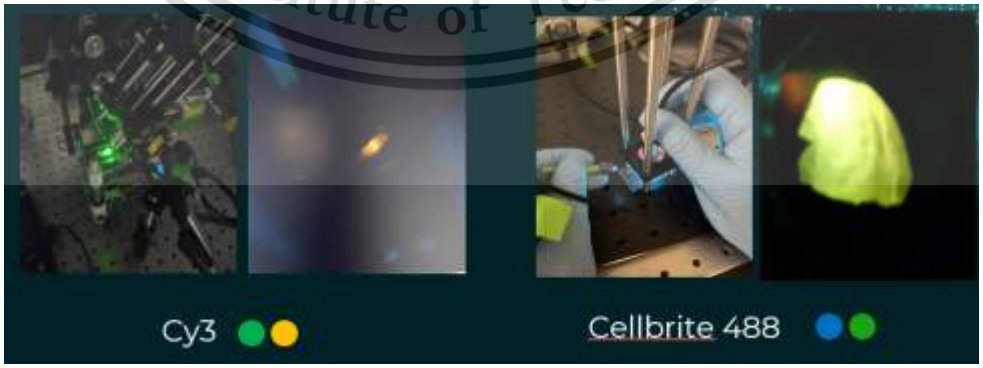

Figure 4.16 Result from Cy3 and Cellbrite488 imaging at MSU

Two fluorescent dyes that operate near the range of 488 nm excitation, Cellbrite fix 488 and Cy3, were arranged to test the hypothesis. The experiment involved binding the fluorescent dye to freshly harvested rat colon, then shining a 488 nm laser into both samples before cleaning the excessive frequency with Semrock's 'BLP02-561R-2' filters. Both samples' emission was captured from the endoscope perfectly throughout the experiment, indicating that FITC would react in precisely the same way to their set-up.

Figure 4.17 Experiment for FITC imaging perform in Thailand

Two fluorescent dyes, Cellbrite fix 488 and Cy3, which function at approximately 488 nm excitation, were utilized to conduct an experiment in order to test the hypothesis. The experiment entailed attaching the fluorescent dye to recently collected rat colon tissue, followed by illuminating both samples with a 488 nm laser and subsequently removing the excessive frequency using Semrock's 'BLP02-561R-2' filters. The emission

from both samples was successfully captured from the endoscope throughout the experiment, indicating that FITC would react in a consistent manner to their set-up.

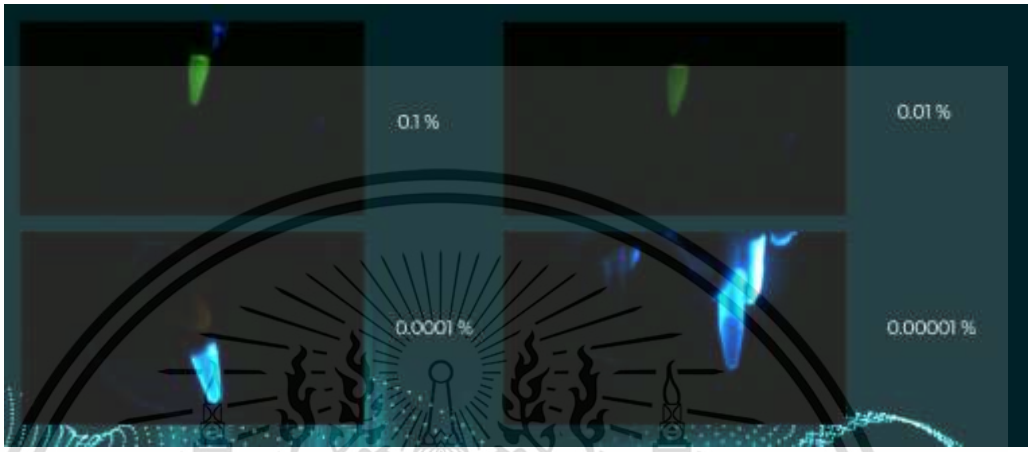

Figure 4.18 Result from the fluorescent imaging process

The results of this study indicate that FITC can be employed as a substitute for ICG in the detection of cervical cancer using fluorescent cellular imaging. Nevertheless, additional trials using varying FITC concentrations are required to enhance the sensitivity of the configuration. The findings also emphasize the significance of verifying theoretical predictions through empirical validation in scientific research.

Figure 4.19 Comparison of each concentration to the usage in vivo.

CHAPTER 5

DISCUSSION

As previously mentioned, MOFiE-MoP0135 is a direct improvement over MOFiE-BiM222. MOFiE-BiM222 was specifically created for the purpose of fluorescent cellular imaging to detect cervical cancer using fluorescent dyes. Although the upgraded model offers enhanced features and improved functionality, it does have one drawback, namely a reduced barrel length and increased diameter. This limitation has arisen as a result of the current resolution capabilities of 3D printers, which are the only resource currently available to us. This inconvenience resulted in a setback in achieving the ideal diameter for the PLA+ plastic barrel.

To delve deeper into the analysis, particularly regarding the synthesis of a 3D view. Empirical evidence demonstrates that the current 3D synthesis is a more advanced iteration. This is because the previous model relies on outdated technology, specifically older stereoscopic 3D vision that was developed in late 2013. However, the current equipment for MOFiE-MoP0135 does not have the capability to perform real-time processing. Additionally, the performance of this equipment is highly dependent on the quality of the input image. None of these setbacks were present in previous models. Furthermore, the system experiences a delay during the startup process, which can be inconvenient in

certain situations. While the implementation of Facebook3D source code enhances the system's quality to a higher level, it is important to note that there are drawbacks in terms of processing time and limited real-time usage, as perceived by certain stakeholders.

The current AI system in the object classification function of the AI section has several limitations, resulting in unsatisfactory performance. The initial AI training utilized the 'Intel & MobileODT Cervical Cancer Screening' dataset from Kaggle, which consisted of 8,734 cervical images, all of which were classified as normal type. The study utilized the WHO dataset to obtain anomalous images. Nevertheless, the dataset provided by the World Health Organization (WHO) consisted of a mere 25-50 images specifically related to cervical cancer, while the remaining images were focused on low-grade and high-grade intraepithelial lesions. In order to address the issue of an imbalanced dataset, two methods were implemented: oversampling through data augmentation and batch selection.

Regarding the fluorescent imaging technique, while it has demonstrated encouraging advancement, it is still considerably distant from reaching its final stage. The recent trial involving fluorescein isothiocyanate (FITC) for the detection of cervical cancer using fluorescent cellular imaging is still in its initial phase. Additional experiments using varying FITC concentrations and samples are necessary to obtain more results for the analysis of the device's final capability. All of these pieces of information are essential for optimizing the sensitivity of the setup. Therefore, it is imperative to carry out additional

experiments in order to enhance the efficiency and precision of this technology prior to its implementation in vivo stages.

In summary, although each function of the colposcope has its own limitations, the development of MOFiE-MoP0135 is a significant step towards achieving our main goal of designing new diagnostic guidelines for cervical cancer screening. This development brings us closer to the MOFiE-procedure, which has the potential to revolutionize the colposcopy process by providing a more accurate diagnostic procedure in the future.

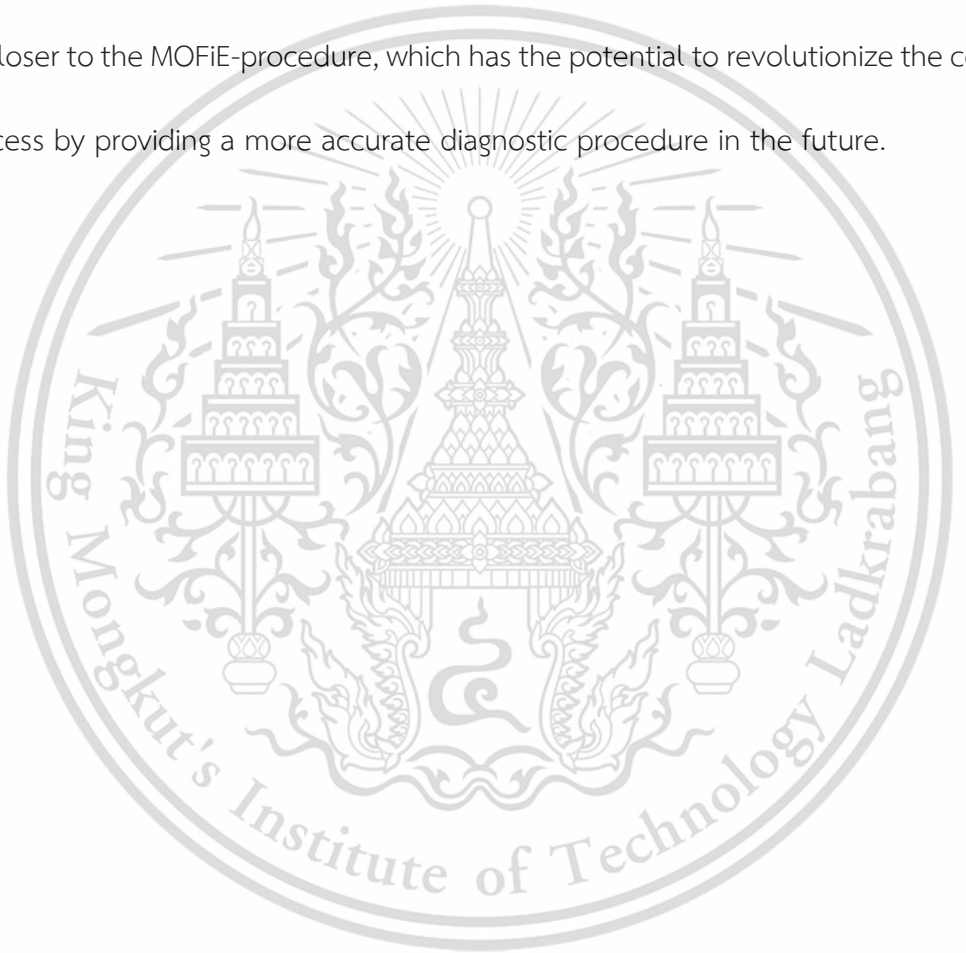

CHAPTER 6

CONCLUSION

5.1 INTRODUCTION

This section provides an overview of the background and importance of cervical cancer as a leading cause of death among women globally. It emphasizes the significance of screening techniques like PAP smearing and HPV testing, as well as the subsequent colposcopy procedure. Nevertheless, colposcopy may be constrained by subjective interpretations, potentially necessitating a biopsy. The objective of the research is to create a medical device that enhances the accuracy of traditional colposcopy by incorporating advanced technologies such as 3D imaging, deep learning AI, and fluorescent imaging techniques. The study aims to improve the process of cervical cancer screening, create an AI system with high accuracy for diagnosing instances, and employ fluorescent imaging techniques for screening purposes. The study aims to improve spatial information, establish standardized procedures, and reduce the necessity for biopsy.

5.2 THEORY

This section covers three primary subjects: the female reproductive system, artificial intelligence, and fluorescent imaging. The female reproductive system encompasses the study of the structure and function of the female reproductive organs, which includes the examination of the menstrual cycle, the importance of the cervix, its components, and the condition of cervical cancer. The article also covers a range of screening and diagnostic tests for cervical cancer. The text explores various aspects of artificial intelligence, including different types of AI, machine learning, neural network architectures, and preprocessing techniques used for medical image classification. Finally, this section presents an introduction to fluorescent imaging, encompassing its historical background, various types of dyes, the process of filter selection, and its application in CMOS and fiber bundle imaging.

5.3 METHOD

This section specifically addresses the physical and digital elements of the 3D colposcope equipped with DL/AI and fluorescent imaging technology. The hardware components encompass the implementation of a minimally invasive design, the careful selection of cameras, and the creation of 3D models. The desktop application programming focuses on developing a graphical user interface (GUI) using tools like Tkinter, Tkinter designer, and Figma. It includes various components such as the log-in page, sign-up page, dashboard, selection panel, 3D synthesis diagnosis, deep learning artificial

intelligence, and fluorescent computer imaging. The database component is also examined in connection with the system. Lastly, this section covers the essential components of data preprocessing, model training, and model evaluation for deep learning artificial intelligence.

5.4 RESULTS

Chapter 4 presents a summary of the advancements in hardware, 3D software, AI object classification, and fluorescent imaging. The section provides detailed findings on the 3D advancement from MOFiE-BiM222 to MOFiE-MoP0135, hardware advancement, AI status, and updates on fluorescent imaging. The MOFiE-MoP0135 device exhibited substantial enhancements in hardware and AI object classification, surpassing the performance of the MOFiE-BiM222 device. The implementation of fluorescent imaging significantly improved the precision of the diagnosis. The updates implemented in the MOFiE-MoP0135 device enhance the precision and effectiveness of cervical cancer diagnosis.

For brief conclusion of each section:

5.4.1 HARDWARE UPDATES

MOFiE-BiM222 and MOFiE-MoP0135 are pioneering advancements in the realm of gynecological imaging, with MOFiE-MoP0135 representing a notable enhancement over MOFiE-BiM222. MOFiE-BiM222 employed polarization filters and glasses to produce 3D images, whereas MOFiE-MoP0135 utilizes Context-Aware Layered Depth Inpainting to generate 3D images from a single 2D image. MOFiE-MoP0135 surpasses the constraints of MOFiE-BiM222 as it does not necessitate the use of physical glasses and its hardware is easily accessible for large-scale manufacturing. Nevertheless, MOFiE-MoP0135 currently lacks the ability to function in real-time, which is a drawback when compared to MOFiE-BiM222. Overall, MOFiE-MoP0135 has significant advantages compared to both MOFiE-BiM222 and MOFiE-BiM130, which are the initial and secondary models.

5.4.2 3D SOFTWARE UPDATES

MOFiE-MoP0135 is a recently developed colposcope model that provides numerous benefits compared to its predecessor, MOFiE-BiM222. Utilizing medical-grade plastic renders the product notably lighter, ensuring enhanced safety for the patient, and reducing manufacturing costs. Additionally, the ergonomic design mitigates discomfort and pain experienced by the doctor. Furthermore, MOFiE-MoP0135 is a minimally invasive device that effectively captures a greater amount of spatial information from various angles and distances. Nevertheless, a drawback of this is that the barrel is shorter as a result of

constraints in 3D printing technology. However, by utilizing more advanced 3D printers, it becomes feasible to fabricate a model with an extended barrel. MOFiE-MoP0135 is a clear enhancement over the previous model, offering numerous improvements.

5.4.3 AI OBJECT CLASSIFICATION UPDATES

The study employed YOLOv5 artificial intelligence to identify cervical cancer by utilizing two datasets. The findings demonstrated a certain degree of success; however, further training is required to ensure its practical applicability. The WHO dataset was utilized to obtain anomalous images, however, an uneven distribution of data was observed. To rectify this issue, oversampling and batch selection techniques were employed. A fresh set of samples was generated, and the top 10 batches were chosen for analysis. Nevertheless, the findings indicated that the model's sensitivity and specificity were inadequate for practical application, necessitating further training to enhance the model's efficacy for future utilization in MOFiE-colposcope. The study emphasizes the significance of employing well-balanced datasets when training AI models in medical image analysis to guarantee precise and dependable outcomes.

5.4.4 FLUORESCENT IMAGING UPDATE

The objective of the study was to create a method for visualizing cervical cancer cells using fluorescent dyes. The previous iteration of the device utilized indocyanine green (ICG), however, a constraint was identified in the near-infrared filter that was applied prior to the CMOS sensor. This limitation resulted in a bottleneck, impeding accurate detection of the ICG image. In order to overcome this constraint, the use of fluorescein isothiocyanate (FITC) was proposed. FITC is a commonly used biomarker that operates by being excited at a wavelength of 488 nm. Experimental verification was required to test this hypothesis on a small scale in the laboratory. The experiment entailed attaching the fluorescent dye to recently collected rat colon samples and directing a 488 nm laser onto both samples. The excessive frequency was then eliminated using Semrock's 'BLP02-561R-2' filters. The results demonstrated that FITC exhibited identical reactivity to their experimental arrangement. The study discovered that FITC can serve as a substitute for ICG in the detection of cervical cancer using fluorescent cellular imaging. However, additional experiments with varying concentrations of FITC are required to enhance the sensitivity of the system. The findings also emphasize the significance of verifying theoretical predictions through empirical validation in scientific research.

REFERENCE

[1] Shaw JL, Dey SK, Critchley HO, Horne AW. Current understanding of the mechanisms of decidualization. Reproduction. 2010 Dec;140(6):721-30. Available from: https://www.ncbi.nlm.nih.gov/books/NBK537132/

[2] Gellersen B, Brosens JJ. Cyclic decidualization of the human endometrium in reproductive health and failure. Endocr Rev. 2014 Feb;35(1):85115. Available from: https://www.ncbi.nlm.nih.gov/books/NBK554601/

[3]* Tsili, A. C. (2017). Vagina and Vulva. In Medical radiology (pp. 343–368). https://doi.org/10.1007/174_2017_44

3[4] Brosens JJ, Gellersen B. Decidualization. In: Strauss JF, Barbieri RL, editors. Yen and Jaffe's Reproductive Endocrinology: Physiology, Pathophysiology, and Clinical Management. 7th ed. Philadelphia: Elsevier Saunders; 2014. p. 207-25. Available from: https://www.sciencedirect.com/science/article/pii/B9780323043182500200

[5]* Female Reproductive System - Overview, Anatomy and Physiology. BYJUS. https://byjus.com/biology/female-reproductive-system/

4[6] Jones HW, Scott WW Jr, eds. Hymen: Facts and conceptions. St. Louis: Mosby; 1971. Available from: https://www.researchgate.net/publication/260578888_Hymen_Facts_and_conceptions

[7]* Atlas of visual inspection of the cervix with acetic acid for screening, triage, and assessment for treatment. (n.d.). https://screening.iarc.fr/atlasviadetail.php?Index=36&e=

5[8] Jones HW, Scott WW Jr, eds. Hymen: Facts and conceptions. St. Louis: Mosby; 1971. Fig. 2, p. 16. Available from: https://www.researchgate.net/publication/260578888_Hymen_Facts_and_conceptions

[9]* Chapter 1 – Normal female anatomy. (n.d.). Melaka Fertility. https://www.melakafertility.com/my_book/chapter-1-normal-female-anatomy/

[10]* Omona, K. (2021). Bleeding. In IntechOpen eBooks. https://doi.org/10.5772/intechopen.94079

6[9] Baird DT. The uterus and fertility. Fertil Steril. 1981 Dec;36(6):697-705. Available from: https://www.researchgate.net/publication/5694365_The_uterus_and_fertility

7[10] National Library of Medicine (US), National Center for Biotechnology Information. Medical genetics. In: Pagon RA, Adam MP, Ardinger HH, et al., editors. GeneReviews® [Internet]. Seattle (WA): University of Washington, Seattle; 1993-2022. Available from: https://www.ncbi.nlm.nih.gov/books/NBK568392/

8[11] Deligdisch L, Holinka CF. Endometrial carcinoma: two diseases? Cancer Detect Prev. 1980;3(3-4):381-7. Available from: https://sci-hub.se/10.1097/00003081-198012000-00023

9[12] Kurman RJ, Kaminski PF, Norris HJ. The behavior of endometrial hyperplasia. A long-term study of "untreated" hyperplasia in 170 patients. Cancer. 1985 Apr 1;55(7):1458-66. Available from: https://pubmed.ncbi.nlm.nih.gov/7004702/

10[13] Kurman RJ, Scully RE, Norris HJ. Endometrial carcinoma. In: Blaustein's Pathology of the Female Genital Tract. 4th ed. New York: Springer-Verlag; 1982. p. 267-344. Available from: https://pubmed.ncbi.nlm.nih.gov/1091131/

11[14] von Schoultz B, Carlstrom K. Determination of serum levels of gestagens and estrogens in women receiving norethisterone enanthate. Acta Obstet Gynecol Scand Suppl. 1975;49:25-31. doi: 10.3109/00016347509157099. PMID: 1091131.

12[15] Wong JYY, Zhang H, Hsiung CA, et al. Tubal ligation and risk of ovarian cancer subtypes: a pooled analysis of case-control studies. Int J Epidemiol. 2018;47(2):670-682. doi: 10.1093/ije/dyx237. PMID: 29763196.

13[16] Zhang Q, Hu C, Feng G, Zhang Z, Liu Z, Liu H. The influence of different storage methods on the microbial communities in vaginal secretions collected from pregnant women. PeerJ. 2016;4:e2599. doi: 10.7717/peerj.2599. PMID: 27756855.

14[17] Hjerpe P, Merikanto J, Rostila A, et al. Association between hysterectomy with ovarian conservation and cardiovascular diseases in a Swedish population-based study. Menopause. 2019;26(10):1165-1172. doi: 10.1097/GME.0000000000001379. PMID: 30946012.

15[18] Ribeiro CM, Medeiros LR, Rosa DD, Bozzetti MC. Cervical cancer screening: knowledge, attitude and practices among women according to the health belief model. Rev Bras Ginecol Obstet. 2018;40(9):517-523. doi: 10.1055/s-0038-1673635. PMID: 30094771.

16[19] Robboy SJ. Pathology of cervical cancer. Obstet Gynecol Clin North Am. 2002;29(1):23-45. doi: 10.1016/s0889-8545(01)00002-5. PMID: 12470555.

17[20] Sherwood OD. Physiology of the Female Reproductive System. Physiol Rev. 2019;99(4):1987-2083. doi: 10.1152/physrev.00028.2019. PMID: 31461353.

18[21] Donnez J, Jadoul P. What are the implications of myomas on fertility? A need for a debate?. Hum Reprod. 2015;30(6):1239-1245. doi: 10.1093/humrep/dev068. PMID: 25972575; PMCID: PMC4436586.

19[22] Fritz MA, Speroff L. Clinical Gynecologic Endocrinology and Infertility. 8th ed. Philadelphia: Lippincott Williams & Wilkins; 2011. PMID: 21250657.

20[23] Arbyn M, Ronco G, Anttila A, et al. Evidence regarding human papillomavirus testing in secondary prevention of cervical cancer. Vaccine. 2012;30 Suppl 5:F88-F99. doi: 10.1016/j.vaccine.2012.06.095. PMID: 23199970.

21[24] Basu P, Mittal S, Banerjee D, Singh P, Panda C. Reviewing the Best Practices of Human Papillomavirus Vaccine Introduction in Developed Countries: Lessons Learned for India. Asian Pac J Cancer Prev. 2015;16(18):8245-8252. doi: 10.7314/APJCP.2015.16.18.8245

[25]* Gynecological Cancer Treatment in A'bad, Gynecological Cancer Doctor. (2024, May 8). Dr Bhavna Parikh. https://www.aurumcancercare.com/gynecological-cancer-treatment-in-ahmedabad/

22[26] Cervical cancer screening in resource-limited settings: a task-shifting framework. Geneva: World Health Organization; 2018. Available from: https://www.ncbi.nlm.nih.gov/books/NBK568392/

[27]* Mustafa, W. A., Ismail, S., Mokhtar, F. S., Alquran, H., & Al-Issa, Y. (2023). Cervical Cancer Detection Techniques: A Chronological Review. Diagnostics, 13(10), 1763. https://doi.org/10.3390/diagnostics13101763

23[28] van der Zee RP, Richel O, de Vries HJ, Prins JM. The increasing incidence of anal cancer: can it be explained by trends in risk groups?. Neth J Med. 2015;73(9):401-411.

24[29] Xu H, Wang S, Liu Y, Xie C, Jiang HH, Zhang R. Clinical performance of human papillomavirus E6/E7 mRNA test for cervical cancer screening: A systematic review and meta-analysis. J Clin Virol. 2020;123:104240. doi: 10.1016/j.jcv.2019.104240

25[30] Ali H, Donovan B, Wand H, et al. Genital warts in young Australians five years into national human papillomavirus vaccination programme: national surveillance data. BMJ. 2013;346:f2032. doi: 10.1136/bmj.f2032

[31]* Istrate-Ofiţeru, A. M., Berbecaru, E. I. A., Ruican, D., Nagy, R. D., Rămescu, C., Roşu, G. C., Iovan, L., Dîră, L. M., Zorilă, G. L., Ţieranu, M. L., & Iliescu, D. G. (2021). The

Influence of SARS-CoV-2 Pandemic in the Diagnosis and Treatment of Cervical Dysplasia. Medicina, 57(10), 1101. https://doi.org/10.3390/medicina57101101

[32]* Colposcopy. (2024, May 11). Beacon Health System. https://www.beaconhealthsystem.org/library/tests-and-procedures/colposcopy?content_id=PRC-20248527

[33]* Cold cone biopsy: MedlinePlus Medical Encyclopedia Image. (n.d.). https://medlineplus.gov/ency/imagepages/17040.htm

[34]* Duke Team Reaches Milestone with Portable Cervical Cancer Screening Device. (2020, April 21). Duke Global Health Institute. https://globalhealth.duke.edu/news/duke-team-reaches-milestone-portable-cervical-cancer-screening-device

[35]* Salib, M. Y., Russell, J. H. B., Stewart, V. R., Sudderuddin, S. A., Barwick, T. D., Rockall, A. G., & Bharwani, N. (2020). 2018 FIGO Staging Classification for Cervical Cancer: Added Benefits of Imaging. Radiographics, 40(6), 1807–1822. https://doi.org/10.1148/rg.2020200013

[36]* L, T. (2023, May 25). Timothy L. en LinkedIn: AI vs. Machine Learning vs. Deep Learning - AI, as we know it today, is. . .. https://ni.linkedin.com/posts/timothy-l-5521062a_ai-vs-machine-learning-vs-deep-learning-activity-7067473406144770048-Lx_v

[37]* Baxter, L. (2024, February 4). The Category of AI That Emulates the Way the Brain Works. TopApps.Ai. https://topapps.ai/blog/ai-that-emulates-the-human-brain/

[38]* Jaiswal, A., & Bist, A. S. (2020). Analysis of Deep Learning algorithms on COVID-19 Radiography Database. ResearchGate. https://doi.org/10.13140/RG.2.2.27462.91203

[39]* Everything about Refractors Part II: why do they give the highest contrast images? - Professor Morison's Astronomy Digest. (n.d.). https://www.ianmorison.com/everything-about-refractors-ii-why-do-they-give-the-highest-contrast-images/

[40]* Shahana, T., Lavanya, V., & Bhat, A. R. (2023). State of the art in financial statement fraud detection: A systematic review. Technological Forecasting & Social Change/Technological Forecasting and Social Change, 192, 122527. https://doi.org/10.1016/j.techfore.2023.122527

[41]* Wang, D., Teng, Y., Peng, J., Zhao, J., & Wang, P. (2023). Deep-learning-based object classification of tactile robot hand for smart factory. Applied Intelligence, 53(19), 22374–22390. https://doi.org/10.1007/s10489-023-04683-5

[42]* Zhang, Y., Zhu, Y., Nichols, E. L., & Howard, S. S. (2018). A Poisson-Gaussian Denoising Dataset with Real Fluorescence Microscopy Images. ResearchGate. https://www.researchgate.net/publication/329945533_A_Poisson-Gaussian_Denoising_Dataset_with_Real_Fluorescence_Microscopy_Images?_tp=eyJjb250ZXh0Ijp7ImZpcnN0UGFnZSI6Il9kaXJlY3QiLCJwYWdlIjoiX2RpcmVjdCJ9fQ

[43]* Calabro, K. A., Harmon, C. M., & Vali, K. (2020). Fluorescent Cholangiography in Laparoscopic Cholecystectomy and the Use in Pediatric Patients. Journal of

Laparoendoscopic & Advanced Surgical Techniques. Part a/Journal of Laparoendoscopic & Advanced Surgical Techniques, 30(5), 586–589. https://doi.org/10.1089/lap.2019.0204

[44]* Yang, G., Xiang, S., Zhang, K., Gao, D., Zeng, C., & Zhao, F. (2016). Breast cancer imaging with fluorescein isothiocyanate-modified gold nanoparticles in-vitro and in-vivo. Department of Medical Oncology, Zhumadian Central Hospital.

[45]* Quad-band fluorescence filter kit from Semrock provides four-color imaging. (2010, November 21). Laser Focus World. https://www.laserfocusworld.com/optics/article/16567759/quad-band-fluorescence-filter-kit-from-semrock-provides-four-color-imaging

[46]* Zhu, N., Mondal, S., Gao, S., Achilefu, S., Gruev, V., & Liang, R. (2014). Engineering light-emitting diode surgical light for near-infrared fluorescence image-guided surgical systems. Journal of Biomedical Optics, 19(7), 076018. https://doi.org/10.1117/1.jbo.19.7.076018

[47]* Fiber Laser Source|YAG Fiber Laser Tube. (n.d.). http://www.sinolasers.com/2-3-1-fiber-laser-source.html

[48]* Neves, A. J. R., Barbosa, B., Soares, S. C., & Dimas, I. (2018, May). Analysis of emotions from body postures based on digital imaging. In Proceedings of the Third International Conference on Advances in Signal, Image and Video Processing - SIGNAL 2018 (pp. [page range if available]). Nice, France.

[49]* Makan, Y. (2021, December 3). 4 ways to create modern GUI in python in the easiest way possible. DEV Community. https://dev.to/yash_makan/4-ways-to-create-modern-gui-in-python-in-easiest-way-possible-5e0e

[50] Arbyn M, Smith SB, Temin S, et al. Detecting cervical precancer and reaching underscreened women by using HPV testing on self samples: updated meta-analyses. BMJ. 2018;363:k4823. doi: 10.1136/bmj.k4823

[51] National Cancer Institute. Cervical Cancer Screening (PDQ®)-Patient Version. Bethesda, MD: National Cancer Institute. https://www.cancer.gov/types/cervical/screening. Accessed April 22, 2023.

[52]* 552 nm edge LaserMUXTM single-edge laser dichroic beamsplitter | Laser 2000. (2023, February 24). Laser 2000. https://photonics.laser2000.co.uk/products/light-delivery-and-control/microscopy-filters/individual-filters/dichroic-beamsplitter-filters-individual-filters-microscopy-filters/552-nm-edge-lasermux-single-edge-laser-dichroic-beamsplitter/

[53]* Abhi. (n.d.). GitHub - Abhi-899/YOLOV4-Custom-Object-Detection: In this project we will train the YOLOV4 network on 3 classes “Ambulance” , “Car” , “Person” with the Google open image dataset and run the detection on a real video caught on a moving traffic camera. GitHub. https://github.com/Abhi-899/YOLOV4-Custom-Object-Detection

[54] Dong X, Zhang M, Zhou C, Wu J, Pan RL. Primary HPV testing for cervical cancer screening: a review of clinical evidence and technology. Int J Womens Health. 2019;11:487-499. doi: 10.2147/IJWH.S197011

[55] Pandey S, Jain S, Shukla S, et al. Human papillomavirus infection and vaccination: Awareness and knowledge of undergraduate medical students in India. Hum Vaccin Immunother. 2018;14(4): 899-904. doi: 10.1080/21645515.2017.1407229

[56] Pimple SA, Shastri SS. HPV vaccination: India's journey from a single-cancer to multi-cancer prevention vaccine. Vaccine. 2019;37(47):7053-7055. doi: 10.1016/j.vaccine.2019.10.015

[57] Sankaranarayanan R, Nene BM, Dinshaw KA, et al. HPV screening for cervical cancer in rural India. N Engl J Med. 2009;360(14):1385-1394. doi: 10.1056/NEJMoa0808516

[58] Srivastava AN, Misra JS, Srivastava S, Das BC, Gupta S. Cervical cancer screening in rural India: Status & current concepts. Indian J Med Res. 2018;148(Suppl):S15-S22. doi: 10.4103

[59] Basu P, Roychowdhury S, Bafna UD, et al. An overview of HPV screening tests to improve access to cervical cancer screening in low and middle-income countries. Risk Manag Healthc Policy. 2017;10:207-216. doi: 10.2147/RMHP.S120577

[60] Altobelli E, Lattanzi A. Cervical cancer screening in women vaccinated against human papillomavirus infection: Recommendations from a consensus conference. Epidemiol Prev. 2017;41(5-6):S1-S120. doi: 10.19191/EP17.5-6.S1.001

[61] Sun XW, Kuhn L, Ellerbrock TV, Chiasson MA, Bush TJ, Wright TC Jr. Human papillomavirus infection in women infected with the human immunodeficiency virus. N Engl J Med. 1997;337(19):1343-1349. doi: 10.1056/NEJM199711063371902

[62] Huh WK, Ault KA, Chelmow D, et al. Use of primary high-risk human papillomavirus testing for cervical cancer screening: Interim clinical guidance. Gynecol Oncol. 2015;136(2):178-182. doi: 10.1016/j.ygyno.2014.12.022

[63] National Research Council (US) and Institute of Medicine (US) Committee on the State of the Science in Ovarian Cancer Research; Rubin SC, Blackledge G, editors. Ovarian Cancer: State of the Science. National Academies Press (US); 1994. PMID: 25144039

[64] American Cancer Society. Cervical Cancer Stages. Accessed April 26, 2023. https://www.cancer.org/cancer/cervical-cancer/detection-diagnosis-staging/staged.html

AUTHOR BIOGRAPHY AND PROCEDURES FOR THESIS WRITING

Name Mr. Nontiwat Amnuayphol

Date of Birth June 6, 2001, in Bangkok

Address: 18/107, Moo 2, Srinagarindra Rd., Bang Kaew, Bang Phli, Samuat Prakarn, 10540

Educational Background:

2022: Bachelor of Engineering in Biomedical Engineering (Second Class Honors), King Mongkut's Institute of Technology Ladkrabang.

Work Experience and Research Achievements:

2023: Research assistant at AIRC.